ENERGY COUPLING BETWEEN THE SOLAR WIND AND THE MAGNETOSPHERE

S.-I. AKASOFU

Geophysical Institute, University of Alaska, Fairbanks, AK 99701, U.S.A.

(Received 12 February, 1981)

Abstract. This paper describes in detail how we are led to the first approximation expression for the solar wind-magnetosphere energy coupling function ε, which correlates well with the total energy consumption rate U_T of the magnetosphere. It is shown that ε is the primary factor which controls the time development of magnetospheric substorms and storms. The finding of this particular expression ε indicates how the solar wind couples its energy to the magnetosphere; the solar wind and the magnetosphere constitute a dynamo. In fact, the power P generated by the dynamo can be identified as ε by using a dimensional analysis. Furthermore, the finding of ε indicates that the magnetosphere is closer to a directly driven system than to an unloading system which stores the generated energy before converting it to substorm and storm energies. Therefore, the finding of ε and its implications have considerably advanced and improved our understanding of magnetospheric processes. The finding of ε has also led us to a few specific future problems in understanding relationships between solar activity and magnetospheric disturbances, such as a study of distortion of the solar current disk and the accompanying changes of ε. It is also pointed out that one of the first tasks in the energy coupling study is an improvement of the total energy consumption rate U_T of the magnetosphere. Specific steps to be taken in this study are suggested.

1. Introduction

Since the successful formulation of the magnetosphere formation by Chapman and Ferraro (1931), the problem of energy coupling between the solar wind and the magnetosphere has been long-standing. Before 1960, it had simply been thought that geomagnetic storms arise as a result of impact of a solar gas cloud upon the magnetosphere. However, Akasofu and Chapman (1963) found that the magnitude of storm sudden commencements (ssc) has little relation to the magnitude of the main phase decrease (*Dst*). The magnitude of an ssc is proportional to $(\sqrt{p_2}-\sqrt{p_1})$, where p_1 and p_2 denote the solar wind pressure before and after an ssc. Figure 1 shows a collection of low latitude magnetic records (H) which demonstrates the variety of the main phase development. One can easily see that a variety of the main phase development follows for a similar magnitude of ssc's and thus of pressure and kinetic energy flux increases. The first two examples show a large ssc and a long initial phase, without a definite indication of the development of the main phase. On the other hand, the last example shows that an intense main phase developed even without ssc and the initial phase. The other examples can be considered to fall in between these two types of storms. For example, the third storm developed eventually an appreciable main phase after a long initial phase. The fourth storm has been considered to be more or less a 'typical' storm. On the basis of these findings, Akasofu and Chapman (1963) concluded: "The variety of development of the storms seems to suggest some intrinsic differences between the solar streams far beyond what we would expect from a mere difference between their pressures. The nature of their intrinsic differences is at present unknown." It was with this statement

Space Science Reviews **28** (1981) 121–190. 0038-6308/81/0282-0121 $10.50.

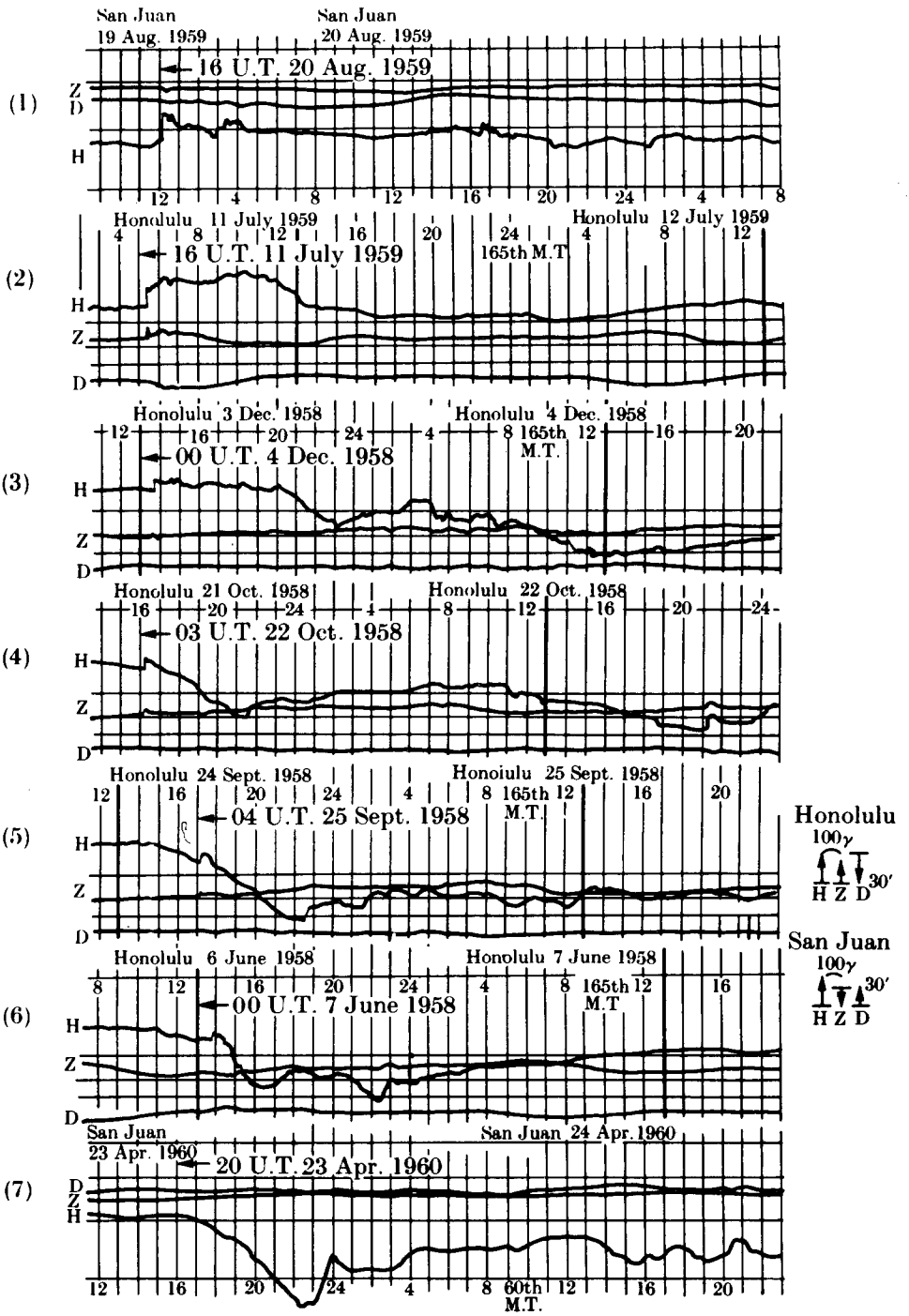

Fig. 1. Collection of the *H* component magnetic records from low latitudes (San Juan and Honolulu) showing the variety of the development of geomagnetic storms. The top one was associated with a large ssc and initial phase, without any significant main phase. The bottom one was associated with a large main phase, without any significant ssc and initial phase. The other examples fall in between these two extreme types.

that our search for the energy coupling process between the solar wind and the magnetosphere began.

In the meantime, the importance of the interplanetary magnetic field (IMF) on substorm activity has become increasingly clear, as suggested originally by Alfvén (1939, 1950), Hoyle (1949), and particularly by Dungey (1961). The first observational support of the importance of the IMF came from a work by Fairfield and Cahill (1966). Since then a large number of papers have been written on the correlation between various magnetospheric phenomena and the IMF southward component. By 1971 the importance of the IMF southward component on substorm activity was confirmed (cf. Rostoker and Fälthammar, 1967; Arnoldy, 1971; Meng *et al.*, 1973; cf. Akasofu, 1977).

It is now clear that the magnetosphere studied by Chapman–Ferraro is a special case in which the solar wind is considered as an unmagnetized plasma. In this special case, their theory indicates that the unmagnetized solar wind simply flows around the Earth, confining completely the Earth's magnetic field into a cavity. Such a magnetosphere is said to be 'closed'.

For the closed magnetosphere the energy coupling with the solar wind can occur in several ways. One possible way is a 'viscous-like' interaction which may take place between the solar wind and the magnetospheric plasma (Axford, 1964, 1969). However, at the present time, it is not possible to demonstrate the presence of such a 'viscous-like' interaction. This is because its presence can be confirmed only when the magnetosphere has a completely closed topology, and there is so far no observation to suggest that the magnetosphere achieves such a closed configuration even when the solar wind magnetic field has a large northward component for several hours. The permanent presence of the auroral oval suggests that the magnetosphere is almost always open, perhaps except for very unusual occasions. Therefore, it is very difficult to identify phenomena which can be attributed to the predicted 'viscous-like' interaction, although they may indeed be present.

Another possibility is that pressure fluctuations of the solar wind generate Alfvén waves and that the wave energy becomes converted into heat energy of plasma in the magnetosphere (Dessler *et al.*, 1961). It is, however, unlikely that this is the main energy coupling process; unusually large wave amplitudes are required to heat magnetospheric plasma in causing geomagnetic storms. Akasofu (1964) suggested that the solar wind contains a significant neutral component (H atoms) which penetrates freely across the magnetopause and becomes energetic protons after exchanging charge with H^+ and O^+ ions in the thermosphere. He suggested that the variety of development of geomagnetic storms might be due to the variety of the degree of ionization of the solar wind. Figure 2 shows schematically how the variety of the development of the main phase could be explained in terms of the variety of the degree of ionization of the solar wind plasma. In particular, he suggested that a geomagnetic storm with a large storm sudden commencement, but with no appreciable main phase was caused by a fully ionized solar wind which simply compresses the magnetosphere (as the Chapman–Ferraro theory indicates). In some cases, the

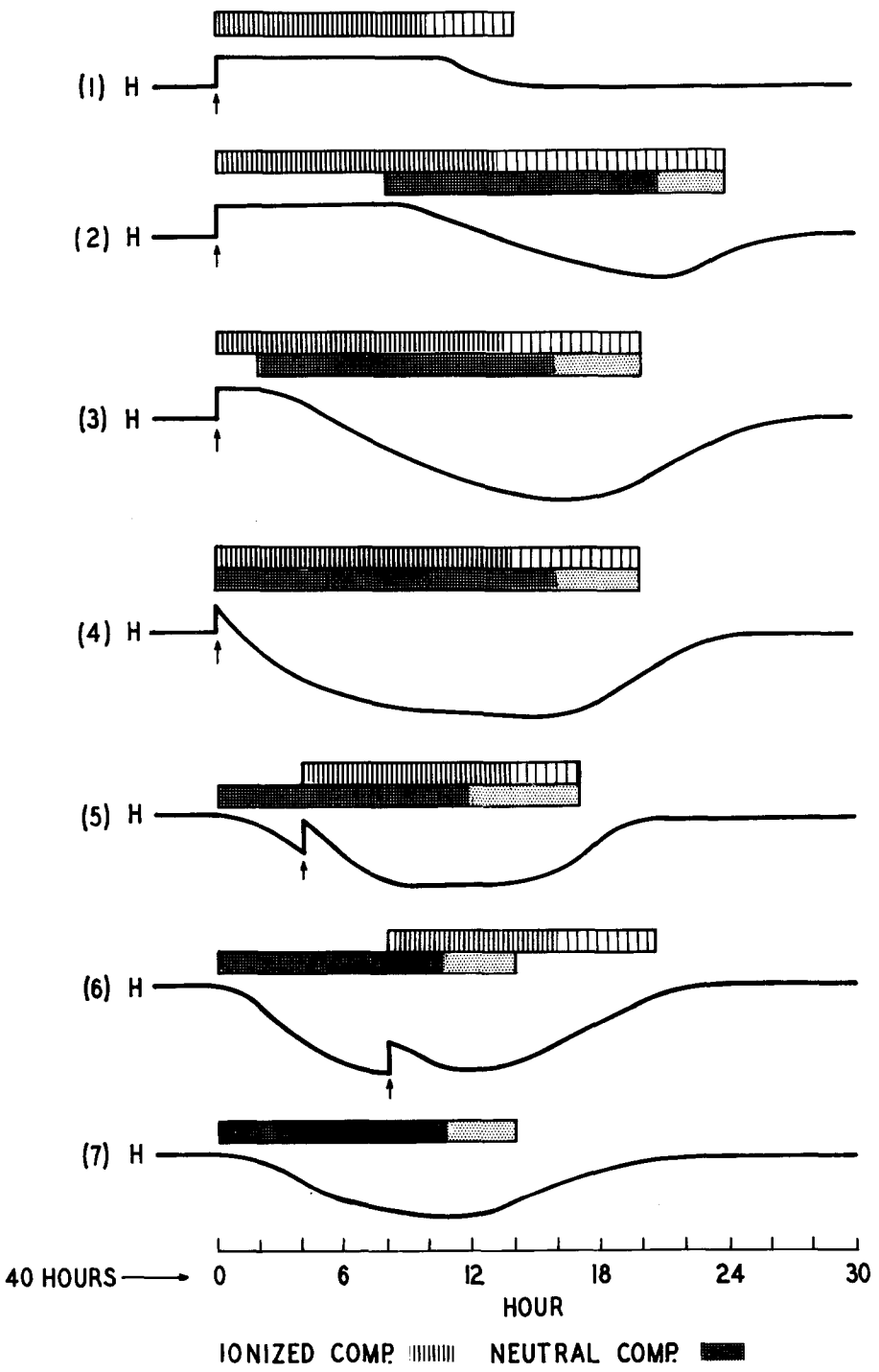

Fig. 2. Attempts to explain the variety of the development of geomagnetic storms by hypothetical distribution of neutral hydrogen atoms in the solar wind.

neutral component might arrive at the Earth long after the arrival of the fully ionized component; such a solar wind could cause a storm with a long initial phase. Although the neutral component appears to be present occasionally (Gosling *et al.*, 1980), it is unlikely that its flux is large enough to cause geomagnetic storms (Brandt and Hunten, 1966). The main point in showing Figure 2 is not to emphasize the importance of the degree of ionization, but to indicate that one must find an 'unknown' quantity in the solar wind to explain the variety of the development of geomagnetic storms. In this paper, it will be shown that the solar wind energy coupling function ε takes the place of the neutral component and the 'unknown' quantity.

The open magnetosphere was first suggested by Dungey (1961). In the open model, a finite amount of magnetic flux from the magnetosphere is interconnected with the solar wind (or interplanetary) magnetic flux. As described in Section 7, the importance of the open model is that it provides correctly the means by which the solar wind couples its energy to the magnetosphere by a dynamo process. In this paper, we shall reach this conclusion by taking the following steps.

(i) Determine the total energy consumption rate U_T (erg s^{-1}) in the magnetosphere.

(ii) Find a solar wind parameter ε (erg s^{-1}) which correlates with the total energy consumption rate U_T (erg s^{-1}).

(iii) Demonstrate that this particular solar wind parameter ε controls the development of the main phase of geomagnetic storms.

(iv) Demonstrate that the solar wind parameter ε can be identified as the power generated by the solar wind-magnetosphere dynamo.

(v) Provide a theoretical basis for the expression of ε.

(vi) Discuss the significance of the above findings.

(vii) Suggest how the energy coupling study might further be pursued in the future.

It should be noted that the approach chosen in the above is considerably different from most of the earlier ones in which one attempted to find a solar wind quantity (or a combination of several quantities) which correlates with a single geomagnetic index (such as the *Kp*, ΣKp, *AE* indices). Such a study has its own merit, but is not necessarily most useful in understanding the energy coupling. For example, there is an excellent correlation between ΣKp and the solar wind speed V (Snyder *et al.*, 1963; Olbert, 1968). However, one can do little with this correlation in understanding the energy coupling, since ΣKp is not really a basic physical quantity (such as B, J, etc.). The results of these studies are summarized in Table I.

2. Definition of Energy Coupling

The *energy coupling* of two systems, say, *A* and *B*, may be described in terms of input energy flux ε (erg s^{-1}) from *A* to *B* and output energy flux U_T (erg s^{-1}) from *B*. In general, a variety of problems between the input and output energies can be

TABLE I

List of the correlation studies between geomagnetic indices and solar wind parameters

Author(s)	Geomagnetic index (Time resolution)		Relation with solar wind parameters
Snyder *et al.* (1963)	ΣKp	(24 hr)	$\Sigma Kp = (V-330)/8.44$
Olbert (1968)	ΣKp	(24 hr)	$\Sigma Kp = (V-262)/6.3$
Ballif *et al.* (1969)	Kp	(3 hr)	$Kp = 9\left\{1-\exp\left(\frac{-\sigma B_T, N^{-0.35}}{7.70}\right)\right\}$
Arnoldy (1971)	AE	(1 hr)	$AE = -0.26\,(\Sigma B_s\tau)_0 - 0.91\,(\Sigma B_s\tau)$, $= -0.33\,(\Sigma B_s\tau)_2 + 0.12P_0$
Bobrov (1973)	Kp	(3 hr)	$Kp = f(V, B_z\Delta B_z)$
Garrett *et al.* (1974)	ap, AE	(1 hr)	ap, $AE \propto C_1 + C_2 V\langle B_s\rangle + C_3 V\sigma$
Murayama and Hakamada (1975)	AE	(1 hr)	$AE = CB_s V^2$
Burton *et al.* (1975)	Dst	(2.5 min)	$\frac{d}{dt}Dst_0 = F(E) - aDst_0$
Crooker *et al.* (1977)	Ap		$Ap = 3.5\times10^{-5}\bar{B}_z\bar{V}^2 - 1.9$
Svalgaard (1977)	am	(3 hr)	$am = 6.6q(f,\alpha)\left\{\frac{BV_0}{21}\right\}\left[\frac{nV_0^2}{105}\right]^{1/3}\times \times\frac{1.157}{(1+3\cos^2\psi)^{2/3}}$
Maezawa (1979)	Al, AU, am	(1 hr)	$AL \propto B^{0.85}V^{2.08}(\sin\theta)^{0.54}$ $AU \propto B^{0.67}V^{1.15}(\sin\theta)^{0.34}$ $am \propto B^{1.03}V^{2.34}(\sin\theta)^{0.37}n^{0.2}$
Holzer and Slavin (1979)	AL	(1 hr)	Rate of erosion $\frac{d\phi_e}{dt} = 0.2\,(1.9\times10^{10}\text{ cm})\,B_z V_{sw}\ (\text{km s}^{-1})$ Rate of return $\frac{d\Phi_r}{dt} = 1.8\times10^{10}\,AL(\gamma)$
Murayama (1979)	AL	(1 hr)	$AL = 60(B_s+0.5)\,V^2F(X,B_y)n^{0.13}$

Note: For details of the expressions and definitions of each notation, see the referenced papers.

expected, depending on different situations we deal with on A and B. In a simplest case, both $\varepsilon(t)$ and $U_T(t)$, as well as the conversion mechanism from ε to U_T, are known; in such a case, the conversion efficiency may be the main problem. In some cases, the nature of both ε and U_T is known, but the conversion mechanism is not known. In some other cases, one can estimate U_T, but the nature of ε is not known; in such a case, the conversion process from ε to U_T is obviously unknown. The study of energy coupling between the solar wind and the magnetosphere belongs to the last case.

Therefore, the first task may be to obtain the total energy consumption rate of the magnetosphere $U_T(t)$ and then attempt to find the input energy flux $\varepsilon(t)$ which

correlates with $U_T(t)$. However, it should be noted that it is not necessarily obvious that one could readily find $\varepsilon(t)$ on the basis of $U_T(t)$. For example, if the magnetosphere is assumed to be a kind of system which initially stores solar wind energy in some form and subsequently converts suddenly the stored energy into substorm energy, one would not necessarily expect a simple relationship between $\varepsilon(t)$ and $U_T(t)$. This point can be illustrated by contrasting the following two systems which are assumed to be energized by hydropower. In the first system, a resistor is directly connected to a dynamo, and we monitor both the hydropower $\varepsilon(t)$ and Joule heat production rate $U_J(t)$ produced in the resistor. In the second system a particular type of device is inserted between the dynamo and the resistor, which is assumed to accumulate electrical energy until it reaches a critical value at which time the accumulated energy is suddenly discharged to the resistor. In the first system, time variations of $\varepsilon(t)$ will be quite similar to those of $U_J(t)$, except for a slight time delay of $\tau = L/R$ where L and R denote the inductance and resistance of the system. However, in the second system $U_J(t)$ will be a series of impulses even when $\varepsilon(t)$ is constant, so that there would be no correlation between $\varepsilon(t)$ and $U_T(t)$. The former system may be called a 'driven' system while the latter may be called an 'unloading' system. Therefore, the identification of the nature of $\varepsilon(t)$ by using $U(t)$ would not necessarily be an easy task and may even fail for an unloading system. On the other hand, if one would succeed in finding $\varepsilon(t)$ which correlates well with $U_T(t)$, the magnetosphere would not necessarily be an unloading system, as it has widely been believed. Therefore the energy coupling study has considerable significance in magnetospheric physics, in particular in understanding magnetospheric substorms and storms.

3. Total Energy Consumption Rate $U_T(t)$ of the Magnetosphere

The first step in our search of this energy coupling process is to determine the total energy consumption rate $U_T(t)$ of the magnetosphere during magnetospheric substorms and storms. Many observable magnetospheric *disturbance phenomena* can be identified as *manifestations of dissipation processes* of the energy produced by solar wind-magnetosphere interaction. The dissipated energy is partially deposited in the inner magnetosphere, resulting in the ring current belt. Fortunately, the ring current energy can continuously be monitored by magnetic observatories in low latitudes under certain assumptions. Another part is deposited in the auroral ionosphere as heat energy which arises partly from Joule heating and partly from the impact of auroral particles. These quantities can also continuously be monitored by magnetic observatories along the auroral zone under certain assumptions. Thus, the total energy consumption rate U_T can be given by the sum of the ring current energy injection rate $U_R(t)$, the Joule heat production rate in the ionosphere $U_J(t)$ and the auroral particle energy flux $U_A(t)$. Fortunately, networks of ground-based magnetometers are capable of monitoring continuously these three quantities, $U_R(t)$, $U_J(t)$, and $U_A(t)$ under certain assumptions (cf. Perreault and Akasofu, 1978).

There may be other magnetospheric dissipation processes which do not deposit energies in the inner magnetosphere or in the auroral ionosphere. For example, a part of the energy dissipated in the magnetotail may be dispersed directly into the solar wind. Unfortunately, there is no way to monitor continuously the amount of energy dissipated in such a way.

Among various geomagnetic indices presently available, there are only two, the *Dst* and *AE* indices, which are suitable in estimating U_T. The *Dst* index gives the average magnetic field intensity of the ring current belt on the Earth's surface and can be considered to be a measure of the total kinetic energy of the belt under several assumptions. The *AE* index gives the sum of the maximum magnetic field intensity of the westward and eastward auroral electrojets and can be considered to be a measure of the total current of the auroral electrojets, again under several assumptions. Both indices are given in units of γ.

A. RING CURRENT ENERGY INJECTION RATE U_R

The total kinetic energy K_R in the symmetric ring current belt is related approximately to the magnetic field intensity at the Earth's center B_R by

$$K_R = \frac{3}{2}\frac{U_m}{B_0}B_R\,, \tag{1}$$

where U_m and B_0 denote the magnetic energy of the Earth outside the Earth and the magnetic field intensity at the equator (Dessler and Parker, 1959; Sckopke, 1966; Akasofu and Chapman, 1972). Note that the induction effect of the Earth is taken into account in (1). In (1), B_R can be approximated by the absolute value of the *Dst* index under the following assumptions.

(i) The ring current belt is symmetric with respect to the dipole axis.

(ii) The nonlinear distortion of the geomagnetic field by the ring current is not serious.

(iii) The *Dst* index gives the field of the symmetric ring current field if it has a negative value.

Actually, none of the above assumptions can rigorously be justified. The suggested steps to improve the *Dst* index for our particular use are given in Section 9.3. It is relatively simple, however, to subtract effects of changes of the solar wind pressure from the *Dst* index. An increase of the solar wind pressure compresses the magnetosphere, causing an increase of the *Dst* index. This solar wind pressure effect ΔH can approximately be removed by using the following formula given by Siscoe *et al.* (1968).

$$\Delta H = 13.1\times 10^4(\sqrt{p_2}-\sqrt{p_1})\gamma\,,$$

where p_1 and p_2 denote the solar wind pressure before and after the pressure increase. An absolute value of the *Dst* index thus corrected is denoted by $\overline{Dst}$. Under the above assumptions, the corrected $\overline{Dst}$ is related to K_R by

$$K_R = 4\times 10^{20}\overline{Dst}(\gamma)\,. \tag{2}$$

The ring current energy K_R is related to the energy injection rate U_R and the loss rate $\mathscr{L}$ by

$$\frac{\partial K_R}{\partial t} = U_R - \mathscr{L}. \tag{3}$$

The loss rate can be expressed by

$$\mathscr{L} = \frac{K_R}{\tau_R}, \tag{4}$$

where τ_R denotes the life time of the ring current particles. By using (2) and (4), the ring current energy injection rate U_R can be written as

$$U_R = 4 \times 10^{20} \left(\frac{\partial \overline{Dst}}{\partial t} + \frac{\overline{Dst}}{\tau_R} \right). \tag{5}$$

The quantity expressed in (5) must be estimated with great caution by noting that U_R must be a positive quantity. This problem was considered in great detail by Davis and Parthasarathy (1967). Further, it has recently become apparent that τ_R varies considerably during a geomagnetic storm. When the ring current is growing, τ_R can be as short as 1 hr, while it is as long as 20–25 hr when the ring current is slowly decaying during the recovery phase. The reason for such a large change of τ_R is that the ring current is formed rather close to the Earth (at a geocentric distance of $3R_E$) even during a weak storm (Frank, 1971) and protons have a very short lifetime as a result of charge exchange at such distances. On the other hand, He^+ and O^+ become dominant ions as a result of their long lifetime (~20 hr) during the recovery phase (Tinsley, 1976). Here, we take $\tau_R = 20$ hr for $\varepsilon < 5 \times 10^{18}$ erg s^{-1} and $\tau_R = 1$ hr for $\varepsilon \geq 5 \times 10^{18}$ erg s^{-1}.

B. JOULE HEAT PRODUCTION RATE IN THE IONOSPHERE

The production rate of Joule heat U_J in the entire auroral ionosphere is defined by

$$U_J = \int\int \mathbf{J}_P \cdot \mathbf{E} \, d\lambda \, d\phi, \tag{6}$$

where $\mathbf{J}_P$ and E_P are the height-integrated Pedersen current intensity and the associated electric field; both quantities are a function of latitude ϕ and longitude λ. At present, there is no way to monitor $\mathbf{J}_P$ and $\mathbf{E}$, and the AE index is, as a first approximation, a measure of the intensity of the Hall current J_H, integrated over latitude ϕ, namely $\int J_H \, d\phi$.

In order to find how U_J might be related to the AE index, it is reasonable to assume that J_P is proportional to J_H and E is proportional to E. Since the auroral electrojet flows mainly in the east–west direction, the quantity $\mathbf{J}_P \cdot \mathbf{E}$ may be proportional to $\mathbf{J}_H \cdot \mathbf{E}_y$, where $\mathbf{E}_y$ is the east–west component of the electric field. In order to proceed further at this point, one must rely on specific observations as to how E_y varies during magnetospheric substorms. Rino *et al.* (1974) showed, by using

the Chatanika radar, that E_y remains fairly constant during magnetospheric substorms in spite of the fact that J_H greatly varies. Therefore, we conclude that the Joule heat production rate U_J is proportional to J_H and $\int J_H \, d\phi$ and thus to the AE index. The Chatanika radar observations seem to support our assumption (Brekke and Rino, 1978). Note that such elaborate steps should be taken to find the dependence of U_J on the AE index, since the conductivity of Σ_3 of the ionosphere is not a constant during magnetospheric disturbances. The longitudinal extent of the electrojet is expected to vary in time, but there is at present no way to monitor it continuously. However, the main part of the electrojet is known to establish itself during an early epoch of the expansive phase of magnetospheric substorms (~30 min); see Akasofu *et al.* (1968). Therefore, we assume that the longitudinal extent is constant as a first approximation.

Altogether, thus, we assume that U_J is proportional to the AE index. By using the fact that U_J is a fraction of U_R (Axford, 1967; Akasofu, 1968, 1977), we adopt the proportionate constant to be 2×10^{15} (erg s^{-1}(γ)), so that the Joule heat production rate for $AE = 1000\gamma$ becomes 2×10^{18} erg s^{-1}.

C. KINETIC ENERGY INJECTION RATE OF AURORAL PARTICLES

The kinetic energy flux U_A carried by auroral particles has been estimated by several workers (Cole, 1962, 1971; Hays *et al.*, 1973; Rees, 1975) and it is generally accepted that it is significantly less than U_J or is at most comparable to it. There is so far no way to monitor this quantity as a function of time, but it is expected to vary in harmony with the AE index. In this paper, we assume $U_A = AE(\gamma)\times10^{15}$ erg s^{-1}.

D. THE TOTAL ENERGY PRODUCTION RATE U_T OF THE MAGNETOSPHERE

On the basis of the above consideration, we arrive at the following equations for the total energy consumption rate U_T of the magnetosphere.

$$\begin{aligned} U_T &= U_R + U_J + U_A \\ &= 4\times10^{20}\left(\frac{\partial\overline{Dst}}{\partial t}+\frac{\overline{Dst}}{\tau_R}\right)+3AE\times10^{15}. \end{aligned} \tag{7}$$

4. Empirical Formulation

As mentioned earlier, our study of the energy coupling between the solar wind and the magnetosphere belongs to the category in which the only known quantity is the total energy consumption rate $U_T(t)$ of the magnetosphere, so that we know neither the nature of input energy flux $\varepsilon(t)$, nor its conversion mechanism to $U_T(t)$.

A. ENERGY FLUX

In this situation, Perreault (1974) and Perreault and Akasofu (1978) had to take an empirical approach in determining the functional form of input energy flux $\varepsilon(t)$. However, *their empirical approach was greatly simplified by the fact that there are*

only two obvious forms of solar wind energy flux; they are ρV^3 (erg s^{-1}) and VB^2 (erg s^{-1}). Furthermore, Akasofu and Chapman (1963) and Arnoldy (1971) have already shown that there is no obvious correlation between ρV^3 and geomagnetic activity. Therefore, they had no alternative but to choose the latter form. Furthermore, the importance of the IMF north–south component B_z in substorm phenomena has been well established. Thus, Perreault and Akasofu (1978) assumed that the solar wind energy flux ε responsible for magnetospheric substorms and storms would have the following form:

$$\varepsilon = VB^2 F(\theta) l_0^2 \text{ (erg s}^{-1}\text{)}, \tag{8}$$

where $F(\theta)$ denotes a function of the angle θ, the polar angle of the IMF vector, projected onto the Y–Z plane, namely

$$\theta = \tan^{-1}(|B_y|/|B_z|) \quad \text{for} \quad B_z > 0$$

$$\theta = 180° - \tan^{-1}(|B_y|/|B_z|) \quad \text{for} \quad B_z < 0.$$

B. FUNCTIONAL FORM OF $F(\theta)$

Since the importance of the IMF B_z component on substorm activity has been well established, this dependence should be included in the formulation. This dependence on the B_z component had widely been discussed in the past in terms of the so-called 'southward turning' of the IMF vector. That is to say, it had been thought that the southward turning of the IMF vector 'switches on' the aurora and triggers a substorm, while the northward turning 'switches them off'. The basic idea behind this belief was that the magnetosphere acted like a half-wave rectifier (Burton *et al.*, 1975), namely $F(\theta) \neq 0$ if $B_z < 0$ and $F(\theta) = 0$, if $B_z = 0$. However, a study of all-sky photographs obtained from the Alaska meridian chain of observatories and DMSP satellite photographs showed clearly that the auroral oval and auroral substorms are present even when the IMF vector is directed northward ($B_z > 0$) for many hours after the northward turning (Akasofu *et al.*, 1973; Akasofu, 1974). During the period when the IMF B_z component is positive, the auroral oval contracts poleward, outside the poleward field of view of most of the auroral zone stations. This phenomenon was misinterpreted as an indication of the absence and also of switching off of the aurora and auroral substorms by the negative IMF B_z component. These observations suggested that $F(\theta)$ is finite even when $B_z > 0$ or $\theta < 90°$. Furthermore, it is reasonable to assume that $F(\theta)$ varies monotonically from 1.0 to 0 as the angle decreases from 180° to 0°, since the brightness of the aurora and the intensity of auroral substorms tend to become progressively weaker as the auroral oval contracts poleward. On the basis of these considerations, Perrault and Akasofu (1978) chose $F(\theta) = \sin^4(\theta/2)$. (In the original formulation, Perreault and Akasofu (1978) considered one of the simple cases in which the energy flux density is given by VB'^2 (erg s^{-1} cm^{-2}) where $B' = B(1 - \sin\theta')/2$ where θ' denotes the angle between the IMF vector and the equatorial plane, $\theta = \pi/2 - \theta'$; note that $(1 - \sin\theta')/2 = \sin^2\theta/2$ and $B'^2 = B^2 \sin^4\theta/2$.)

C. EFFECTIVE CROSS-SECTIONAL AREA

In order to equate the solar wind energy flux and U_T, one must find an 'effective cross-sectional area' l_0^2 of the magnetosphere where l_0 denotes the linear dimension of the cross-sectional area. As a first empirical step, Perreault and Akasofu (1978) assumed that l_0 is a constant and found that ε and U_T can roughly be equated by taking l_0 to be $7R_E$. Note that our simple empirical approach would fail if l_0 is a strong function of ρ, V, B, and θ, etc.

D. SUMMARY

In general, an empirical formulation should, by necessity, be as simple as possible. If such a simple formulation, based on a simple physical observation, would fail, one could do little in obtaining a reasonable first approximation expression for ε. This is particularly the case in our problem of the energy coupling between the solar wind and the magnetosphere, since one must deal with a large number of variable quantities which are not necessarily accurately known. In particular, our estimate of U_T is very crude.

Let us review here our physical observations:

(i) An approximate total energy consumption rate U_T of the magnetosphere can be monitored as a sum of U_R, U_J, and U_A, and these three quantities can be expressed as a function of the *Dst* and *AE* indices.

(ii) The solar energy flux density associated with magnetospheric disturbances has the form of VB^2 (erg s^{-1} cm^{-2}), not ρV^3 (erg s^{-1} cm^{-2}).

(iii) Effects of the IMF vector orientation may be expressed in the form $F(\theta)$ which varies from 1.0 to 0 as the angle θ varies from 180° to 0°, as the auroral observations suggest.

(iv) The effective cross-sectional area l_0^2 would not strongly depend on solar wind quantities, such as ρ, V, B, and θ, etc. The Chapman–Ferraro theory suggests that the distance between the Earth and the magnetopause is only a weak function of ρ and V.

In spite of such great uncertainties, it was a surprise to find that $\varepsilon(t)$ correlates well with $U_T(t)$. This was particularly the case because we would not be able to find ε in the form of (8), if the magnetosphere would be an unloading system, as had widely been discussed. Figure 3 is one of the examples which was obtained by Perreault and Akasofu (1978). One can see that $\varepsilon(t)$ follows $U_T(t)$ reasonably well over three orders of magnitude. This example and others examined by them establish firmly that the energy coupling function (8) is a reasonable first approximation. One can see, however, a serious discrepancy during the recovery phase. They found that this discrepancy arises from the fact that they adopted a single value of $\tau_R = 8$ hr. The discrepancy can be removed easily by assuming that τ_R is much less during the developing phase than during the recovery phase.

In the rest of this paper, we shall see that the solar wind energy input rate ε thus found on the basis of $U_T(t)$ can be considered to be, as a first approximation, the

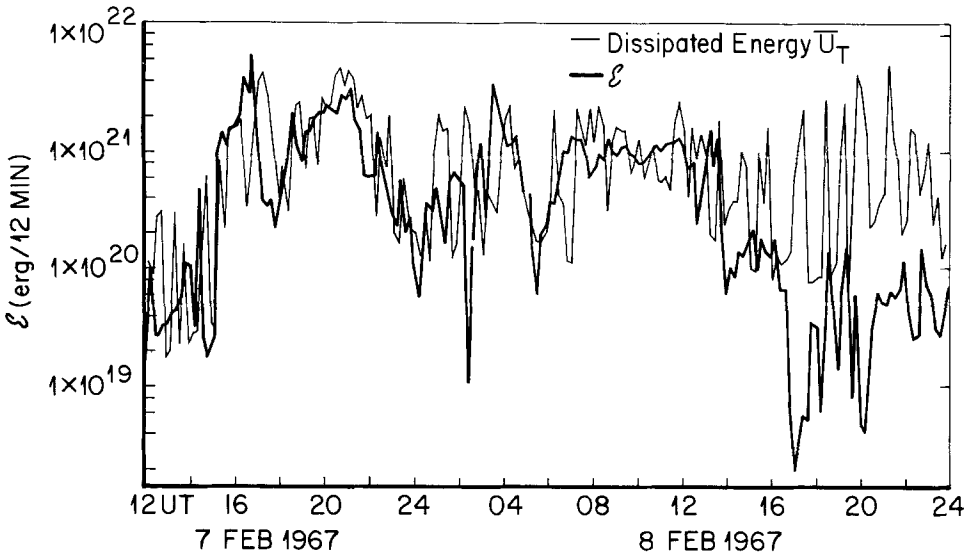

Fig. 3. The solar wind-magnetosphere energy coupling function ε (erg/12 min) and the total energy dissipation rate U_T of the magnetosphere for the February 7–8, 1967 storm.

'unknown' quantity which Akasofu and Chapman (1963) considered. We shall see that it controls the development of geomagnetic storms and replaces the proposed neutral component of the solar wind in Figure 2. In Section 7.2, we shall verify the expression (8) as the energy coupling function.

E. EXAMPLES

In this subsection, we examine ε for three fairly intense storms. All the figures used here have the same format. For each storm period, it shows, from the top, the kinetic energy flux $K = \rho V^3 l_0^2$ (assuming the same effective cross-sectional area for ε), the solar wind-magnetosphere energy coupling function ε, the total energy consumption rate U_T, the AE index and the Dst index. All the energy fluxes are given in units of 10^{18} erg s^{-1} and the two geomagnetic indices are given in units of γ. For each storm we show also ε, U_T, the ring current energy injection rate U_R and the combined energy injection rate $U_J + U_A = UJ = 3 \times AE(\gamma) \times 10^{15}$ erg s^{-1}. The solar wind quantities are taken from King (1977) and the two geomagnetic indices AE and Dst are produced by the WDC-A, NOAA, Boulder and the Goddard Space Flight Center, respectively. Note that all the quantities used in this paper are hourly average values.

We examine first the storm of March 31–April 3, 1973. The first two curves in Figure 4a show how the kinetic energy flux K and the energy coupling ε varied during the storm. As expected, K is far greater than ε and U_T. One can see that K and ε varied quite differently from the beginning of April 1, while the total energy consumption rate U_T followed fairly well changes of ε, but not of K, indicating that U_T is primarily controlled by ε. An intense main phase began to develop rapidly

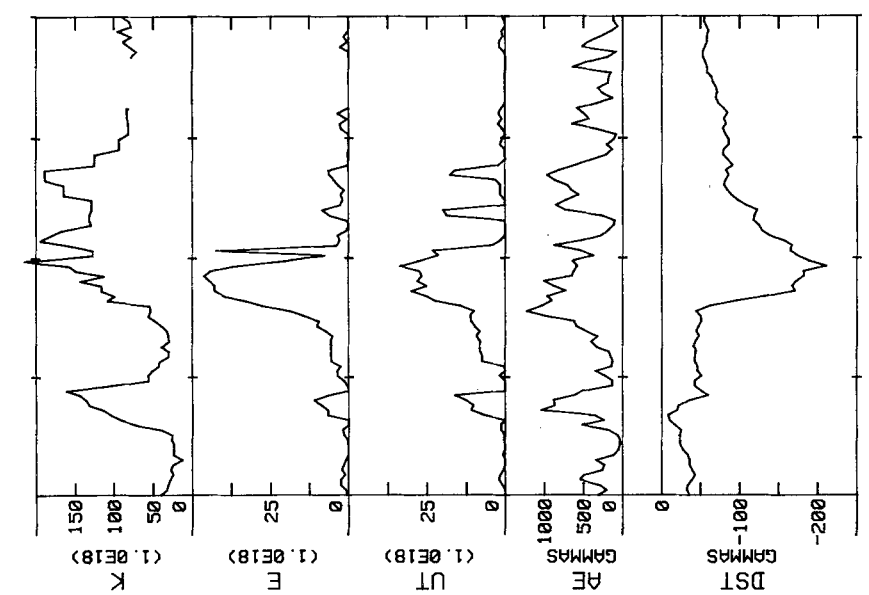

Fig. 4a. The kinetic energy flux K, the solar wind-magnetosphere energy coupling function ε, the total energy consumption rate U_T, the AE and Dst indices for the storm of March 31–April 3, 1973.

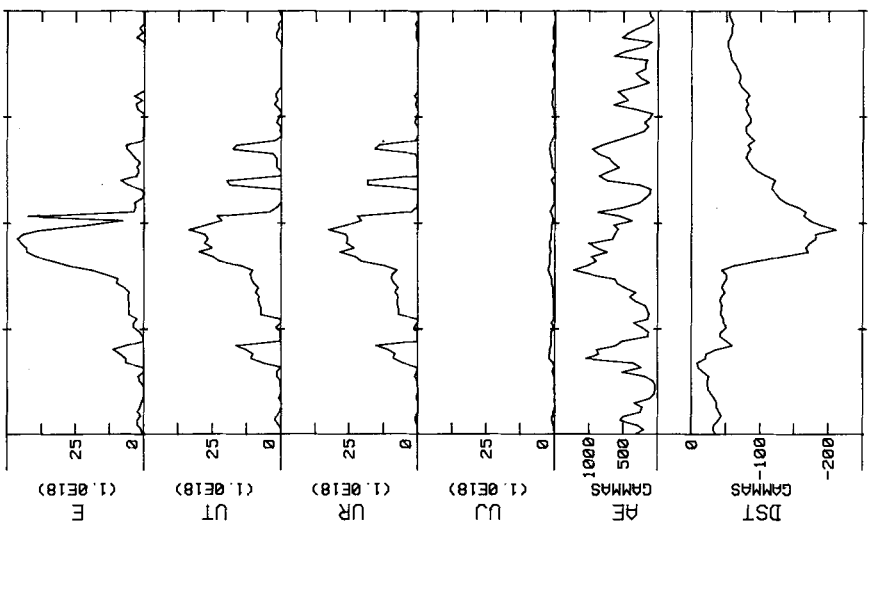

Fig. 4b. The solar wind-magnetosphere energy coupling function ε (denoted by E), the total energy consumption rate U_T, the ring current energy injection rate U_R, Joule heat production rate and the auroral particle injection rate $(U_J + U_A)$; the last quantity is denoted by UJ.

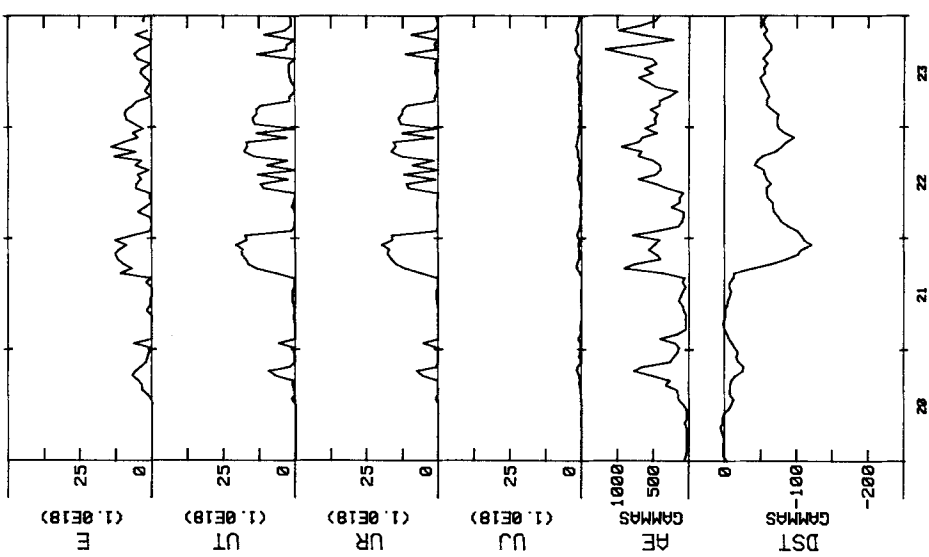

Fig. 5b. Same as Figure 4b, for the February 20–23, 1973 storm.

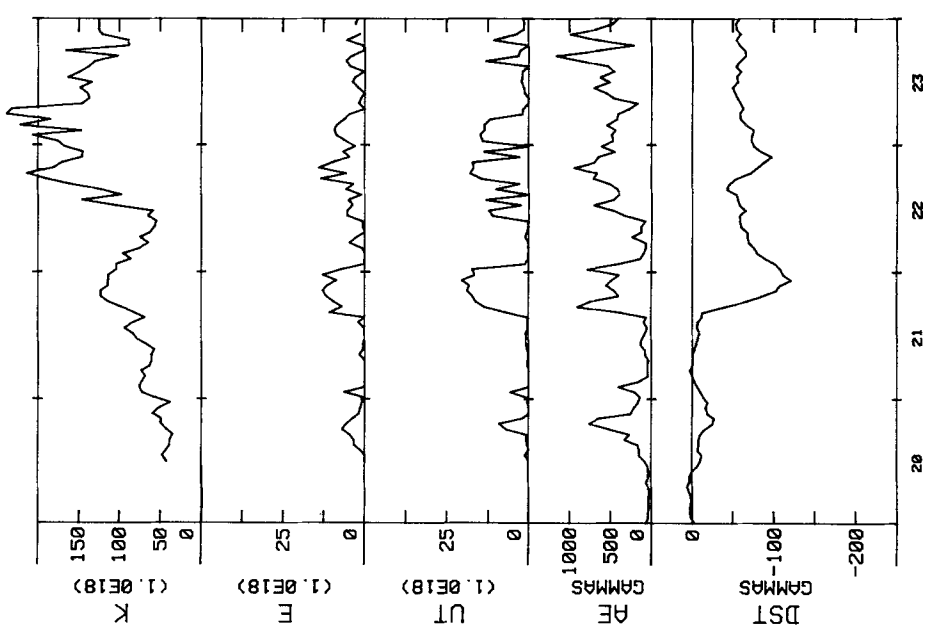

Fig. 5a. Same as Figure 4a, for the February 20–23, 1973 storm.

when ε reached a value of $\sim 10^{19}$ erg s^{-1}. This feature will be seen repeatedly in many of the examples we shall examine in this paper. However, note that when ε exceeded 2.5×10^{19} erg s^{-1}, U_T was significantly less than ε. Before speculating on causes of this discrepancy, it is important to improve the estimate U_T (Section 9.3). Figure 4b shows ε, U_T, U_R and $(U_J + U_A)$, as well as the *AE* and *Dst* indices. One can easily see that the main contribution to U_T comes from the ring current energy injection rate U_R. Furthermore, note that when ε exceeded $\sim 2.5 \times 10^{19}$ erg s^{-1}, the *AE* index and thus *UJ* indicated some decline. This interesting phenomenon is discussed by Akasofu (1981).

Figure 5a shows K, ε, U_T, *AE* and *Dst* for the storm of February 21–23, 1973. It is quite obvious that the total energy consumption rate of the magnetosphere is well controlled by ε, not by K. The main phase developed rapidly from 15 UT to 24 UT on February 21 when ε was greater than $\sim 10^{19}$ erg s^{-1}. When this increase of ε subsided, the main phase began to recover. A new increase of $\varepsilon \sim 10^{19}$ erg s^{-1} on February 22 caused a new development of the main phase. Figure 5b shows again that U_T arises mainly from U_R.

5. The Solar Wind-Magnetosphere Energy Coupling Function ε and the Variety of Development of Geomagnetic Storms

In this section, it will be demonstrated in detail that the variety of development of geomagnetic storms is primarily controlled by $\varepsilon(t)$. The format of the figures used in this section is the same as that in Section 4.

A. GEOMAGNETIC STORMS WITHOUT AN APPRECIABLE MAIN PHASE

A geomagnetic storm without an appreciable main phase belongs to the first and second types in Figure 2. This type of storm begins with a distinct ssc which indicates that there occurs a significant increase of the solar wind pressure. On the other hand, it fails to develop an appreciable main phase, indicating that the increased flow failed to deliver its energy to the magnetosphere or contained little amount of ε. The storm of February 13–14, 1973 belongs to such a type. The ssc was at 21 : 19 UT. Figure 6 shows that the ssc was indeed associated with a distinct increase of the kinetic energy flux which lasted for about 24 hr, while this solar wind flow contained only a very little amount of ε. One can easily appreciate the small values of ε for this particular storm by comparing them with those of the storms which were examined in Figures 4 and 5. At about 06 UT on February 14, there was a small increase of $\varepsilon \sim 4 \times 10^{18}$ erg s^{-1} which was associated with a weak substorm (indicated by an increase of the *AE* index) and a weak depression of the *Dst* index. Since K remained high at that time, this depression can reasonably be attributed to the growth of a weak ring current. Note the simultaneous increase of the total energy consumption rate $U_T(t)$, but it was also very small. After the increase of K almost subsided (at about 06 UT on February 14), there occurred a small increase of ε which caused a

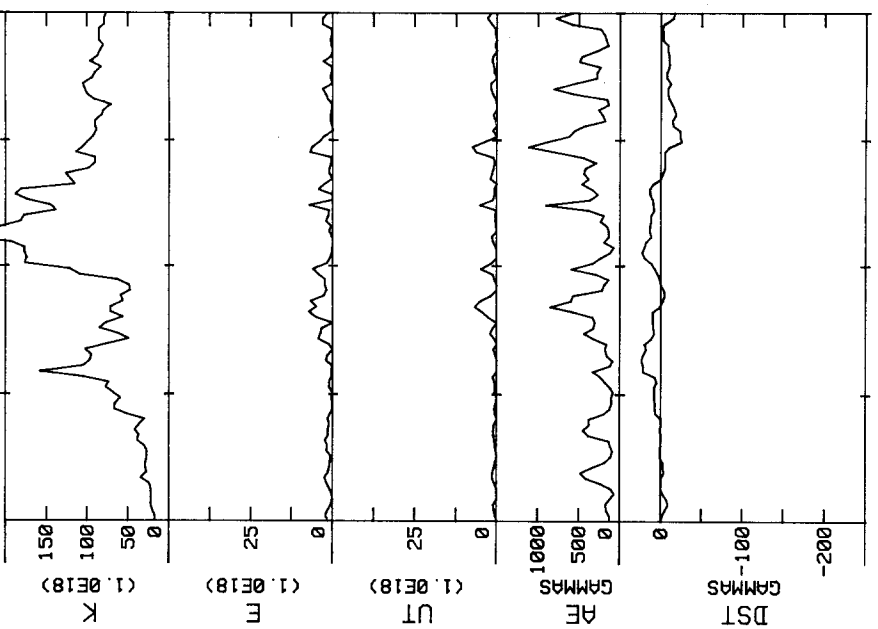

Fig. 7. Same as Figure 4a, for the May 29–June 1, 1974 storm.

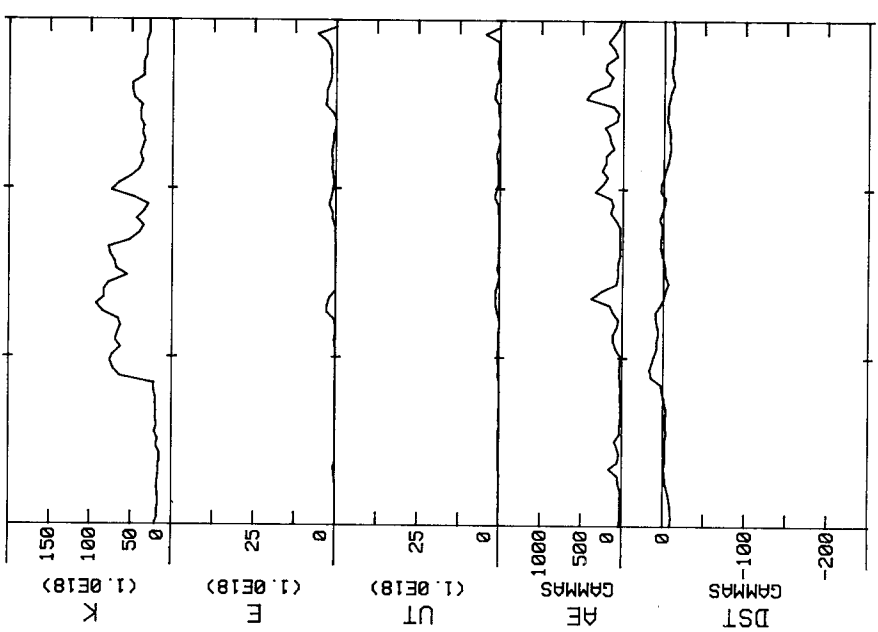

Fig. 6. Same as Figure 4a, for the February 13–15, 1973 storm.

very weak depression of the *Dst* index, indicating the development of a very weak ring current.

The storm of May 29–June 1, 1974 also belongs to this category (Figure 7). It was associated with a double increase of the kinetic energy flux K. In fact, the increase of K at about 06 UT on May 31 was one of the largest increases in the examples examined in this paper. However, this intense solar wind flow contained only a very small amount of ε ($<10^{19}$ erg s^{-1}). Note that a number of minor increases of ε throughout the strong solar wind flow caused magnetospheric substorms, as indicated by the corresponding increases of U_T and AE.

B. GEOMAGNETIC STORMS WITH A LONG INITIAL PHASE

A geomagnetic storm with a long initial phase belongs to the third type in Figure 2. The geomagnetic storm of January 18–21, 1973 belongs to this type (Figure 8). The ssc was at 00:00 UT on January 18, which was caused by a large increase of K (although it was not registered as an ssc because of a slow rise of the H component). However, the main phase did not begin until after 15 UT on January 19, about 15 hr later; there occurred a new increase of K at 15:44 UT, causing an ssc. One can see easily that this long delay of the main phase onset was due to the fact that this particular solar wind flow contained little ε until about 12 UT on January 19. Note that there is no correlation between K and ε, while the correlation between ε and U_T is high. One can also see that the details of the development and decay of the main phase are also well correlated with an increase and decrease of ε. Note that the largest depression of the *Dst* index occurred well after the subsidence of the large increase of K, namely near the end of January 20, as a result of a weak, but prolonged increase of ε.

C. MINI-STORMS

Mini-storms are often associated with a very large K, but only a weak main phase ($|Dst| < 100\gamma$). This type of storm is not included in Figure 2. The storm of March 6–7, 1972 belongs to this type (Figure 9). The storm was associated with a very large ssc at 21:08 UT on March 6 which was caused by an intense impact of a strong solar wind flow; see a large increase of K at that time. However, in spite of such a large K, the magnitude of the main phase was not more than 100γ. This was due to the fact that this solar wind flow contained relatively small amounts of ε. As a result, U_T was also very small. There were two impulsive increases of ε which caused a double main phase. Note that U_T was well correlated with ε, indicating that the total energy consumption rate is well controlled by ε.

Two other examples of mini-storms are shown in Figures 10 and 11. The storm of March 6–7, 1973 was also caused by an intense impact of the solar wind flow which caused a large ssc at 00:11 UT on March 5. However, the main phase was even weaker than that of the March 6–7, 1972 storm (Figure 9) and consisted mainly of two short-duration pulses. One can see that U_T was almost identical to ε in this particular example, resulting in a double storm. The storm of March 16–17, 1974

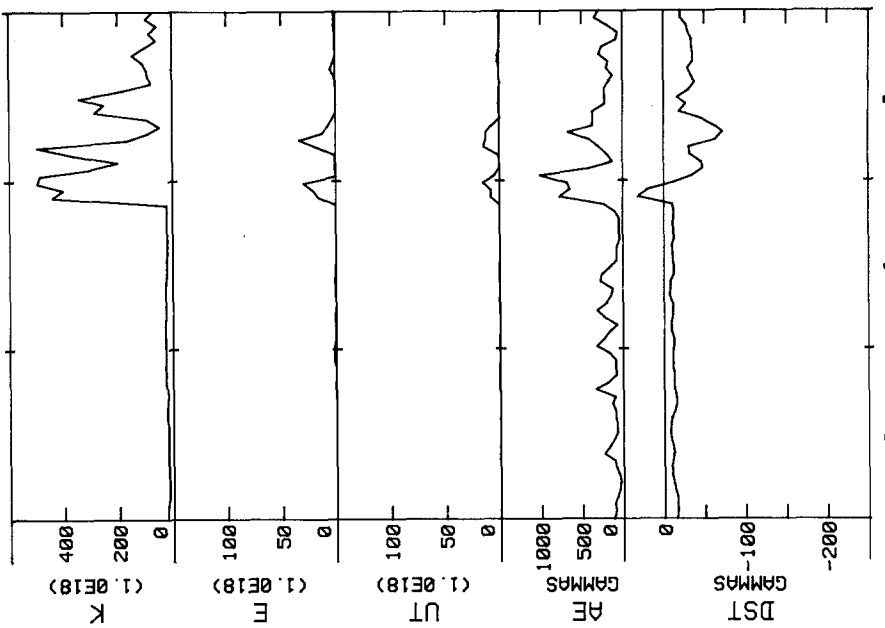

Fig. 9. Same as Figure 4a, for the March 5–7, 1972 storm.

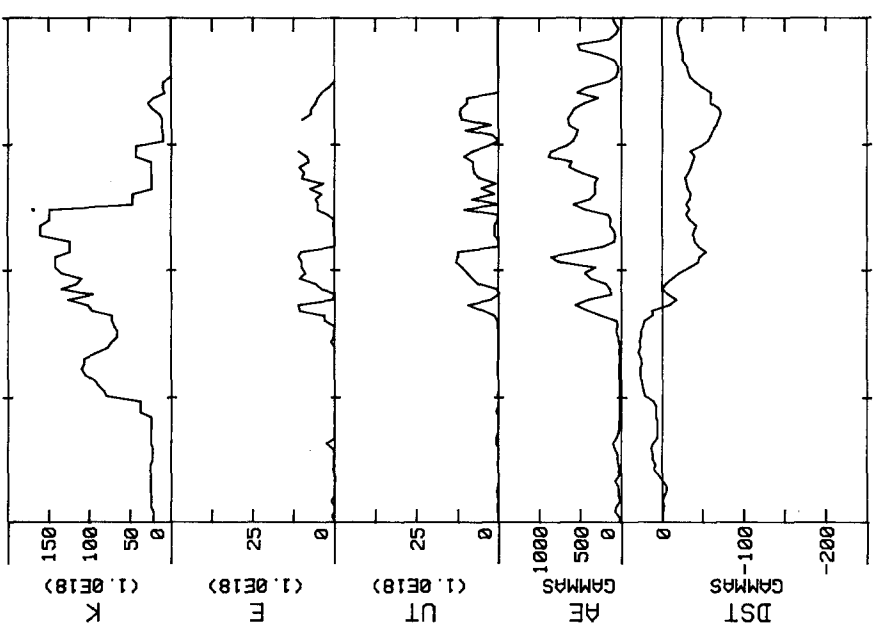

Fig. 8. Same as Figure 4a, for the January 12–21, 1973 storm.

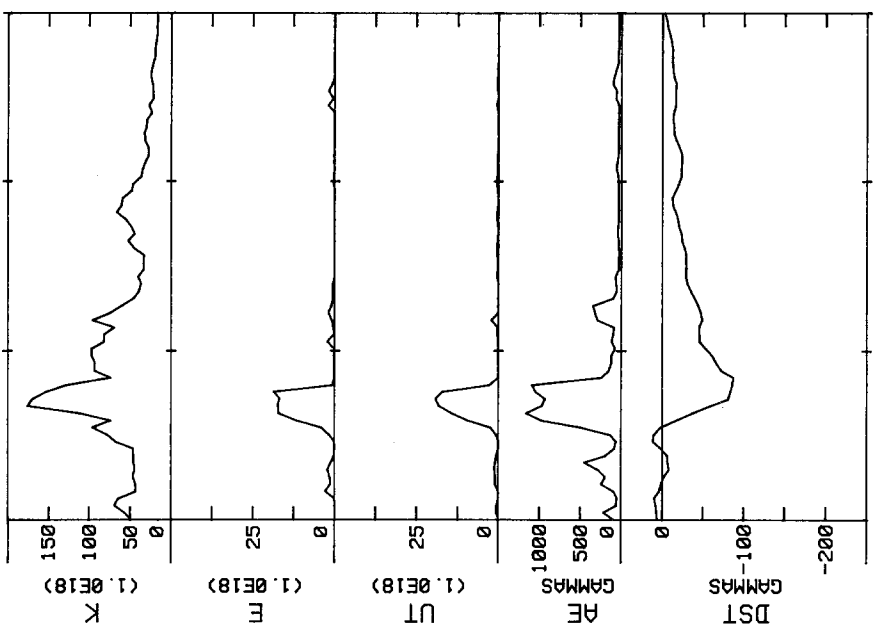

Fig. 11. Same as Figure 4a, for the March 16–18, 1974 storm.

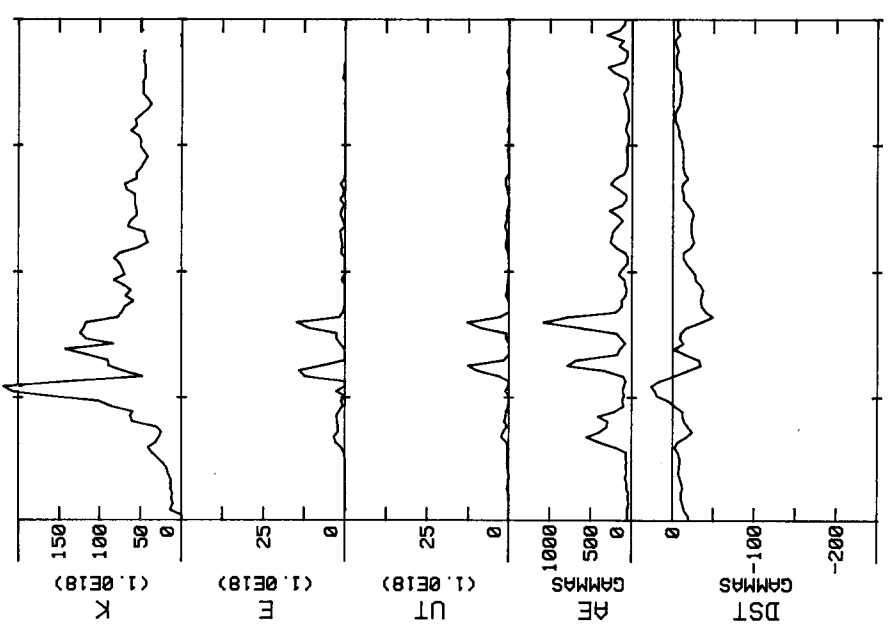

Fig. 10. Same as Figure 4a, for the March 5–8, 1973 storm.

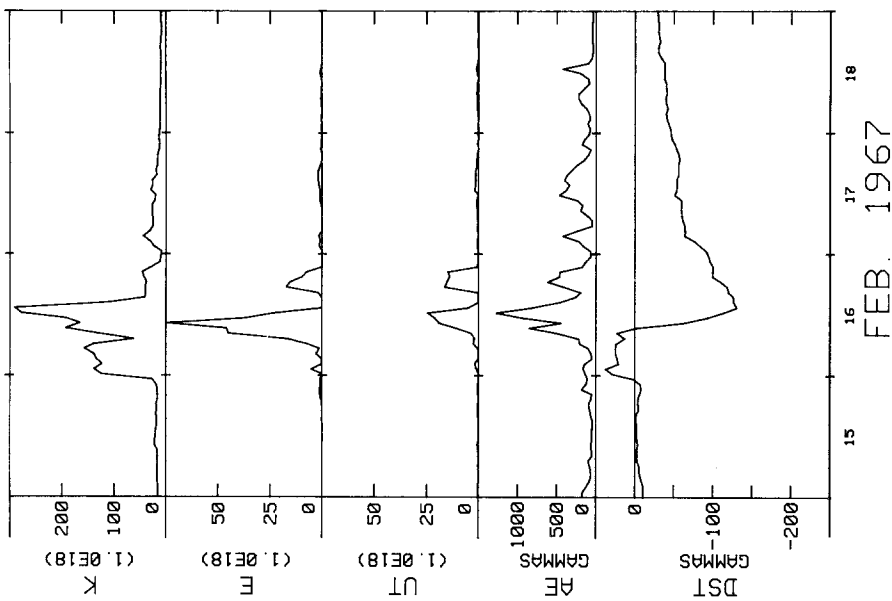

Fig. 13. Same as Figure 4a, for the February 15–18, 1967 storm.

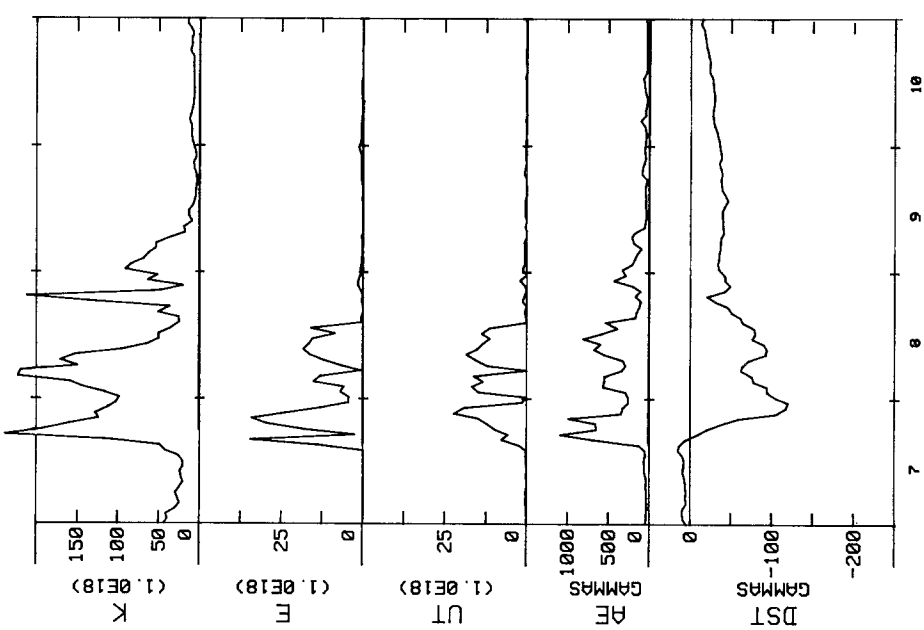

Fig. 12. Same as Figure 4a, for the February 7–10, 1967 storm.

is another example of mini-storms. Again, note that the total energy consumption rate U_T was well controlled by ε. In this particular storm, ε consisted of a single increase of about 2×10^{19} erg s^{-1}, lasting for about 6 hr. The total energy consumption rate U_T had a similar time variation, resulting in a weak main phase.

The failure of the development of an intense main phase of more than $|Dst| > 100\gamma$ by a large kinetic energy flux indicates that it is not possible to predict the intensity of geomagnetic storms in terms of the intensity of solar wind flows and thus perhaps in terms of the intensity of solar flares and of high speed streams. It is crucial to infer the amount of ε in the flow in predicting accurately the intensity and time development of geomagnetic storms.

D. INTENSE STORMS

The storm of February 7–9, 1967 is a typical intense storm (Figure 12). Its main phase began soon after the impact of an intense solar wind flow. This is understandable as ε sharply increased at the time of ssc. The total energy consumption rate U_T is fairly well correlated with ε, except for the first large pulse. This failure of the correlation may partly be due to the fact that the correction of the solar wind pressure effect on the *Dst* index was not sufficient. One can also see little correlation between K and ε. It is interesting to compare such an intense storm with a mini-storm. The first increase of K for the storm of March 6–7, 1973 (Figure 10) was comparable to that of the storm under study here. However, the amount of ε contained in the two flows was considerably different for the two storms, resulting in a large difference of the magnitude of the main phase.

The storm of February 16–17, 1967 was also a typical storm which was caused by an intense solar wind flow associated with a solar flare (Figure 13). This storm had a typical initial phase which was followed by a sudden growth of the main phase. The kinetic energy flux K had a two-step increase during the storm. The first increase contained only a very small amount of ε. This resulted in the long compression period without the development of an intense main phase. On the other hand, the second increase of K was associated with a very large amount of ε. It is due to this increase of ε by which the main phase was produced. However, ε declined rather sharply after reaching a peak value of about 7.5×10^{19} erg s^{-1}, which was followed by another smaller increase. The total energy consumption U_T had also two peaks. However, the first peak was appreciably smaller than what one expects from ε.

The storm of March 8–9, 1970 is also a typical example of intense storms which are caused by an impact of intense solar wind flow (Figure 14). The initial phase was very brief. This was because of a large increase of ε at the time of the impact. This initial increase of ε did not last long and was followed by an increase of a larger magnitude. This is well reflected in the growth of the main phase. It began to grow a little, but recovered rather quickly. The large main phase began as a result of the second increase of ε. The total energy consumption rate U_T had also a double peak. However, the second increase was significantly less than what we expect from ε. The

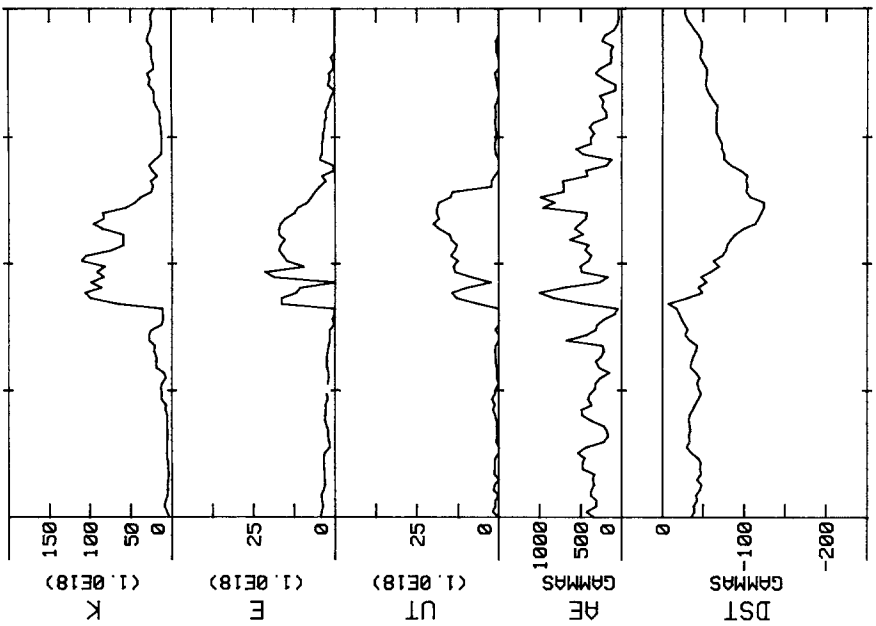

Fig. 15. Same as Figure 4a, for the February 9–12, 1968 storm.

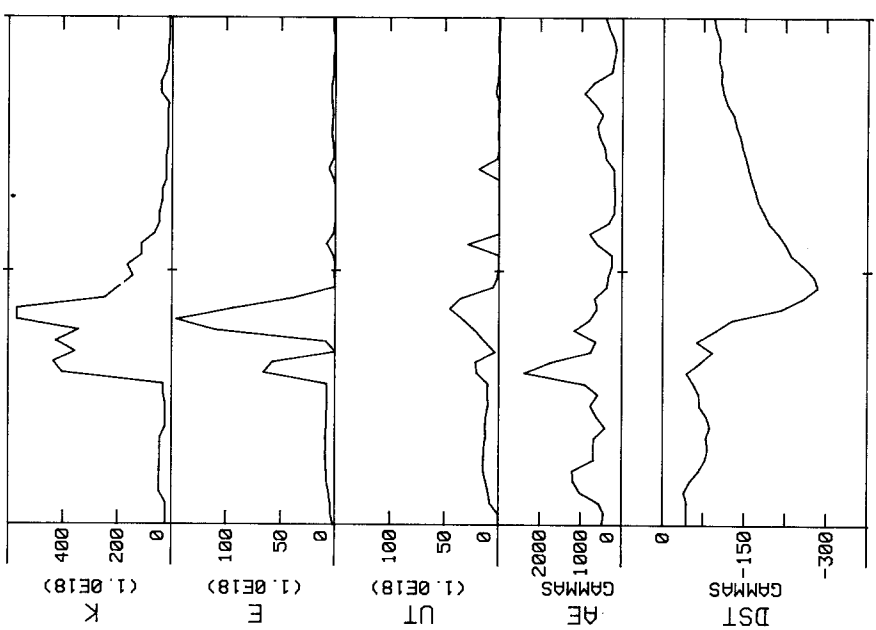

Fig. 14. Same as Figure 4a, for the March 8–9, 1970 storm.

storm of February 10–12, 1968 was also a typical intense storm (Figure 15). In this particular storm, K and ε had similar time variations. However, it is clear that U_T correlated better with ε than K, and ε and U_T had a comparable magnitude.

E. STORMS WITH A WEAK, BUT LONG-LASTING MAIN PHASE

The storm of September 27–30, 1967 is a typical storm with a weak, but long-lasting main phase (Figure 16a). Such a type is not included in Figure 2, but is fairly common. One can easily see that such a storm was caused by a succession of small impulsive changes of ε. Variations of U_T during the storm were similar to those of ε. The storm of March 18–21, 1973 was similar to the previous example in many ways (Figure 16b).

F. STORMS WITHOUT THE STORM SUDDEN COMMENCEMENT

The double storm of March 26–28, 1972 is an example of storms which began without the storm sudden commencement (Figure 17a). It belongs to the last type in Figure 2. It is quite obvious that the development of the storm was well controlled by ε, not by K at all. Time variations of K and ε were entirely different. On the other hand, ε and U_T correlate well. The storm of December 30, 1967–January 3, 1968 was another example of a double geomagnetic storm which began without the ssc (Figure 17b). There was no obvious correlation between K and U_T.

6. Solar Current Disk and Geomagnetic Storms

In this section, we examine the solar wind speed, V, and the IMF magnitude B, the IMF angles Ⓗ, ϕ, the energy coupling function ε, and two geomagnetic indices AE and Dst during a number of 27-day periods, rather than during selected major geomagnetic storm periods. In this way, one can recognize clearly which of the above solar wind quantities differ significantly during major geomagnetic storms from those during the rest of the period and which quantities contribute most to the energy coupling function ε; note that θ in Equation (8) is related to Ⓗ by $\theta \simeq 90° - Ⓗ$ (cf. Akasofu, 1979c).

In this particular study, it is important to know a large-scale magnetic field structure in interplanetary space. Schulz (1973), Saito (1975), Svalgaard and Wilcox (1976), and Smith *et al.* (1978) suggested that the Sun has a very extensive current disk. Figure 18 shows schematically the geometry of the solar current disk (Saito, 1975). Note that the current disk is warped. As a result, as the Sun rotates every 27 days, the Earth will be located above the current disk for a certain period(s) and below during the rest of the period. In this section, we shall see that intense geomagnetic storms are often associated with the passage of the solar current disk near the Earth. We interpret a sudden change of the IMF azimuth angle ϕ from $\sim 135°$ to $\sim 315°$ or from $\sim 315°$ to $\sim 135°$ as the passage of the solar current disk at the location of the Earth, or its large-scale upward or downward motion, instead of the so-called 'sector boundary crossing' (Wilcox and Ness, 1965). The direction of

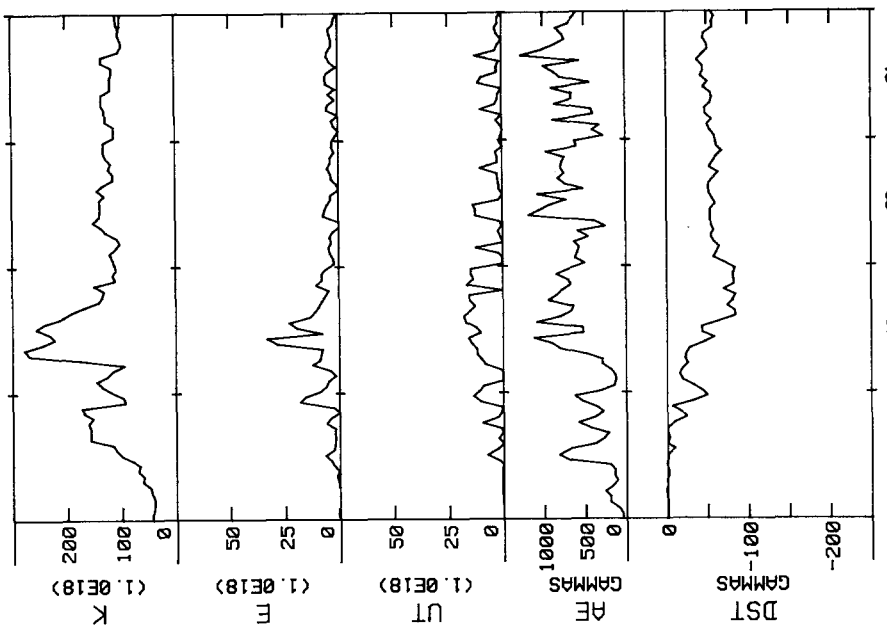

Fig. 16b. Same as Figure 4a, for the March 18–21, 1973 storm.

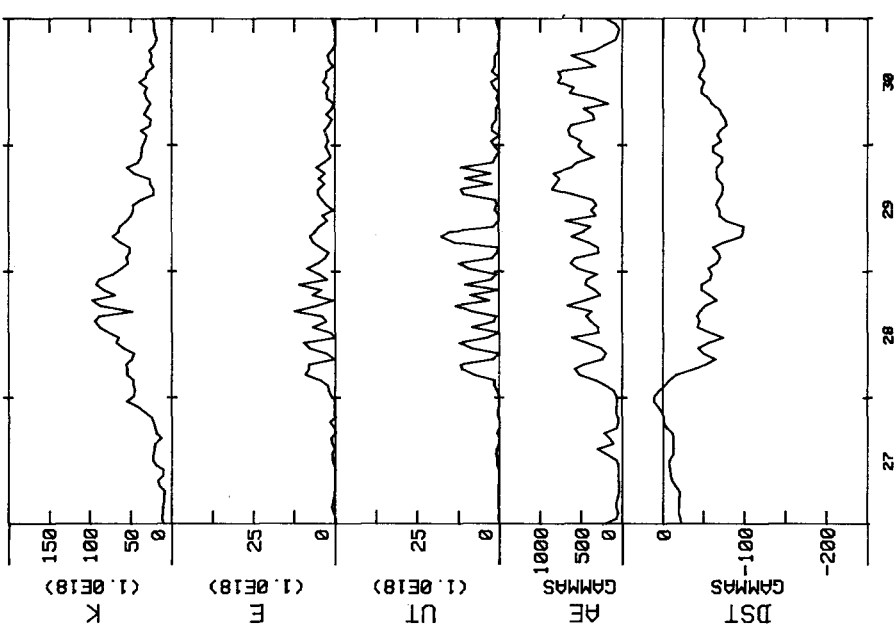

Fig. 16a. Same as Figure 4a, for the September 27–30, 1967 storm.

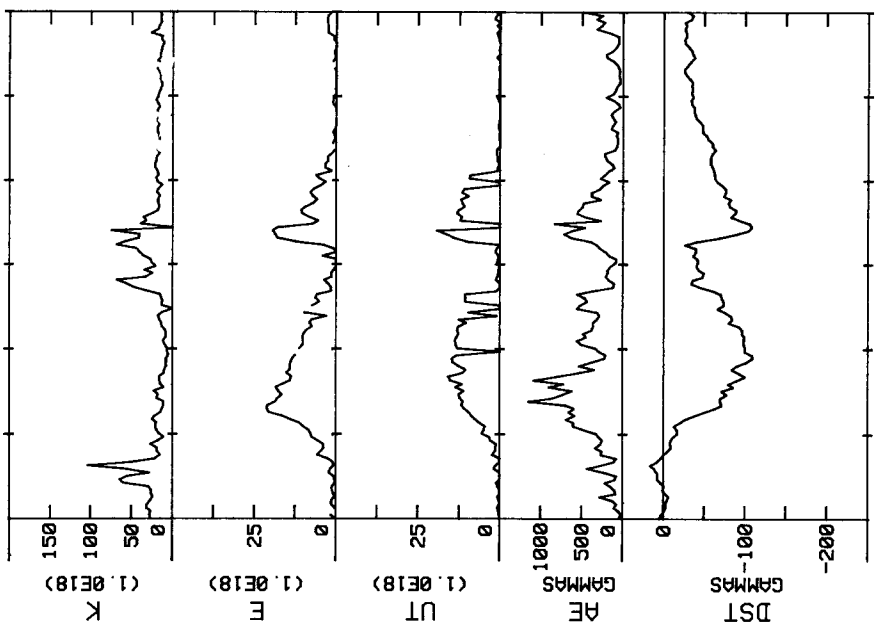

Fig. 17b. Same as Figure 4a, for the December 30, 1967–January 4, 1968 storm.

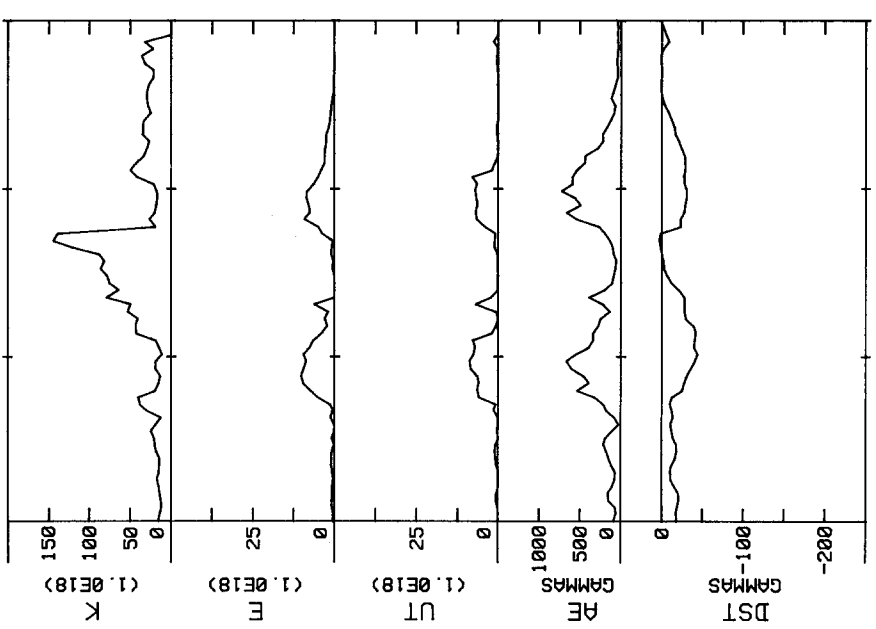

Fig. 17a. Same as Figure 4a, for the March 26–28, 1972 storm.

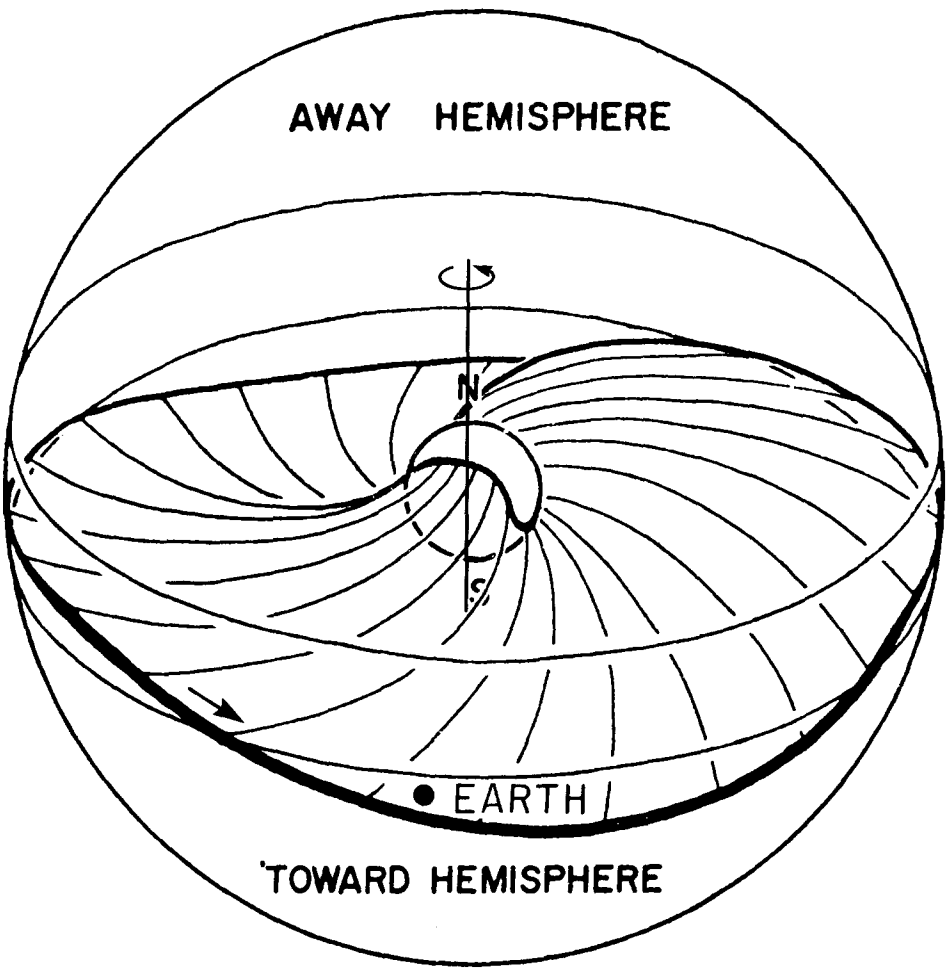

Fig. 18. Schematic illustration of the solar current disk (Saito, 1975).

the up-down motions must be determined by considering the polarity of the solar magnetic field. In 1967–1970, the dipole moment of the solar field was pointing southward. Thus, the Earth was above the current disk when $\phi \sim 315°$, and below when $\phi \sim 135°$. After the change of the polarity in 1970, the Earth was above the current disk when $\phi \sim 135°$ and below when $\phi \sim 315°$.

6.1. Passages of the Solar Current Disk Associated with the Solar Rotation

Figure 19a shows the solar wind speed V, the IMF magnitude B, IMF angles Ⓗ, ϕ and two geomagnetic indices AE and Dst for a 27-day period between July 17 and August 12, 1974. It shows two medium intensity storms. Both are associated with a sudden change of ϕ either from $\sim 315°$ to $\sim 135°$ or from 135° to 315°; the general

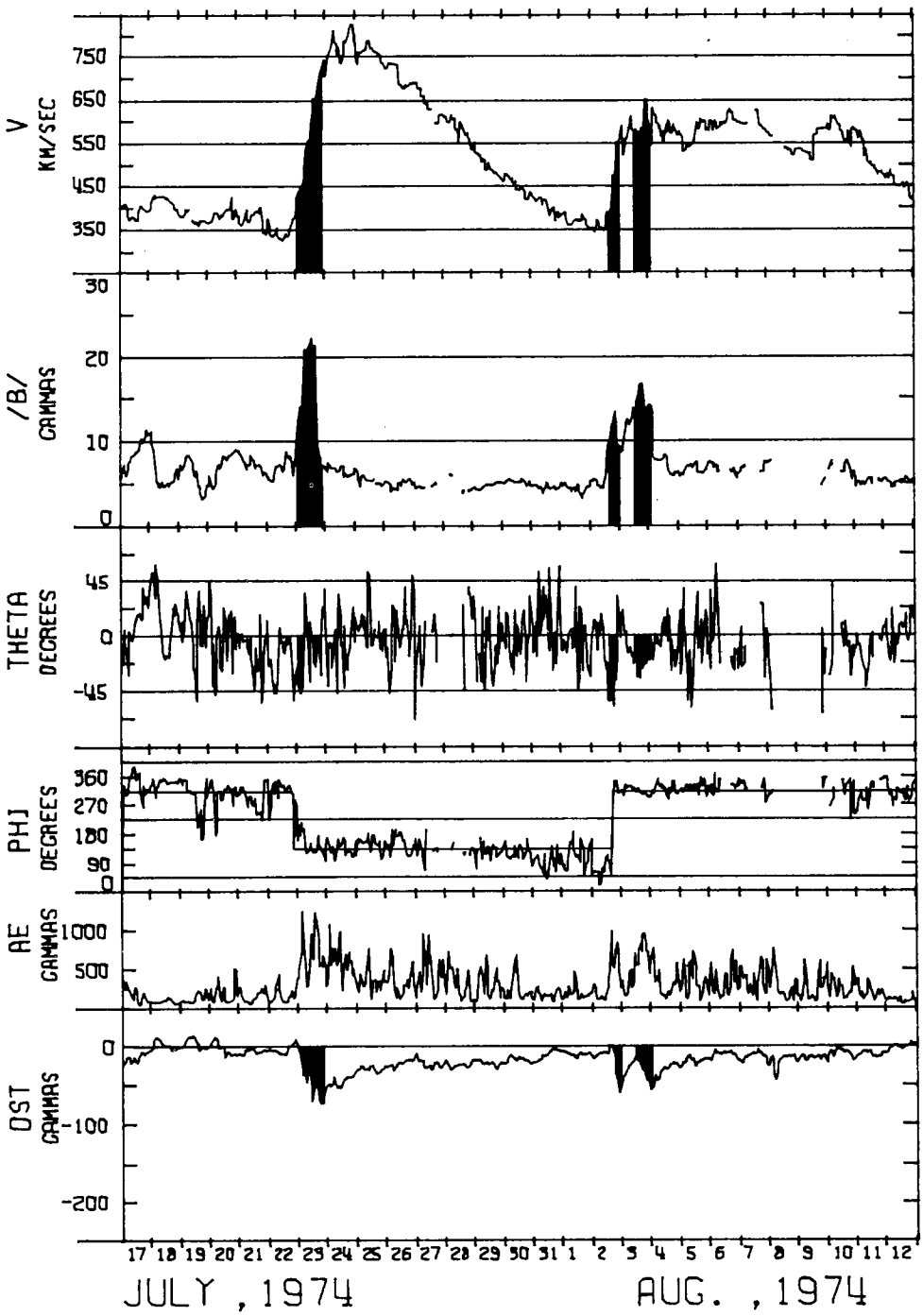

Fig. 19a. The solar wind speed V, the IMF magnitude B, IMF angles Theta (H) and Phi (ϕ) and two geomagnetic indices AE and Dst for the period between July 17 and August 12, 1974. Changes of ϕ are roughly indicated by straight lines. Periods of $\partial|Dst|/\partial t < 0$ are also indicated.

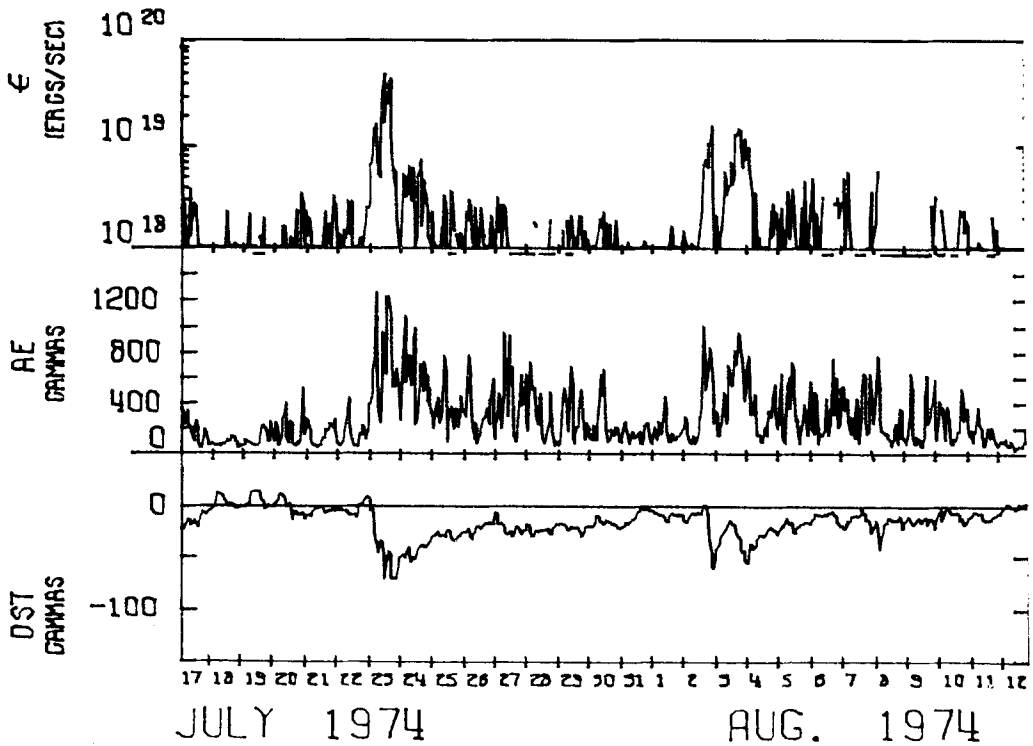

Fig. 19b. The solar wind-magnetosphere energy coupling function ε, and two geomagnetic indices, *AE* and *Dst* for the period corresponding to Figure 19a. Note that the periods of lacking data in computing ε are indicated by horizontal lines at the bottom.

trend of ϕ changes is indicated by straight lines. The Earth had been below ($\phi \sim 315°$) the current disk until July 22. The warped current disk passed on that day, placing the Earth above ($\phi \sim 135°$) it until August 2. Prolonged geomagnetic activity associated with the so-called 'sector boundary crossing' which we interpret here as the passage of the current disk, was studied first by Wilcox and Ness (1965).

As we learned in Section 5, a large input of solar wind energy into the magnetosphere occurs particularly when the main phase is growing, namely when $\partial|Dst|/\partial t < 0$. Thus throughout this section, we concentrate our effort mainly in examining V, B, and Ⓗ during the period when $\partial|Dst|/\partial t < 0$ and $|Dst| \geqslant 100\gamma$. Those periods are shaded in the *Dst*, V and B diagrams. Figure 19b shows the energy coupling function ε, the *AE* and *Dst* indices during the same period.

Note that there is a reasonable correlation between $\varepsilon > 10^{18}$ erg s^{-1} and the *AE* index. Here, we examine specifically the development of the two medium intensity geomagnetic storms on July 22–23, 1974 and August 3 and 4–5, 1974; note that the latter was a double storm. The development of the main phase of the three moderate storms occurred during three impulsive increases of $\varepsilon > 10^{19}$ erg s^{-1}. Let us now study in detail, by examining Figures 19a and 19b, how the solar wind speed, the IMF B and Ⓗ varied during these periods. During the first storm (July 22–23), the solar

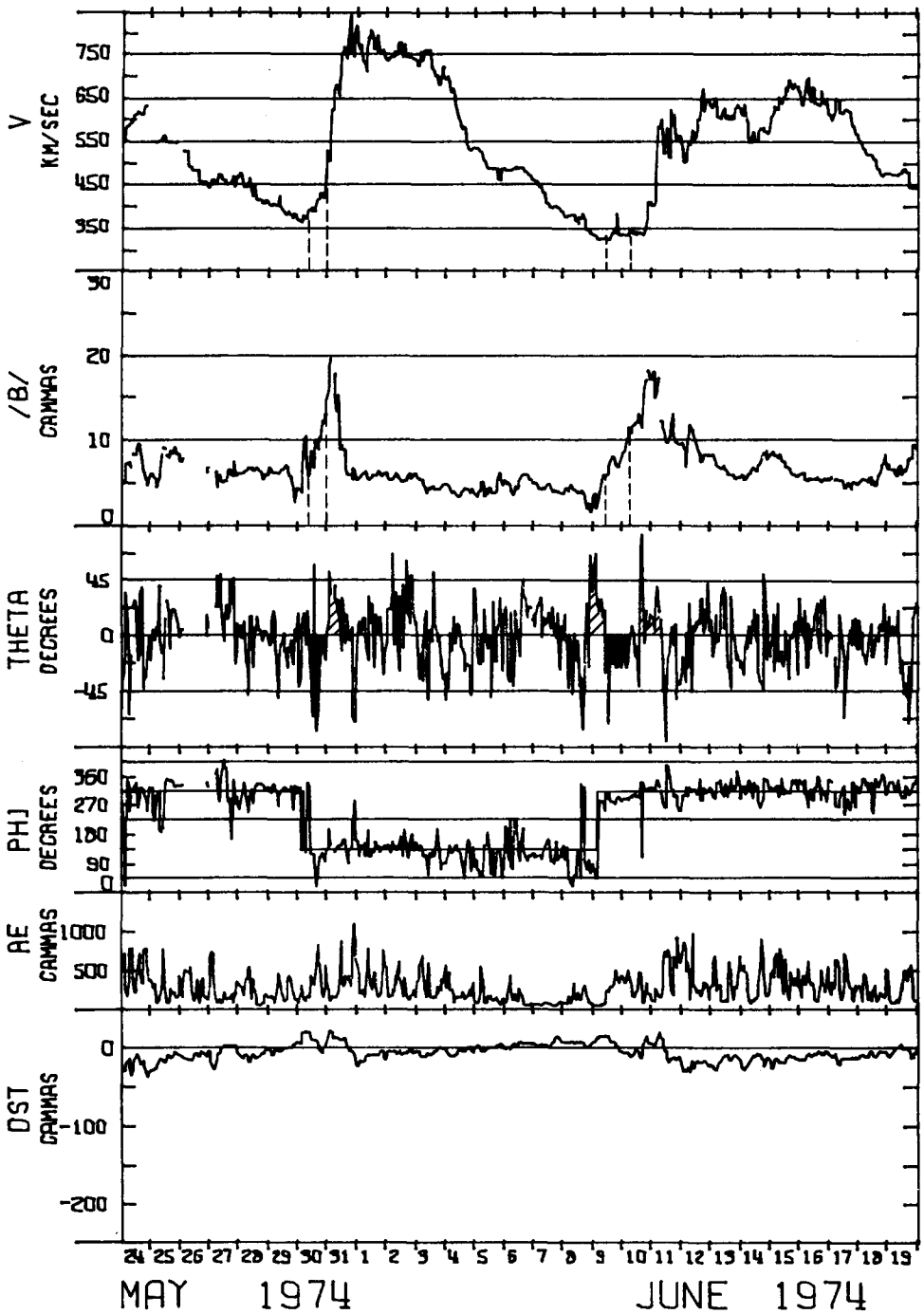

Fig. 20a. Same as Figure 19a, for the period between May 24–June 19, 1974. Note that some of large Ⓗ > 0 are hatched.

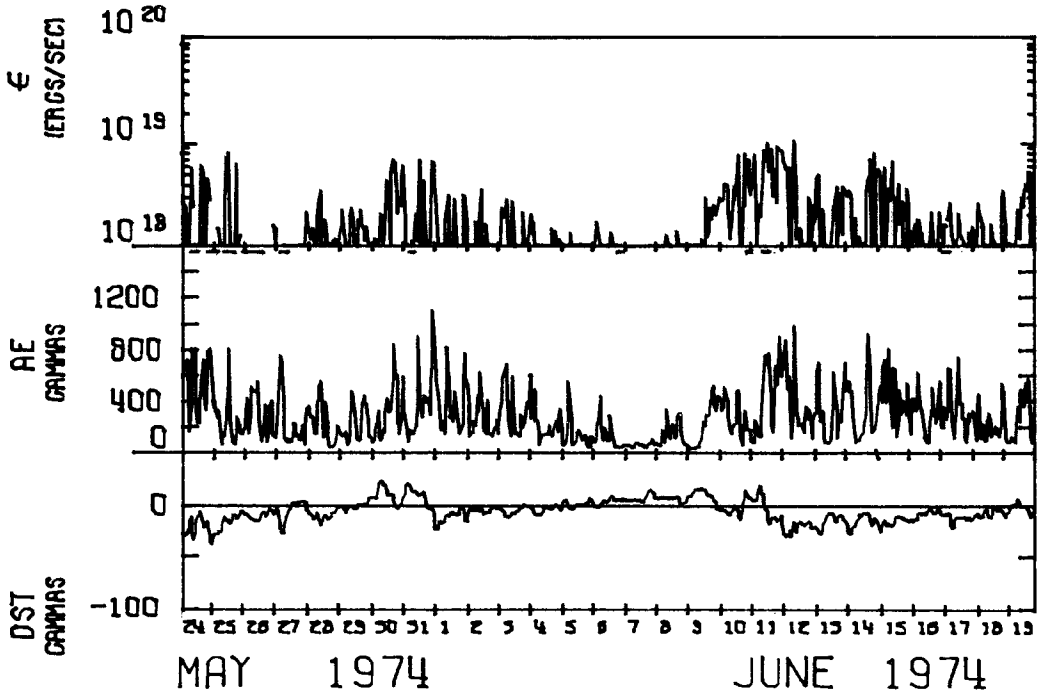

Fig. 20b. Same as Figure 19b, for the period corresponding to Figure 20a.

wind speed was rapidly increasing, while B had an impulsive increase just during the largest energy input. Negative variations of Ⓗ during the corresponding periods are also shaded. It is quite clear that a large B was a very important ingredient in causing the first storm. The degree of importance of the solar wind speed V is less than that of B, since the largest energy input ended even before V reached the maximum value. The contribution of V is overwhelmed by changes of B and Ⓗ. However, it should be noted that V was rapidly increasing when B had an impulsive increase. Similar statements can be made for the second storm. The degree of importance of Ⓗ will be discussed in association with later examples.

In Figure 20a we examine a situation similar to that in Figure 19 in terms of the passage of the current disk, but a major geomagnetic storm failed to develop on May 30–31 and June 8–10, in spite of the occurrence of large negative values of Ⓗ. This failure can be associated with the fact that B was less than 10γ when Ⓗ had a large negative value ($\sim -30°$ or less). The solar wind speed was also very low. A large increase of both B and V occurred only *after* large changes of Ⓗ. As a result, ε did not exceed 10^{19} erg s^{-1} during the entire 27-day period (Figure 20b). As we shall see in later examples, it is important to note that the passage of the current disk is often associated with a large positive-negative or negative-positive change of Ⓗ; periods of positive values are hatched in Figure 20a. Note also that there is a reasonable correlation between $\varepsilon > 10^{18}$ erg s^{-1} and the AE index.

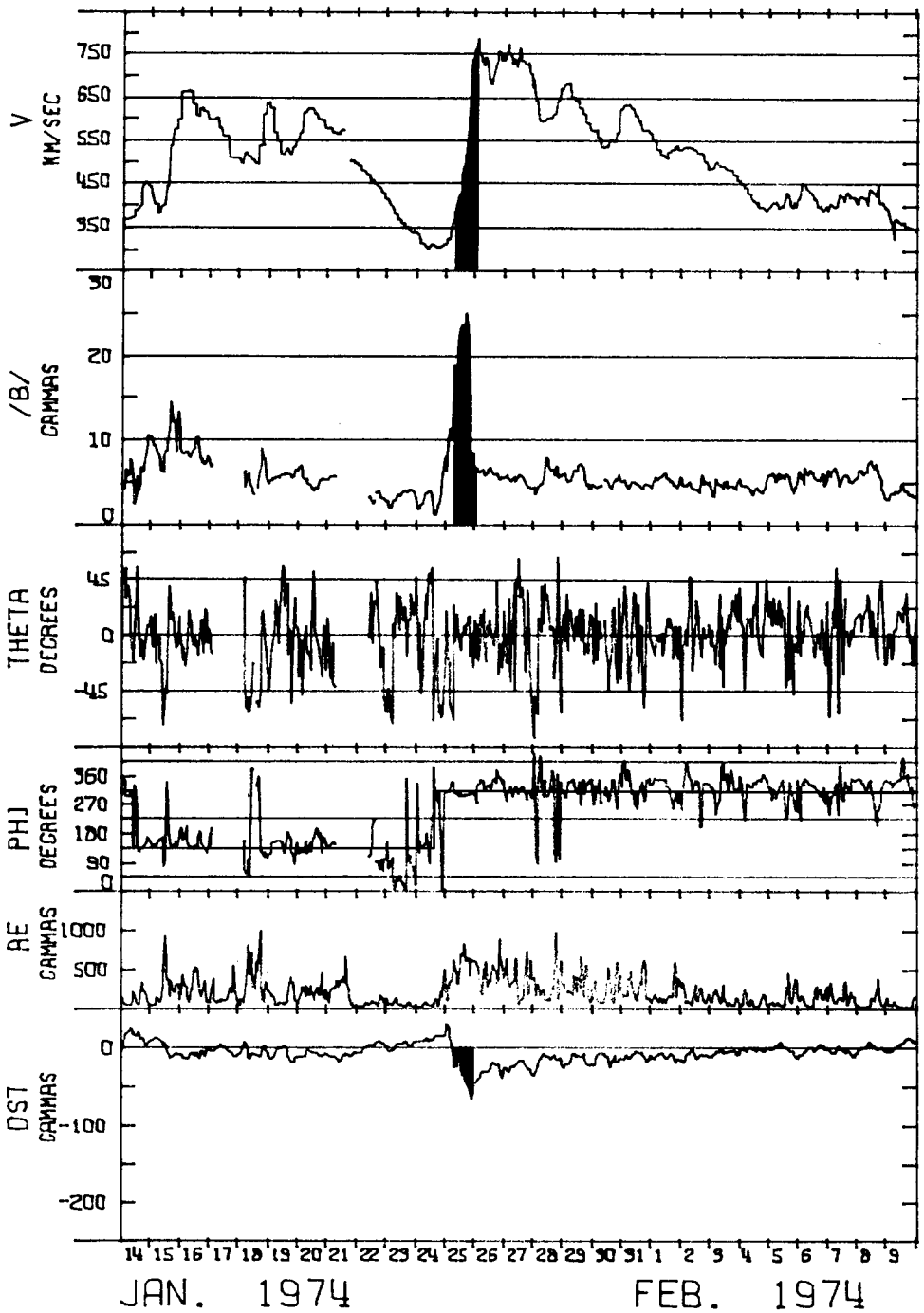

Fig. 21a. Same as Figure 19a, for the period between January 14 and February 9, 1974.

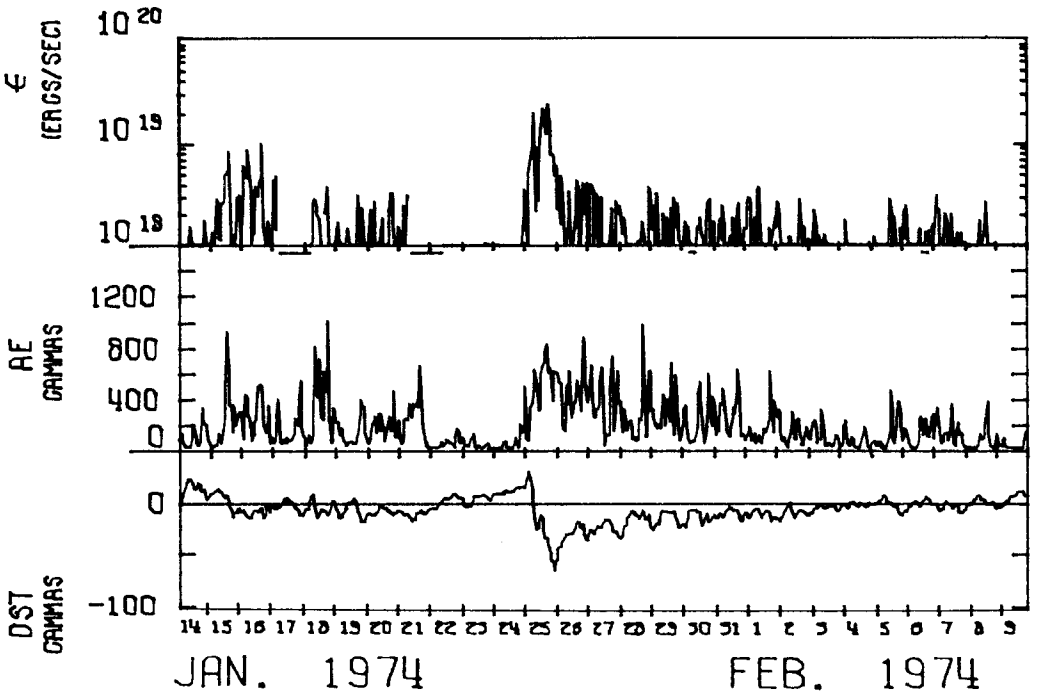

Fig. 21b. Same as Figure 19b, for the period corresponding to Figure 21a.

Figure 21a shows an interesting example of the passage of the current disk (January 24–25, 1974). A medium intensity main phase developed rapidly on January 25, and the corresponding period is shaded in both the solar wind speed V and the IMF B data, while only negative changes of Ⓗ are shaded for the same period. This example is very similar to the first storm in Figure 19a. The overwhelming importance of B for the development of the main phase is quite obvious; a large value of $B > 20\gamma$ overcame even the fact that Ⓗ > 0. In Figure 21b the development period coincides with a large increase of $\varepsilon \geq 10^{19}$ erg s^{-1}. The solar wind speed V was rapidly increasing during the impulsive increase of B.

6.2. Transient passages

So far, we have dealt with the passage of the warped solar current disk associated with the 27-day solar rotation. In this section, we examine transient passages and the associated storms, in addition to the 27-day solar rotation. A series of storms between July 4–7, 1974 was associated with a complicated series of changes of ϕ, superposed on the passage associated with the 27-day rotation (Figure 22a). It is of great interest to examine why the magnitude of the three successive storms was so different. In Figure 22b, one can see clearly that ε increased in three steps; note that ε is plotted with a logarithmic scale, so that there is a considerable difference in ε for the three increases, namely approximately one order of magnitude between the first and the third storm. The first storm was weak because both B and V were

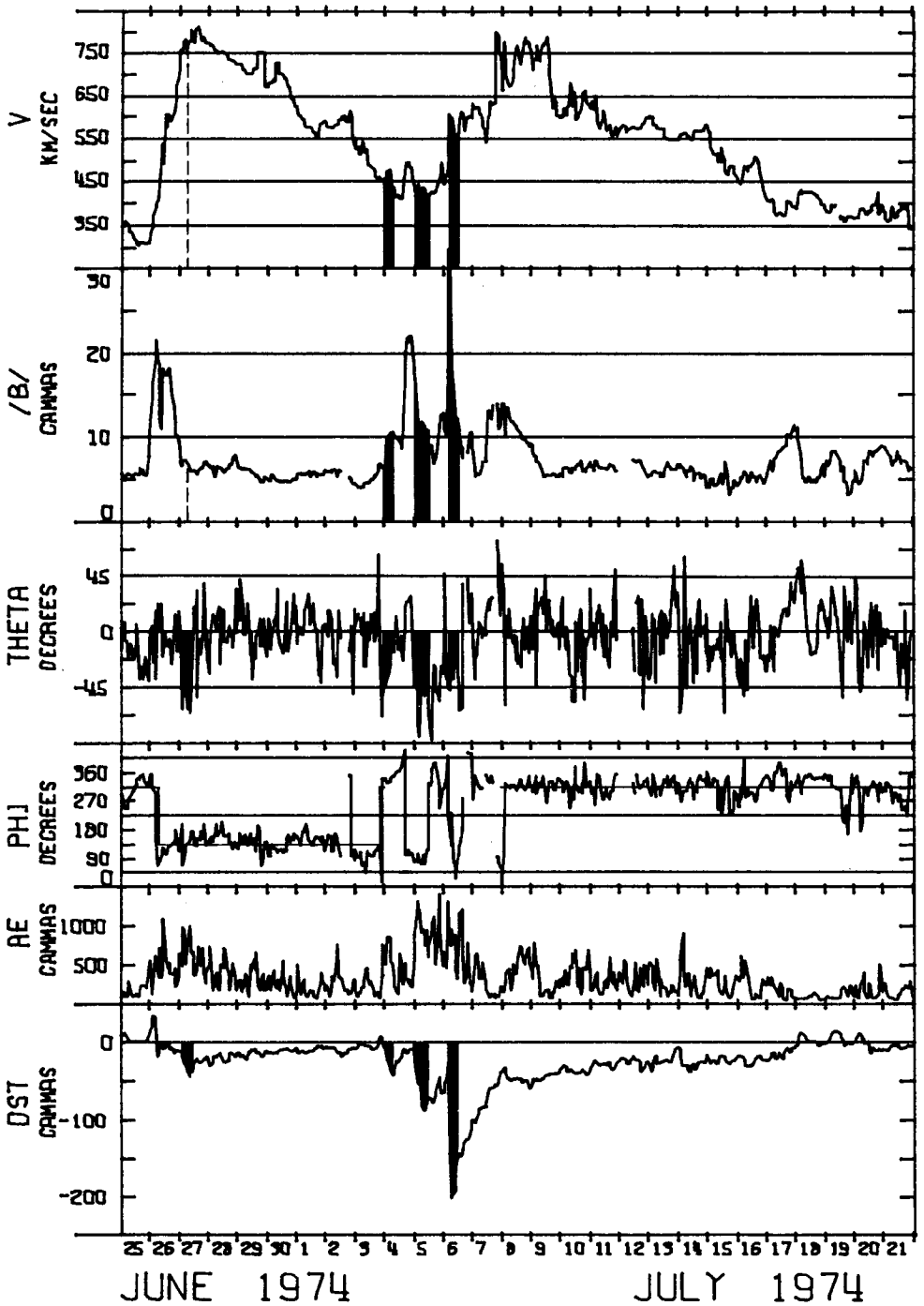

Fig. 22a. Same as Figure 19a, for the period between June 25 and July 21, 1974.

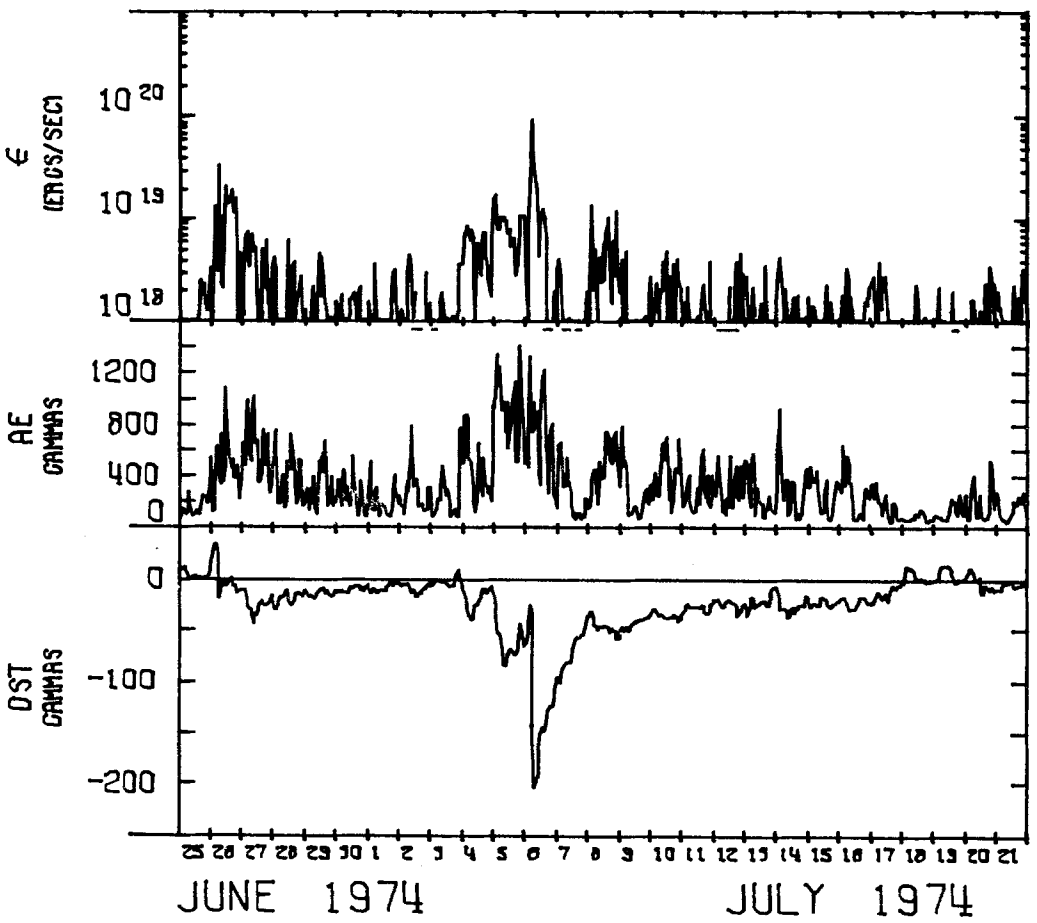

Fig. 22b. Same as Figure 19b, for the period corresponding to Figure 22a.

small. The second storm developed when Ⓗ reached a large negative value during the decay of a large impulsive change of B (it did not develop earlier because Ⓗ was positive). For the third storm, the period of a very rapid development of the main phase coincided with an impulsive change of B as large as 33γ. Note that the $|Dst|$ index was as large as 200γ and the associated peak of ε was about 10^{20} erg s^{-1}. It may also be noted that the earlier movement of the current disk on June 26–27 caused a fairly large negative Ⓗ near the end of a large impulsive change of B, so that an intense storm failed to develop.

Figure 23a represents changes of the solar wind and the IMF during the sunspot maximum phase. The current disk passed the location of the Earth, placing the Earth above it on February 2. Then the current disk passed again on February 19, placing the Earth below it. Note that the polarity of the solar magnetic field is different during this maximum period and the declining period (namely, after 1970). In addition to this basic pattern of ϕ, there occurred at least once a brief excursion of

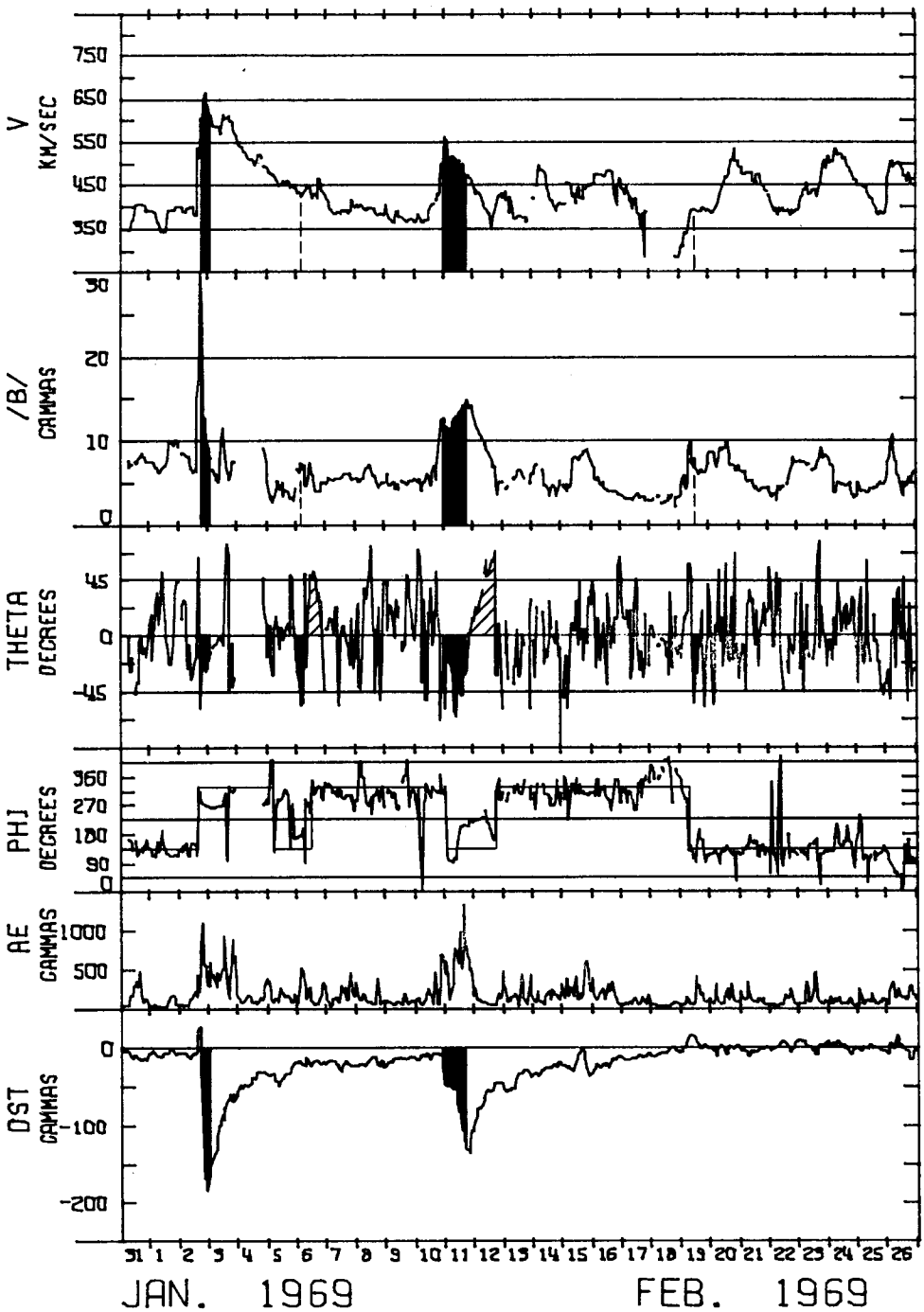

Fig. 23a. Same as Figure 19a, for the period between January 31 and February 26, 1969.

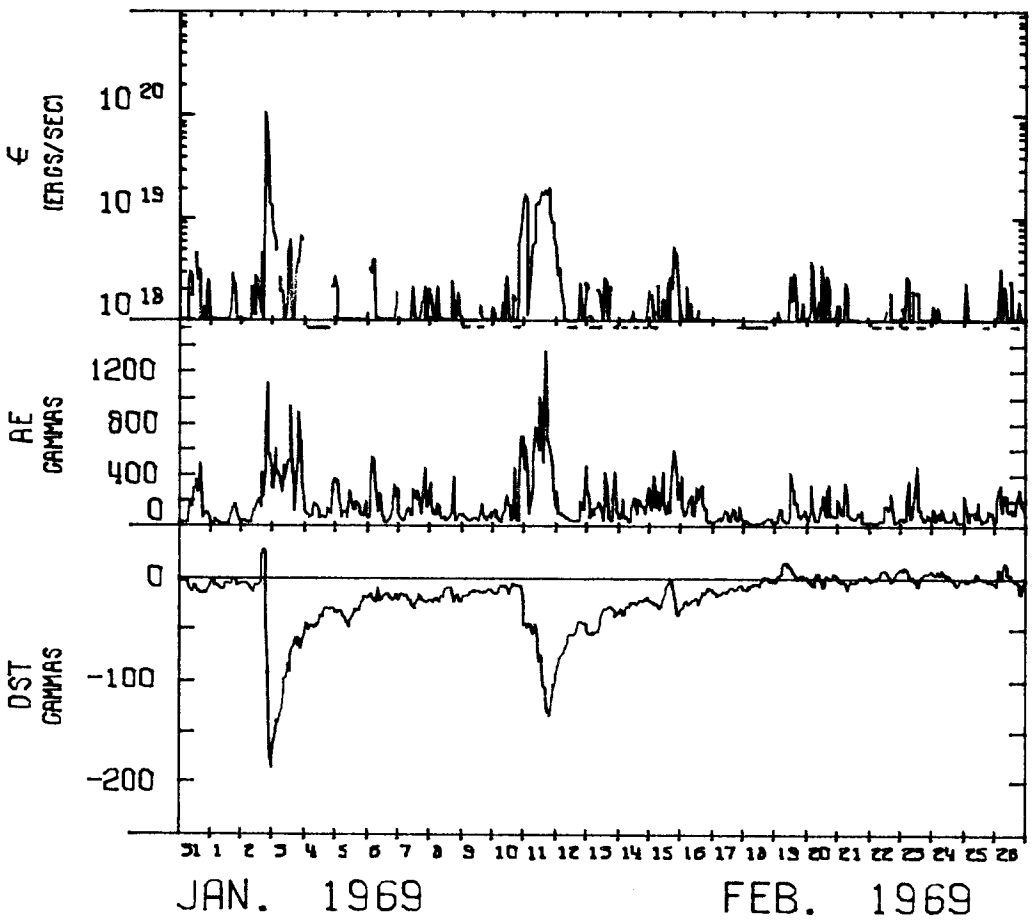

Fig. 23b. Same as Figure 19b, for the period corresponding to Figure 23a.

the current disk on February 11–12. Another similar brief excursion also occurred on February 5–6. These excursions differ from the passages associated with the 27-day rotation of the warped current disk and may be due to a temporal up-down movement of the current disk. The first passage of the current disk was associated with an extremely rapid development of a large main phase ($|Dst| \sim 180\gamma$) of the storm of February 2–4. Indeed, in Figure 23b, one can see a large impulsive increase of $\varepsilon \sim 10^{20}$ erg s^{-1}, coinciding with this brief period during which a rapid increase of V and an impulsive change of B occurred. A close examination of the data shows, however, that a large energy input ε occurred only during a later half of the large impulse of B. This is because Ⓗ was positive during the first half of the B impulse. On the other hand, a storm failed to develop when the current disk passed on February 19. It is easy to see the cause of this failure; both B and V were small. There occurred only a very minor change of ε at that time.

Let us now examine the development of a major geomagnetic storm during the brief excursion of the current disk on February 10–11. The angle Ⓗ had a large

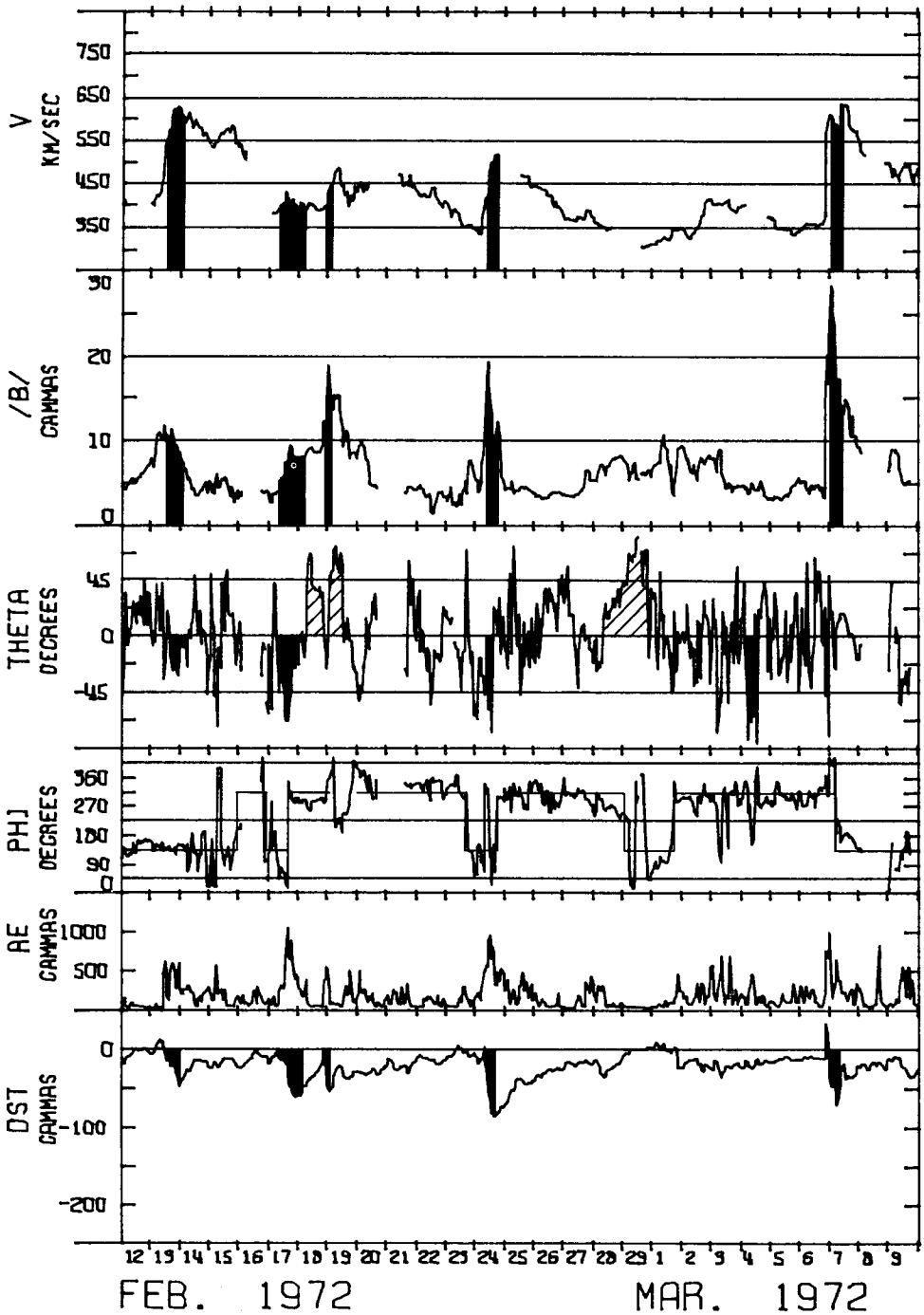

Fig. 24a. Same as Figure 19a, for the period between February 12 and March 9, 1972.

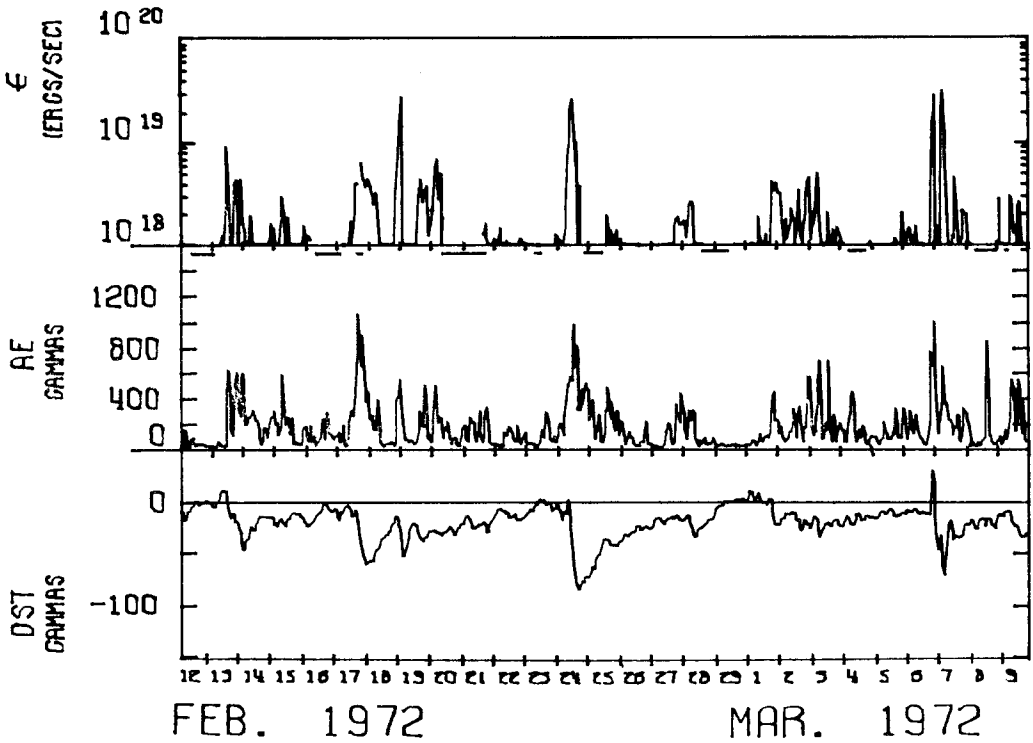

Fig. 24b. Same as Figure 19b, for the period corresponding to Figure 24a.

negative–positive excursion, and the storm grew during the period of Ⓗ<0, although V and B were not particularly large; a fortunate combination of the three quantities (although none of them were particularly large). Note that the main phase grew in two steps and that ε had a double peak. The largest $|Dst|$ value was about 150γ and the corresponding ε was about 2×10^{19} erg s^{-1}. There was a similar excursion of the current disk on January 5–6. However, a storm failed to develop in spite of a fairly large negative excursion of Ⓗ. Again, the reason for the failure is clear: a small value of B.

Figure 24a is basically quite similar to Figure 23a, but is somewhat more complicated. The corresponding changes of ε are shown in Figure 24b. The solar current disk passed the location of the Earth on February 16–17 and March 6–7. Both passages were associated with the development of geomagnetic storms of $|Dst|\sim50\gamma-\sim75\gamma$. In the former, B did not reach 10γ and V was small, but a relatively large value of Ⓗ was an important factor. On the other hand, in the latter storm (March 6–7), the main phase developed when B had a large impulsive change and V was rapidly increasing, in spite of the fact that Ⓗ was negative during only a very short period. There also occurred brief excursions of the solar current disk on February 19, 24 and February 29–March 1. The first excursion caused a very brief development of the main phase, which resulted from a very brief period of Ⓗ<0, a large value of B and a slight increase of V. The second excursion was associated

with the development of a major geomagnetic storm. Both V and B were quite similar for the first and the second storm; the difference of the development can thus be associated with a large difference in Ⓗ. In addition to these events, there occurred another storm on February 13–14. There was no associated change of ϕ, but the storm was only a medium one.

6.3. Summary

(a) The passage or a brief excursion of the warped solar current disk is often, but not always, associated with a large impulsive increase of the IMF magnitude to $B > 10\gamma$ and an increase in solar wind speed V.

(b) The current disk passage is often, but not always, associated with a variety of changes of Ⓗ.

(c) A major geomagnetic storm ($|Dst| > 100\gamma$) can develop only when the regions of a large $B \geq 10\gamma$ and Ⓗ < 0 coincide in the solar wind, resulting in a large value of $\varepsilon \geq 10^{19}$ erg s^{-1}.

(d) A very large increase of $B > 20\gamma$ occurs only during a very short period (6–24 hr). This is the main reason for the fact that very intense storms develop in such short periods. The most intense storms ($|Dst| \sim 200\gamma$) cannot develop even if Ⓗ has a large negative value, unless $B > 20\gamma$.

(e) There is a rather simple relationship between ε and the $|Dst|$ index.

$$|Dst| < 50\gamma \qquad \varepsilon < 10^{19} \text{ erg s}^{-1}$$

$$|Dst| \sim 50\gamma \qquad \varepsilon \sim 10^{19} \text{ erg s}^{-1}$$

$$|Dst| \sim 100\gamma \qquad 10^{19} \text{ erg s}^{-1} < \varepsilon < 10^{20} \text{ erg s}^{-1}$$

$$|Dst| \geq 200\gamma \qquad \varepsilon > 10^{20} \text{ erg s}^{-1}.$$

Figure 25 shows that the relationship between ε and Dst can be approximated by

$$|Dst| \sim 60(\log \varepsilon - 18)^2 + 25. \tag{9}$$

The nonlinearity of this curve can be understood by the fact that a more intense ring current tends to form at a closer distance to the Earth, namely in the atmosphere of an exponentially increasing density.

(f) Since a geomagnetic storm (and thus a magnetospheric storm) period is defined as the period when an appreciable ring current grows (namely, $|Dst| > 50\gamma$), the main difference between a magnetospheric substorm and a magnetic storm can be described easily in terms of ε. Magnetospheric disturbances which are caused by $\varepsilon < 10^{19}$ erg s^{-1} can mostly be classified as magnetospheric substorms. Since there is a reasonable correlation between $\varepsilon > 10^{18}$ erg s^{-1} and the AE index, it may be concluded that magnetospheric substorms are associated with 10^{18} erg s$^{-1} < \varepsilon <$ $< 10^{19}$ erg s^{-1}. A substorm begins when ε becomes $\sim 10^{18}$ erg s^{-1}. These points will be discussed further in Section 8.2.

(g) These conclusions do not depend on the phase of the sunspot cycle.

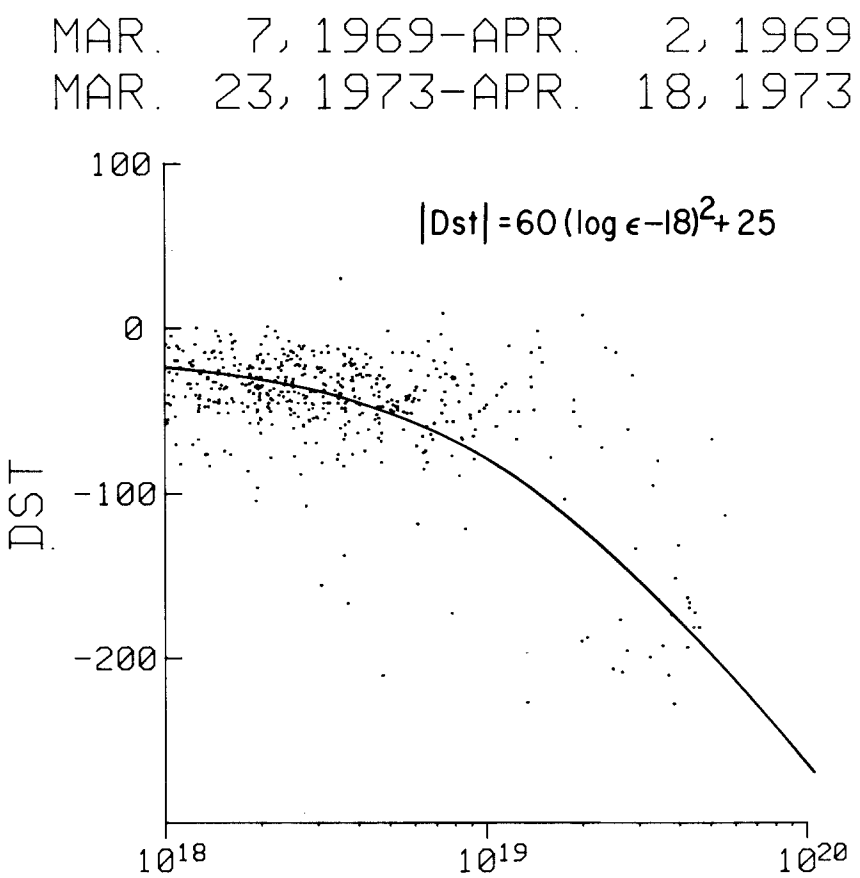

Fig. 25. Relationship between the solar wind energy coupling function ε and the *Dst* index for two 27-day periods, March 7–April 2, 1969 and March 23–April 18, 1973.

It is quite likely that a high speed solar wind stream from coronal holes or solar active regions causes a large impulsive increase of the IMF magnitude B by interacting with a slow solar wind (cf. Dryer, 1975; Dryer and Steinolfson, 1976; Dryer *et al.*, 1978; Smith and Wolfe, 1979). As we shall discuss in Section 9.1, the passage of the solar current disk is often identified as the passage of the interface. The structure of the interface has been extensively discussed by Burlaga (1975). As we shall discuss in Section 9.1, a large dipping of the IMF vector ($\textcircled{H} \sim -60° - -90°$) may arise often from a large-scale distortion of the interplanetary magnetic field and thus of the solar current disk.

7. Identification of ε as the Power of the Solar Wind-Magnetosphere Dynamo

7.1. Dynamo power

The purpose of this section is to show that the energy coupling function ε can be identified as the power generated by the solar wind-magnetosphere dynamo. The

dynamo power is given (Siscoe and Cummings, 1969; Gonzalez and Mozer, 1974) by

$$P = \frac{1}{4\pi}(B_t B_n) VS , \tag{10}$$

where B_n and B_t are, respectively, the normal and tangential field components on the tail magnetopause, V is the solar wind speed, and S is the surface area of the tail magnetopause on which B_n is nonzero.

Under the assumption that the magnetosphere is open and the polar cap field lines are interconnected with the interplanetary magnetic field lines, the polar cap potential can be written as

$$\phi = VBG(\theta) l_R , \tag{11}$$

where l_R is the effective length of the interconnection line on the frontside magnetopause. The form of the function $G(\theta)$ depends on the magnetopause interconnection geometry to be discussed later.

The averaged tangential electric field on the tail magnetopause can be estimated by mapping the polar cap potential on open field lines along the tail lobe, i.e.,

$$E_t = VBG(\theta) l_R (S/L) , \tag{12}$$

where S is the magnetopause surface area defined in (10) and L is the length of the magnetotail. Assuming that B_n is small compared with the lobe field, the tangential field component can be estimated by

$$B_t \cong B_n (S/A) , \tag{13}$$

where A is the cross section of the tail lobe. The normal field component on the magnetopause is related to E_t by the frozen-in condition, i.e.,

$$E_t = VB_n , \tag{14}$$

where V is the solar wind speed along the tail magnetopause which is assumed approximately equal to the upstream solar wind speed.

Upon substitution of (12), (13), and (14) into (10), the power generated by the solar wind-magnetosphere dynamo can be written as

$$P = VB^2 G^2(\theta)(l_R^2 L^2 / 4\pi A) . \tag{15}$$

Let us now examine the form of the function $G(\theta)$. Sonnerup (1974) and others proposed a component interconnection geometry in which the resulting polar cap convection is always anti-sunward. Under the component interconnection assumption (Sonnerup, 1974), combined with the fact that only the perpendicular component of the electric field contributes to the polar cap potential, the function $G(\theta)$ can be written as (Kan and Lee, 1979)

$$G(\theta) = \sin^2 \left(\frac{\theta}{2} \right) \tag{16}$$

Substituting (15) into (14), one obtains

$$P = \varepsilon[(l_R/l_0)^2 L^2/4\pi A]. \tag{17}$$

This result shows that P is proportional to $\varepsilon = VB^2 G(\theta)^2 l_0^2$. To allow the possibility that a fraction of the dynamo power can be stored in the magnetotail, the above result predicts that

$$l_R \geq l_0\sqrt{4\pi A}/L, \tag{18}$$

where the equality sign corresponds to $P = \varepsilon$, without energy storage. If $L = 200R_E$, $R_T = 15R_E$ together with $l_0 = 7R_E$, $A \cong \pi R_T^2/3 = 235R_E^2$, the effective length of interconnection line is $l_R \geq 2R_E$, which is reasonable if interconnection occurs near the cusp latitudes.

From the above derivation, one can see that the power generated by the solar wind-magnetosphere dynamo is proportional to the empirically derived energy coupling function ε which correlates with the total energy consumption rate U_T in the magnetosphere (Kan *et al.*, 1980). This result provides a theoretical basis for the energy coupling function, as well as an observational verification of the solar wind-magnetosphere dynamo theory.

7.2. Poynting flux

From the point of view of electromagnetic fields, the energy enters the magnetosphere by means of Poynting flux $\mathbf{E}\times\mathbf{H}$ (here $\mathbf{H} = \mu_0^{-1}\mathbf{B}$). Consider an exçavated volume (shown by dotted lines in Figure 26a) enclosing the magnetosphere. Integration of the Poynting's theorem $\partial/\partial t(\frac{1}{2}\mathbf{H}\cdot\mathbf{B}) + \nabla\cdot(\mathbf{E}\times\mathbf{H}) = -\mathbf{J}\cdot\mathbf{E}$ yields

$$\iiint -\mathbf{J}\cdot\mathbf{E}\,dV = \frac{\partial}{\partial t}\iiint \frac{\mathbf{H}\cdot\mathbf{B}}{2}\,dV + \iint(\mathbf{E}\times\mathbf{H})\cdot d\mathbf{A}. \tag{19}$$

Note that

$$\mathbf{E}\times\mathbf{H}\cdot d\mathbf{A} = -\mathbf{U}\cdot\left(\mathbf{HB} - \frac{\mathbf{H}\cdot\mathbf{B}}{2}\overleftrightarrow{1}\right)\cdot d\mathbf{A} + \frac{\mathbf{H}\cdot\mathbf{B}}{2}\mathbf{U}\cdot d\mathbf{A}, \tag{20}$$

where $\mathbf{HB}$ is a dyadic and $\overleftrightarrow{1}$ is a unit; the differential area $d\mathbf{A}$ of the magnetopause points inwards toward the Earth and is perpendicular to the solar wind (viz. $\mathbf{U}\cdot d\mathbf{A} = 0$) on the tail magnetopause. The time derivative of the volume integral is zero when the interplanetary medium is in a steady state. The surface integral has no contribution from the exterior surface of the excavated volume, as the solar wind is practically uniform in the region under our consideration. The surface integral on the interior surface represents the Poynting flux entering the magnetopause, or, equivalently, the work done by the Maxwell stress on the magnetopause. The volume integral of $-\mathbf{J}\cdot\mathbf{E}$ amounts to the total current outside the magnetopause times the

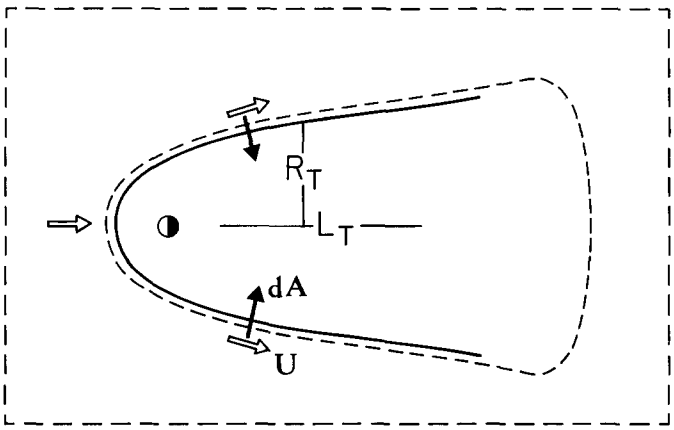

Fig. 26a. Application of the Poynting's theorem to an excavated volume enclosing the entire magnetosphere.

total voltage due to the electromotance. Therefore, we have

$$\Phi I = \int\int \mathbf{U} \cdot \left(\frac{\mathbf{H} \cdot \mathbf{B}}{2} \overleftrightarrow{1} - \mathbf{HB} \right) \cdot \mathrm{d}\mathbf{A} \tag{21}$$

integrated over the entire surface of the magnetopause.

Yeh *et al.* (1981) considered (21) for Dungey's open model to calculate the electromotance and the open flux. In this case, the geometry of the magnetosphere is determined entirely by the two fields and neglects effects of the solar wind pressure. This is obviously an extreme simplification, but an advantage of this procedure is that one can obtain a self-consistent expression for the energy coupling function. Yeh *et al.* (1981) showed that the power P generated for Dungey's model is given by

$$P(t) = 24 \mu_0^{-1} R_E^2 \frac{r_N L}{R_T^2} V B_0^{2/3} B_I^{4/3} \, |\sin \phi_I| \, F(\theta_I) \,, \tag{22}$$

where

B_0 = the intensity of the Earth's field at the equator;
B_I = the intensity of the IMF;
r_N = the geocentric distance of the neutral line;
L = the length of the magnetotail;
R_T = the radius of the tail;
ϕ_I = the longitude (measured eastward from the Sun–Earth line) of the neutral line
θ_I = the polar angle of the IMF vector

and

$$F(\theta_I) = \left[\frac{4}{27} \frac{(8 + \cos^2 \theta_I)^{1/2} - 3 \cos \theta_I}{(8 + \cos^2 \theta_I)^{1/2} + \cos \theta_I} \right]^{1/2} f(\theta_I) \tag{23}$$

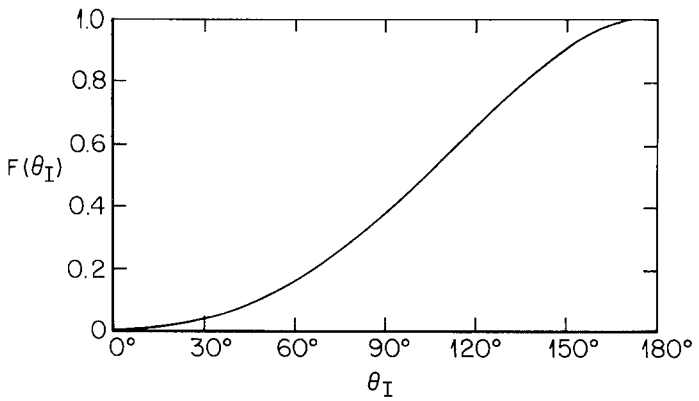

Fig. 26b. Plot of $F(\theta_I)$ showing the functional dependence of the dynamo power on the polar direction of the interplanetary magnetic field.

Figure 26b shows $F(\theta_1)$ as a function of θ_I; it shows a monotonic change between 1.0 and 0.

Equation (22) represents an energy coupling function derived from a theoretical consideration based on Dungey's model. It differs from ε in two aspects. First, $P(t)$ is proportional to $B_I^{4/3}$ whereas $\varepsilon(t)$ is proportional to B_I^2. This discrepancy is rather superficial, for the factor $l_0^2 B_I^2$ in $\varepsilon(t)$ should be compared with the factor $r_E^2 B_0^{2/3} B_I^{4/3}$ in $P(t)$ when the dependence of the size of the magnetosphere on the interplanetary medium is taken into consideration. If the stress exerted by the interplanetary medium on the magnetopause is predominantly magnetic, as is assumed in the interpermeation model, l_0 should vary as the distance between the two neutral points, hence it is proportional to $B_I^{-1/3}$. On the other hand, if the dynamic stress of the solar wind predominates, l_0 will be independent of B_I, but may weakly depend on ρ and V. The realistic situation certainly lies between these two extreme situations. It may be that the distance l_0 can be affected appreciably only during the periods when the IMF has a very large southward component (Kan and Akasofu, 1974). During such periods the rate of energy injection may be proportional to $VB^{4/3}$, instead of VB^2. Except for such extraordinary periods, the distance l_0 can be considered as a constant as a first approximation. This point will be discussed at the end of this section. Secondly, $P(t)$ is proportional to $|\sin\phi_I| F(\theta_I)$, not to $\sin^4(\frac{1}{2}\arctan(|\sin\phi_I|\tan\beta_I)$. Note that

$$\theta = \arctan(|\sin\phi_I|\tan\theta_I) \tag{24}$$

is equal to θ_I when the interplanetary field is entirely perpendicular to the Sun–Earth line, viz. $\phi_I = \pm 90°$. It turns out that $F(\theta_I)$ is well approximated by $\sin^{8/3}(\theta_I/2)$. As to the numerical value of l_0, its value of being 7 Earth radii as used in the initial deduction can correspond to the combination of $R_T \approx 2r_N$ and $L_T \approx 8r_N$. This seems in reasonable order of magnitude. Note that L_T is the effective width of the current sheet, it is not the whole length of the magnetotail.

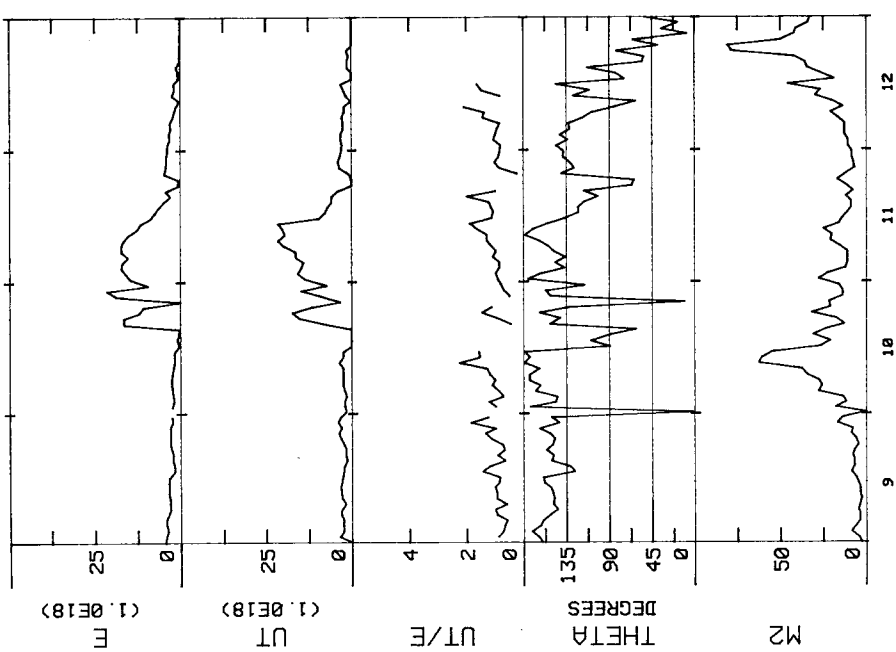

Fig. 27a. From the top, the solar wind-magnetosphere energy coupling function ε, the total energy consumption U_T, the ratio U_T/ε, θ and M^2 (denoted by M2) for the storm of February 9–12, 1968; the ratio U_T/ε is calculated for periods only when U_T and ε are greater than

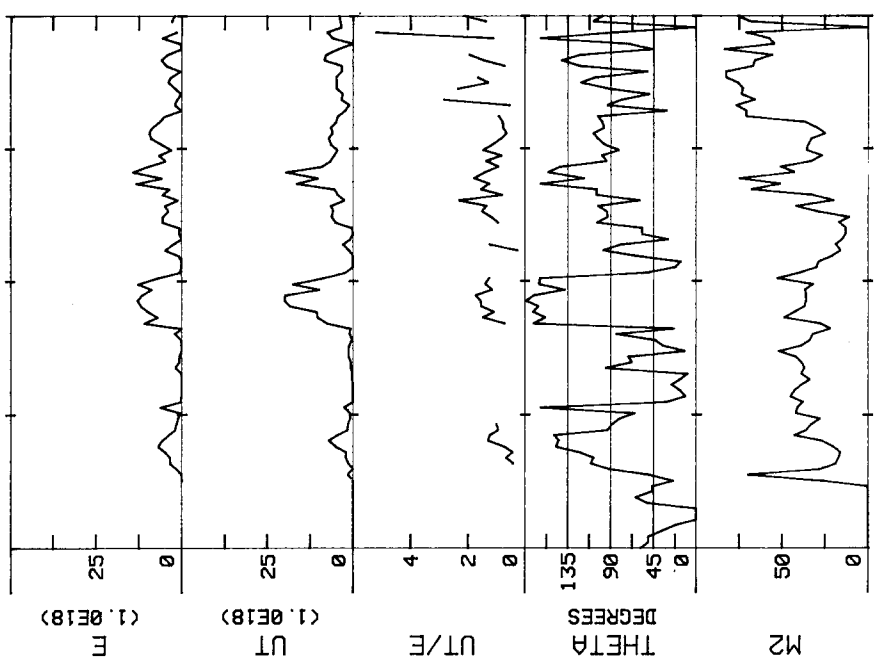

Fig. 27b. Same as Figure 27a for the storm of February 20–23, 1973.

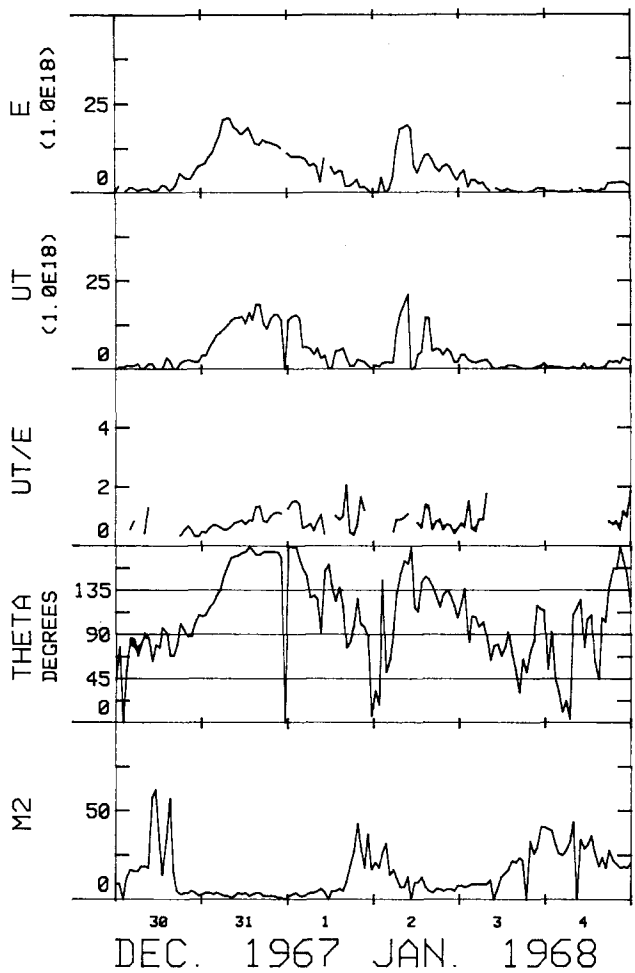

Fig. 27c. Same as Figure 27a for the storm of December 30, 1967–January 4, 1968.

In order to verify the expression for the energy coupling function ε, several tests have been conducted. For example, Figures 27a and 27c show the ratio U_T/ε for the storm of February 9/12, 1968, of February 20–23, 1973, and of December 30, 1967–January 4, 1968. One can see that $U_T/\varepsilon \sim 1$ for the entire storm period (when both U_T and ε are large enough), indicating that ε cannot be expressed in terms VBl_0^2 or $VB^{4/3}l_0^2$. Therefore, one may write:

$$U_T/\varepsilon = (1 + H(\rho, V, B) + \cdots) \tag{25}$$

and

$$H(\rho, V, B) \ll 1.$$

Further, in order to examine the dependence of $H(\rho, V, B)$ on the Alfvén Mach number M, we plot M^2 for the three periods. One can infer that $H(\rho, V, B)$ cannot

be a strong function of M^2 (if any). Further, by assuming that the distance l_0 is given by the Chapman–Ferraro distance l_{CF}.

$$l_{CF} = \left(\frac{M_E}{4\pi\rho V^2}\right)^{1/6} \tag{26}$$

a new coupling function ε' is computed and is compared with ε, where M_E denotes the magnetic moment of the Earth. Both ε' and ε are quite similar, indicating that l_0 may be only a weak function of ρ and V (if any) and can be assumed to be a constant as a first approximation. In order to determine accurately the expression for $H(\rho, V, B)$, however, one must improve U_T (see Section 9.3).

It may be of interest to note that Gonzalez and Mozer (1974) showed that the power P transmitted to the magnetosphere can be expressed by the integral over the tail of the Poynting flux, namely

$$P = \frac{1}{4\pi}\int \mathbf{E}\times\mathbf{B}\cdot d\mathbf{S} = \frac{1}{4\pi}\int dx\, dy\, E_y B_x\,, \tag{27}$$

where E_y denotes the cross-tail electric field and B_x the magnetotail field. Here we assume that the integral $\int B_x\, dx$ can be given by $B_t L$, where B_t is the average tail field intensity and L is the length of the magnetotail. Thus, the above equation may be rewritten as

$$P = \frac{1}{4\pi}\psi B_t L \tag{28}$$

since $\int E_y\, dy = \psi$ is the potential drop across the tail.

Here, B_t may be estimated as the total amount of field line flux connected on the dayside in the time = L (the length of the magnetotail)/V (solar wind speed), divided by the half cross-sectional area of the magnetotail $\pi R_T^2/2$. Thus,

$$B_t = (2\psi/2\pi R_T^2)(L/V)\,. \tag{29}$$

Thus,

$$P = \psi^2 L^2/2\pi^2 V R_T^2 \tag{30}$$

or since

$$\psi = \frac{B_t}{2}\pi R_T^2 \frac{V}{L} \tag{31}$$

$$P = \frac{B_T^2}{8\pi}\pi R_T^2 V = \left(\frac{B_t B_n}{4\pi}\right) SV\,. \tag{32}$$

The last equation is the same as (10) in Section 7.1 and is thus proportional to ε. This proves that the dynamo process takes place on the magnetopause of the magnetotail.

8. Significance of the Findings of the Energy Coupling Function

8.1. Identification of the Interaction Process between the Solar Wind and the Magnetosphere as a Dynamo

Although the derivation given in Section 7.1 was a dimensional analysis, it is significant that the energy coupling function ε can be identified as the power P by assuming that the solar wind and the magnetosphere constitute a dynamo. Furthermore, on the basis of the formulation of P by Siscoe and Cummings (1969) and Gonzalez and Mozer (1974), one can now understand how the dynamo power is generated. The electromotive force arises from $\mathbf{B}_n \times \mathbf{V}$, where $\mathbf{B}_n$ denotes the normal component of the magnetic field on the magnetopause in the magnetotail.

This understanding should serve in finding how the generated power is dissipated in the magnetosphere. In the past, the solar wind-magnetosphere interaction was discussed in terms of 'reconnection' or 'flux transfer' without any concrete understanding, quantitatively or physically, of the energy coupling process. It is through the empirical study described in this paper that a first approximation expression for the energy coupling function is obtained.

8.2. Is a Magnetospheric Substorm a Consequence of Conversion of Magnetic Energy Stored Prior to the Onset?

It has long been thought, actually tacitly, that the magnetosphere stores the solar wind energy in the form of magnetic energy in the magnetotail and that the stored magnetic energy is suddenly converted into substorm energy by internal processes in the magnetosphere. As mentioned in Section 4, we would not expect to find a simple function ε if the magnetosphere were an unloading system. Our finding of ε indicates conclusively, however, that the magnetosphere is, as a first approximation, a directly driven system.

Therefore, our finding suggests strongly that magnetospheric disturbances arise primarily as the power $P\ (=\varepsilon)$ generated by the solar wind-magnetosphere dynamo increases above certain values, rather than by a sudden conversion of the stored energy accumulated prior to the onset of the disturbances. This is an unexpected result. On the other hand, it is not difficult to realize that the concept of an unloading system was simply a hypothesis, since the relationship between the energy input and output rates had not been known before.

The fact that both $\varepsilon(t)$ and $U_T(t)$ have similar time variations indicates indeed, that magnetospheric disturbances arise primarily from a direct consequence of an enhanced dynamo efficiency. For this reason it is of great interest to see how the energy input rate ε, the amount of the magnetic energy in the magnetotail $(B_T^2/8\pi) \times$ $\times$ the volume of the tail, and the total energy consumption rate U_T vary as a function of time. Thus we examine here the relationship among ε, $(B_T^2/8\pi)$ in the magnetotail, and the substorm index (AE). Figure 28 shows the relationship between these three quantities monitored by the Explorer 34, 35 satellites and auroral zone

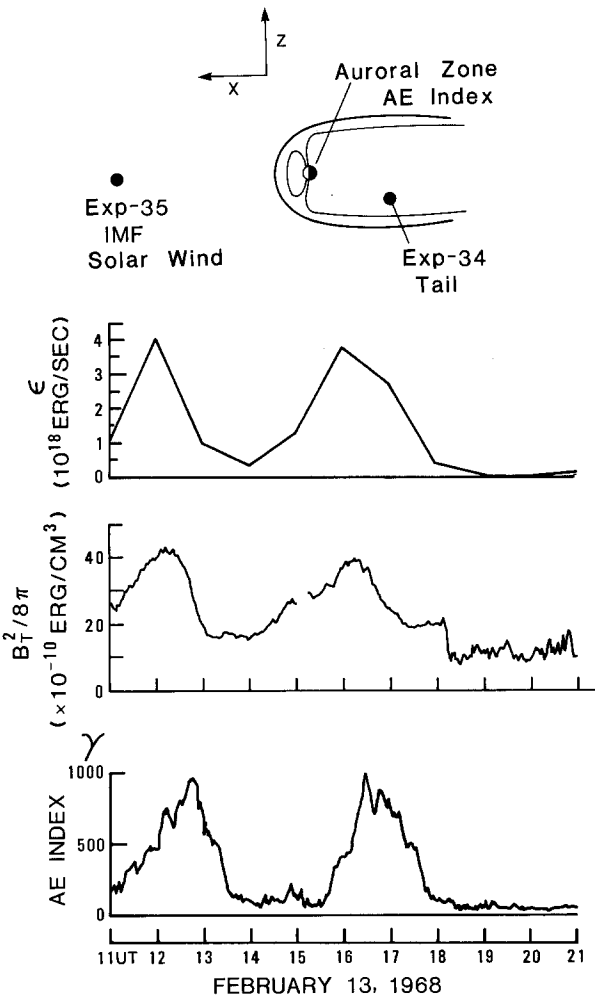

Fig. 28. Relationship between the solar wind-magnetosphere energy coupling function ε and the magnetic energy density ($B^2/8\pi$) in the magnetotail and the AE index during two successive substorms on February 13, 1968. The location of two satellites used in this figure is shown in an insert.

magnetic observatories, respectively. For the relative location of the satellites with respect to the magnetosphere, see the insert in Figure 28. One can see in Figure 28 that the three quantities, ε, $B_T^2/8\pi$ and AE vary roughly in harmony.

This result is in agreement with our earlier conclusion that the development of magnetospheric substorms is a direct consequence of increasing ε above $\sim 10^{18}$ erg s^{-1}. As ε is increased, both the magnetotail (solenoidal) current and the auroral electrojet are enhanced, as can be seen in the corresponding increase of $B_T^2/8\pi$ and AE. If one assumes that the magnetospheric substorm is produced by an explosive conversion of magnetic energy stored prior to substorm onset $T_s = 0$ in the magnetotail (as it has been widely assumed), $B_T^2/8\pi$ should begin to decrease rapidly after ~11:00 UT and 15:30 UT in Figure 28. On the contrary, both the

magnetic energy in the magnetotail and the energy consumption in the magnetosphere began to increase during the expansive phase of the magnetospheric substorm. This fact indicates that an enhanced power of the dynamo increases the magnetic energy in the magnetotail, while magnetospheric substorms develop at the same time. Thus, this result indicates clearly that the magnetospheric substorm is a direct result of an increased ε, rather than a result of sudden conversion of the energy stored prior to $T_s = 0$.

Our conclusion that the development of magnetospheric substorms is a direct consequence of increasing ε above $\sim 10^{18}$ erg s^{-1} can also be tested by examining relationships between ε and auroral activity. Figure 29 shows ε, the *AE* and *Dst* indices on February 21–23, 1973. Some of the DMSP photographs taken during the same period are shown on the left-hand side. The time when each photograph was taken is identified in the ε diagram. One can easily see that the aurora is very dim when ε is less than 10^{18} erg s^{-1} (the photographs 3 and 7). When ε is rapidly increasing from less than 10^{18} erg s^{-1} to $\sim 10^{19}$ erg s^{-1} (at about 16 UT on February 21), the corresponding auroral photograph (4) shows a brightening arc in the midnight sector, an indication of substorm onset. When ε is greater than $\sim 5 \times$ $\times 10^{18}$ erg s^{-1}, the auroral oval is expanded considerably and bright (photographs 5, 6, 8, and 9). Note that this period was examined earlier in Section 4.

In this connection, it may also be interesting to recall that magnetospheric substorms occur sometimes simultaneously with or immediately after storm sudden commencements (Schieldge and Siscoe, 1970; Kawasaki *et al.*, 1971). Burch (1972) noted that this probability is high when the IMF B_z component is negative ($<-1\gamma$) over a period of at least one half hour preceding the ssc, although the magnitude of the ssc is an important factor. Iijima (1973) confirmed Burch's result. On the basis of these studies, it has generally been believed that a strong compression of the magnetosphere by an interplanetary shock wave *triggers* a substorm, if the magnetosphere is preconditioned about one hour prior to the compression. This conclusion was thought to imply that a magnetospheric substorm could arise as a result of a sudden conversion of energy which is *stored* in the magnetotail *prior to substorm onset* and that this conversion could be triggered by an interplanetary shock wave.

Since such an implication appears to contradict the above conclusion, it is of interest to re-examine the phenomenon of so-called 'substorms triggered by ssc's' by examining the energy coupling function ε at the time of ssc's (Akasofu and Chao, 1980). Figure 30 shows, from the top, the interplanetary magnetic field (IMF) magnitude B, the three IMF components (B_x, B_y, B_z), the solar wind speed V, the solar wind-magnetosphere energy coupling function ε, the *AE* index and the *Dst* index. In this event, the interplanetary shock wave reached the magnetosphere at 19:58 UT on March 19, 1969, resulting in compression of the magnetosphere, as indicated by a positive change of the *Dst* index. The ssc was immediately followed by substorm activity, as indicated by a sudden increase in the *AE* index at that time. Therefore, this event is a good example to show the simultaneous occurrence of an ssc and a substorm, in spite of the fact that the IMF B_z component was positive for

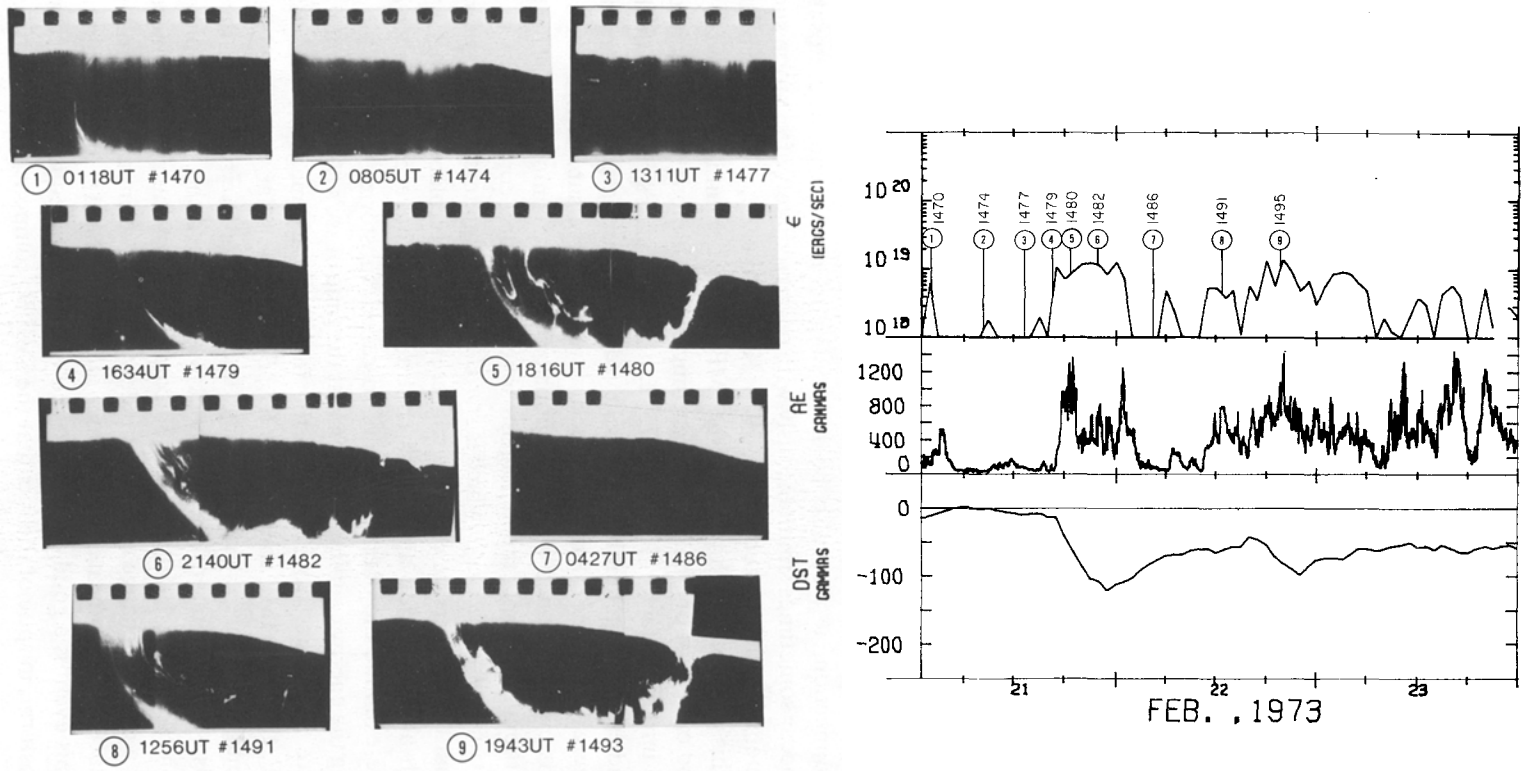

Fig. 29. Relationship between the solar wind-magnetosphere energy coupling function ε and auroral activity (DMSP photographs taken from above the northern polar region; see an insert for an approximate field of view). The times when the DMSP photographs were taken are identified in the ε diagram. The *AE* and *Dst* indices are also shown.

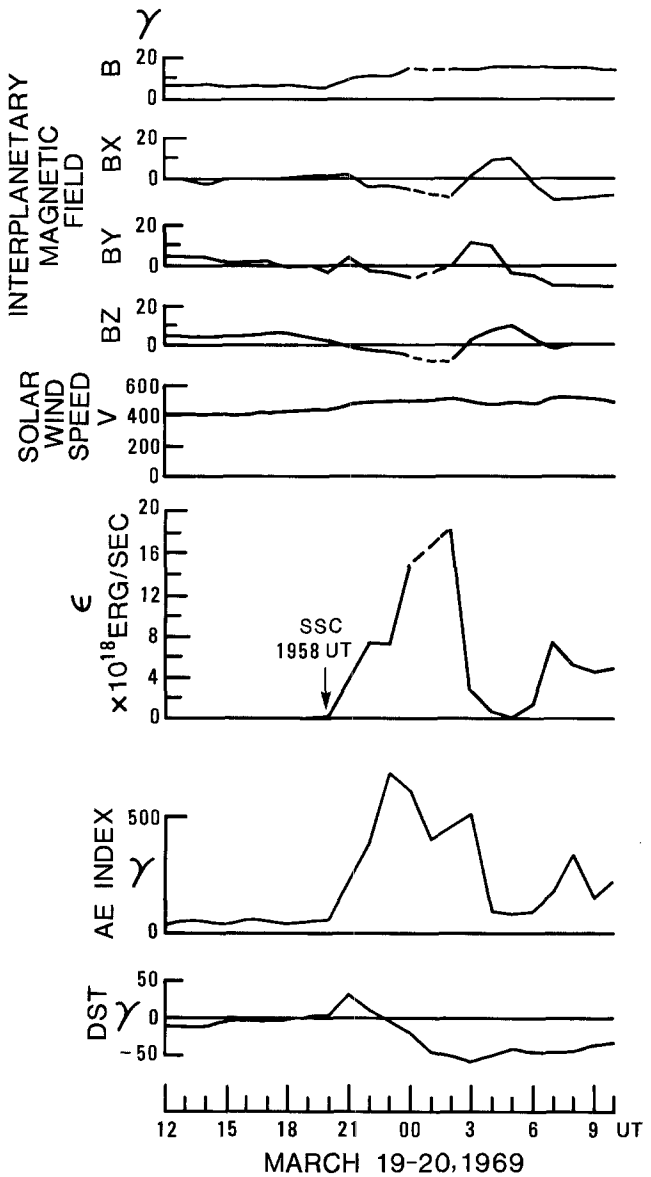

Fig. 30. The interplanetary magnetic field (IMF) magnitude B, the three components (B_x, B_y, B_z), the solar wind speed V, the solar wind-magnetosphere coupling function ε, the magnetosphere substorm index AE and the ring current intensity index Dst for the March 19–20, 1969 storm.

more than 8 hr prior to the ssc. One can see that the energy coupling function ε sharply increased simultaneously with the ssc and that there is a reasonable similarity between ε and the AE index, indicating that the substorm activity was associated with the increase of ε after the ssc, rather than triggered by the ssc. On the other hand, the following example shows a case in which an ssc was not immediately followed by any significant substorm activity (Figure 31). Note that the solar wind

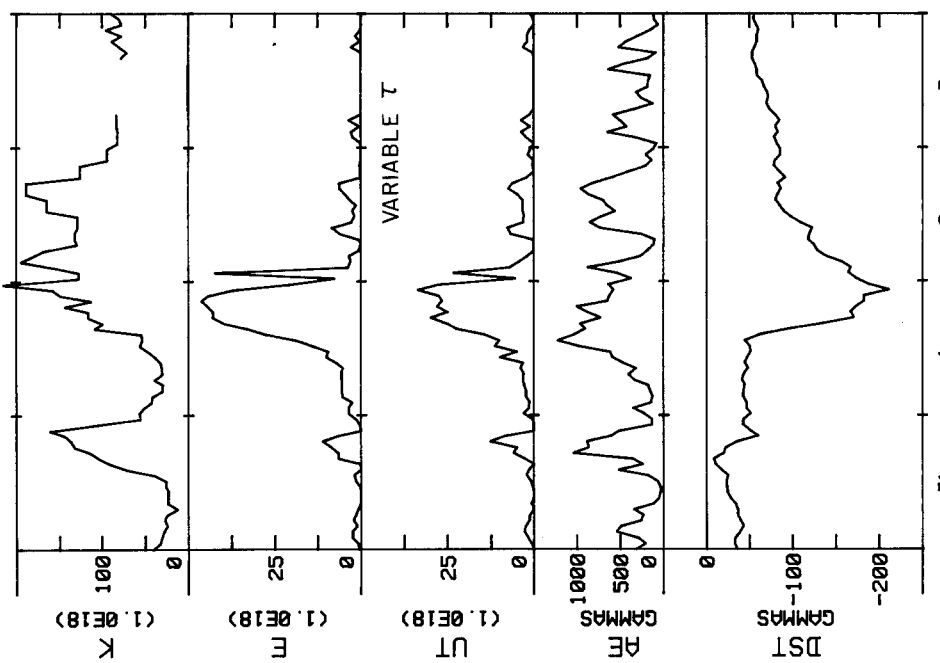

Fig. 32. The kinetic energy flux K, the solar wind-magnetosphere energy coupling function ε, the total energy consumption rate U_T which is estimated on the basis of variable values of τ_R (see the text) and the AE–Dst indices for the storm of March 31–April 3, 1973.

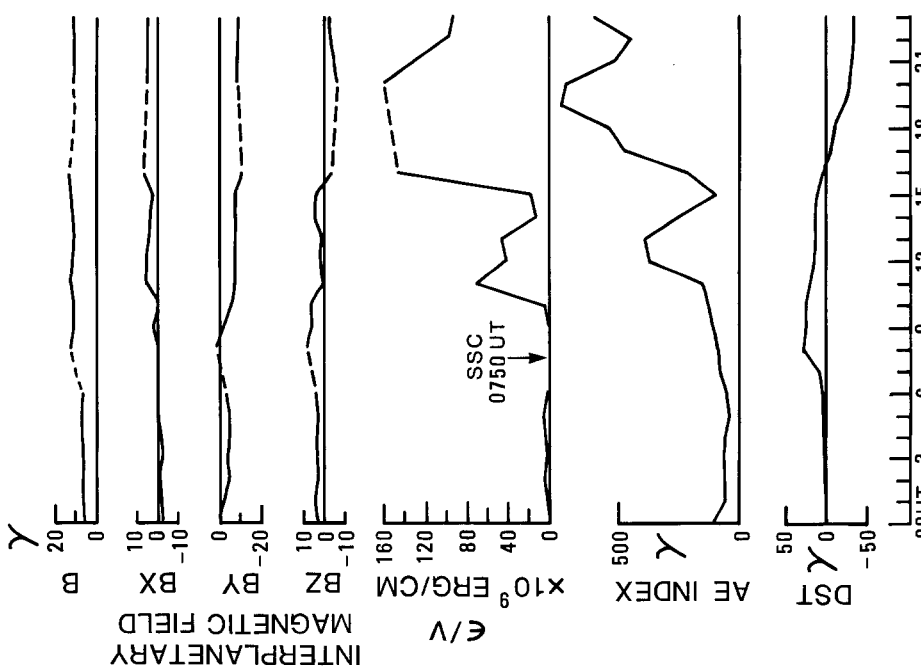

Fig. 31. Same as Figure 30, for the June 17, 1970 storm, except that ε/V is given instead of ε (since the solar wind speed V is not available).

speed was not available for this event, so that the quantity ε/V (erg s^{-1}) is plotted. By comparing the above two examples, one can easily see that the occurrence of substorm activity after the storm sudden commencement depends on whether or not an interplanetary shock wave is accompanied by a large increase of the solar wind-magnetosphere energy coupling function ε. This result implies that a magnetospheric substorm is not a sudden conversion of magnetic energy stored in the magnetotail which is triggered by an ssc, but is a direct consequence of an increased power of the solar wind-magnetosphere dynamo. A number of similar examples for both cases can be found in Section 5.

It may be worthwhile to consider here two contrasting relationships between $\varepsilon(t)$ and $U_T(t)$. In one case, $\varepsilon(t)$ follows closely $U_T(t)$ with a delay of τ_M. In the other case, $\varepsilon(t)$ is stored in the magnetotail and is then suddenly converted into $U_T(t)$. Both cases are illustrated in Figure 32a. The former is a driven process, while the latter is an unloading process. Note that for the latter case, the time constant for both a sharp rise and a slow fall is determined solely by magnetospheric quantities, not by an increase and decrease of $\varepsilon(t)$. It has long been thought that the magnetospheric substorm belongs to the latter. As mentioned repeatedly, one would not necessarily expect similar time variations between $\varepsilon(t)$ and $U_T(t)$ for such a system. On the contrary, it is clear from our study that both the rise and fall of $U_T(t)$ are controlled primarily by $\varepsilon(t)$ so that the magnetospheric substorm is closer to a driven process, rather than to an unloading process. Magnetospheric time constants are not primary factors which determine when $U_T(t)$ begins to increase and subside. This conclusion clarifies some longstanding crucial questions on magnetospheric substorms, namely, (i) why the magnetosphere ceases to convert the magnetic energy

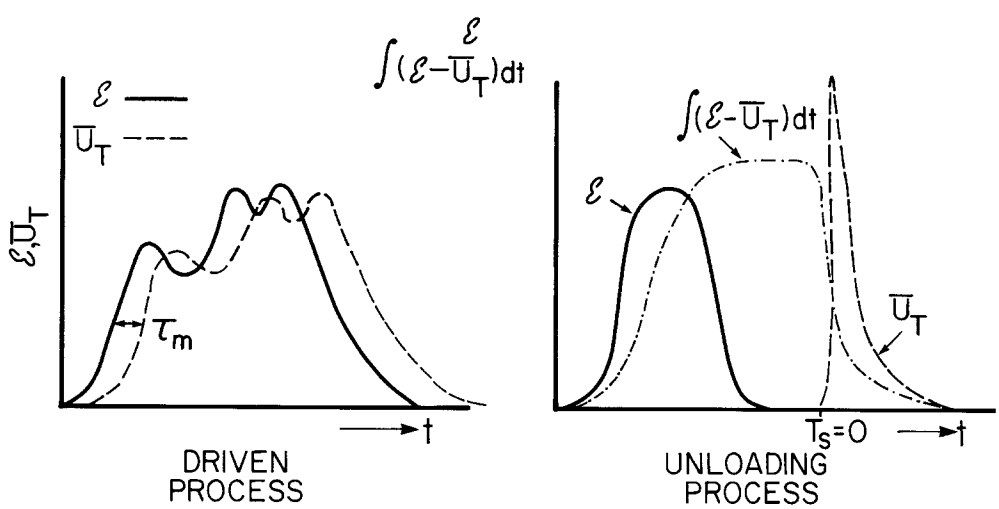

Fig. 32a. Schematic illustration of two different systems indicated by differences of the response $U_T(t)$, the energy dissipation rate of the system to the energy input rate $\varepsilon(t)$. For a driven system, the relationship can be expressed by $\varepsilon(t) \sim U_T(t+\tau_M)$. For an unloading system, $U_T(t)$ depends on various characteristics of the system and may not have any simple relationship with $\varepsilon(t)$.

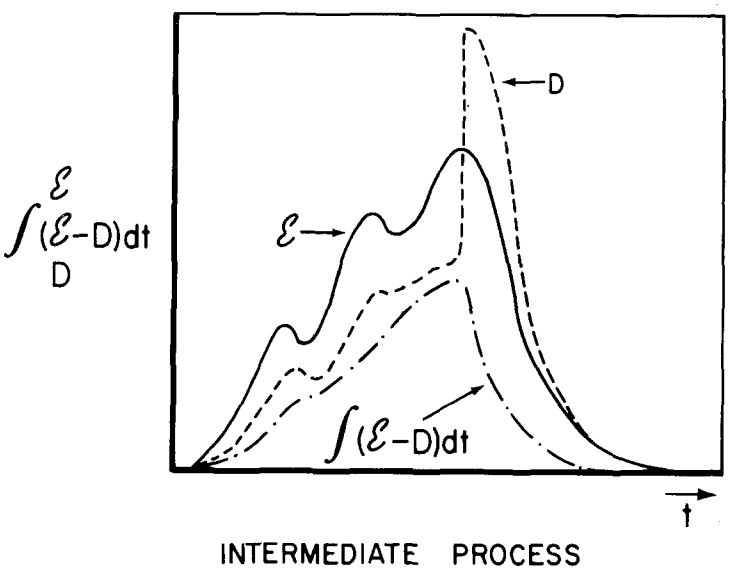

Fig. 32b. Schematic illustration of the $\varepsilon - U_T$ relationship for a system which can be considered to be intermediate between a driven and an unloading system.

for substorms even when there is a considerable amount of magnetic energy left in the magnetotail at the end of a substorm; (ii) why a substorm does not occur during quiet periods ($\varepsilon < 10^{18}$ erg s^{-1}) even if the magnetotail (thus magnetic energy) is available; and (iii) why there is the ground state of the magnetosphere. These questions do not arise once the magnetosphere is understood to be a driven system and magnetospheric substorms are a direct result of an increased power ($\varepsilon > > 10^{18}$ erg s^{-1}).

It should be emphasized that the magnetosphere is not strictly a driven system. It is only closer to a driven system than to an unloading system. This is because the magnetosphere has a large inductance $L = 100 \sim 500H$. It will accumulate magnetic energy in the magnetotail and convert it into substorm energy. It is important to note that such a process will occur only after ε begins to decline, namely near the maximum epoch of a magnetospheric substorm, not at substorm onset. For such an intermediate situation, the relationship between ε and U_T may be illustrated by Figure 32b. It remains to be seen how much the energy released in this way contributes to a substorm. In this connection, it should be noted that one should expect some time delay between $\varepsilon(t)$ and $U_T(t)$ or $AE(t)$; the magnetosphere–ionosphere system has a large inductance. Noting that the total ionospheric resistance is of the order of 0.1Ω, the time constant τ_M of the magnetosphere is of the order of $17 \sim 85$ min. Thus, the magnetosphere cannot respond instantly and fully to time variations of ε of scales of less than τ_M. In the past, such a delay has been considered exclusively in terms of a growth phase, implying that the total magnetic energy required for a substorm is accumulated prior to its onset.

8.3. Prediction of Auroral and Magnetic Activity

The finding of the energy coupling function $\varepsilon(t)$ suggests that one should be able to predict not only the occurrence and intensity of auroral and magnetic activity, but also its time development, provided that one can monitor ε by a satellite which is located at the front of the magnetosphere at a reasonable distance, say $\sim 500 R_E$. Akasofu and Chao (1979) examined one example of the simultaneous observations of ε by the space probe and by an earthbound satellite. A medium size geomagnetic storm occurred at the time when the Mariner 5 space probe was located at a distance of 460 Earth radii (in the ecliptic plane projection) from the Earth on its way to Venus. At that time, the solar wind disturbances were also monitored by an earthbound satellite, Explorer 34. In Figure 33, we plot hourly average values of ε at Mariner 5 and Explorer 34 by shifting the Mariner data by 3.4 hours; for the locations of the two spacecraft with respect to the magnetosphere, see the insert in Figure 33. Similarity of ε at the two locations suggests that ε is well retained during

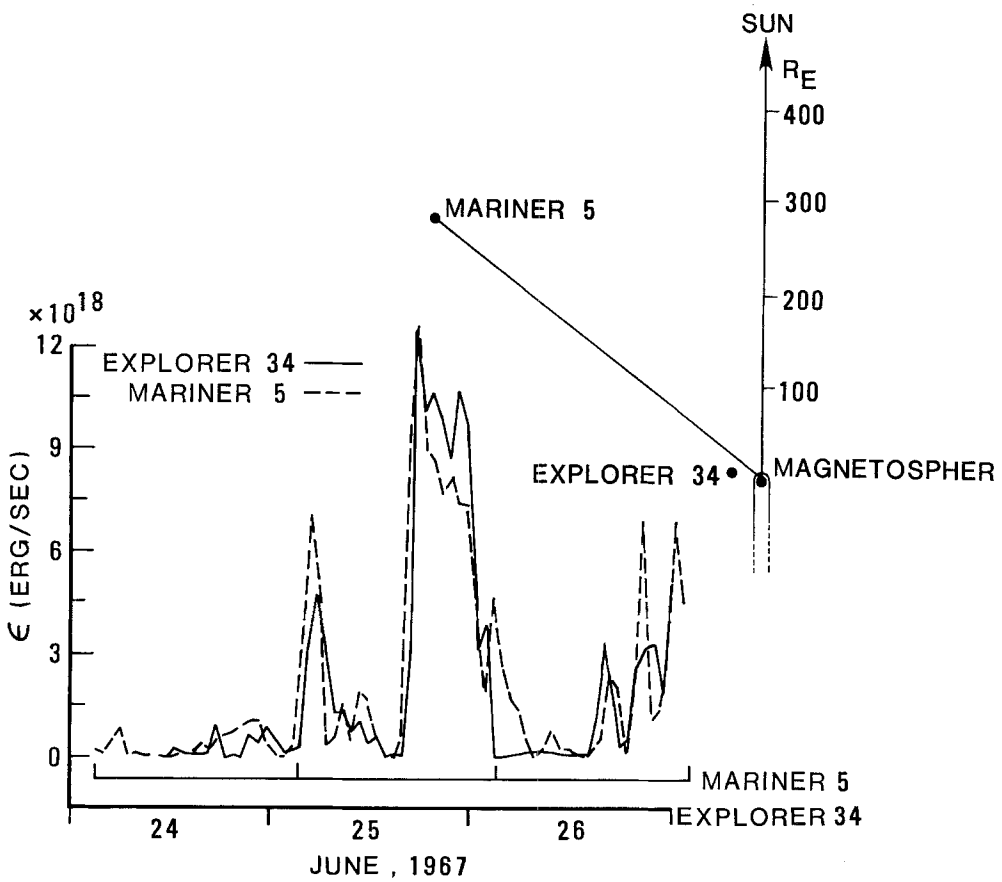

Fig. 33. Comparison of the solar wind-magnetosphere energy coupling function ε observed by the Mariner 5 space probe and the earthbound satellite Explorer 34. The Mariner data are shifted by 3.4 hr. The insert gives the location of the spacecraft.

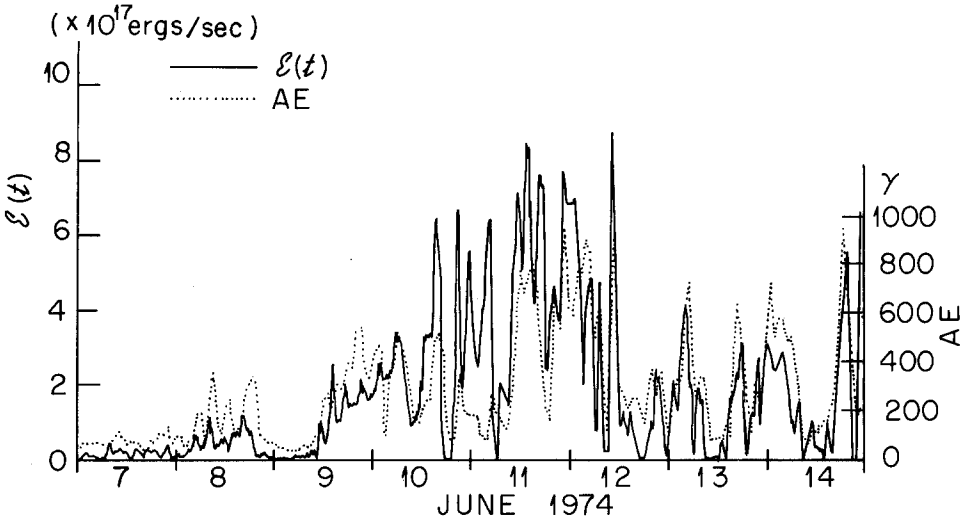

Fig. 34. Comparison of the solar wind-energy coupling function ε and the AE index for the period between June 7–14.

its traverse from Mariner 5 to Explorer 34. This study suggests that it is possible to monitor ε by the ISEE/C satellite at the libration point.

The predicted time variations of $Dst(t)$ can be obtained by replacing U_R in (5) by 0.7ε; this is to assume that 70% of the generated power will be deposited in the ring current belt. The expected maximum Dst index can be obtained from Figure 25 or Equation (9). The dependence of AE on ε is complicated by the fact that AE is a double value function of ε, since AE tends to decline as ε increases beyond $\sim 10^{19}$ erg s^{-1}. For a weak storm ($|\text{Dst}| < 50\gamma$), however, $AE(t)$ may be given approximately by $AE \sim \varepsilon/10^{16}(\gamma)$. Thus for $\varepsilon \sim 10^{19}$ erg s^{-1}, AE will be $\sim 1000\gamma$. A typical example of the relationship between ε and the AE index for weak disturbances is shown in Figure 34 (Akasofu, 1979a).

9. Future Problems Associated with the Energy Coupling

9.1. Causes of a large value of ε

In considering the *energy coupling* between the solar wind and the magnetosphere, it is important to note that the energy input rate ε is expressed by a particular combination of three quantities, V, B, and θ. Among the quantities which contribute to ε, namely V, B, and $\sin^4(\theta/2)$, the solar wind speed is the least variable (350–750 km s^{-1}). During major geomagnetic storms, the IMF magnitude B is found to increase and vary considerably ($3 \sim 30\gamma$); further note that B contributes to ε in the form of B^2 ($9\gamma^2 \sim 900\gamma^2$). The function $\sin^4(\theta/2)$ is most variable, although its range is limited between 0 and 1.0 (usually between 0.1 and 0.9). By examining V, B, and $\sin^4(\theta/2)$ for a large number of geomagnetic storms, Perreault and Akasofu

(1978) showed that the combination of both a large value of B and $\sin^4(\theta/2)$ is an essential ingredient for the development of a major geomagnetic storm. As we learned in the previous section, a large main phase $|Dst| > 100\gamma$ tends to develop when ε becomes greater than $\sim 10^{19}$ erg s^{-1}. Therefore, in order for ε to become $\sim 10^{19}$ erg s^{-1} and at times as large as 10^{20} erg s^{-1}, B should be about 10γ and become at times as large as 30γ for $V = 500$ km s^{-1} and $\sin^4(\theta/2) = 1.0$ and thus $\theta = 180°$. On the other hand, even if the IMF vector is directed southward, an intense storm would not develop if B is only 3γ.

A large value of the IMF magnitude B can be caused by an intense shock wave generated by a solar flare. It is also observed in the vicinity of the interface between a slow solar wind and a high speed solar wind stream (Burlaga and King, 1979). Figures 35 and 36 show two examples of a large B value associated with a shock wave. The standard solar wind quantities, the IMF vectors in the X–Y, X–Z, and

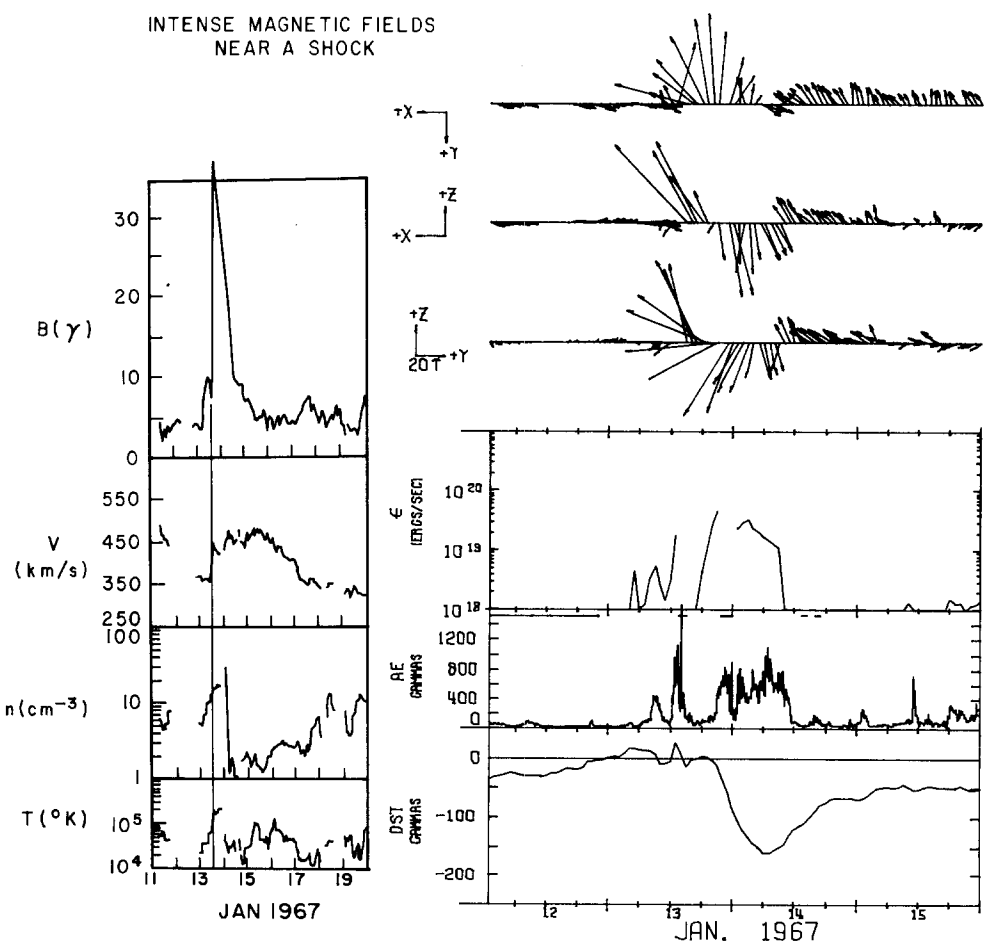

Fig. 35. Solar wind quantities B, V, n, and T (Burlaga and King, 1979), together with the IMF vector projections in the X–Y, X–Z, and Y–Z planes, ε and the AE and Dst indices during an intense magnetic storm of January 12–15, 1967.

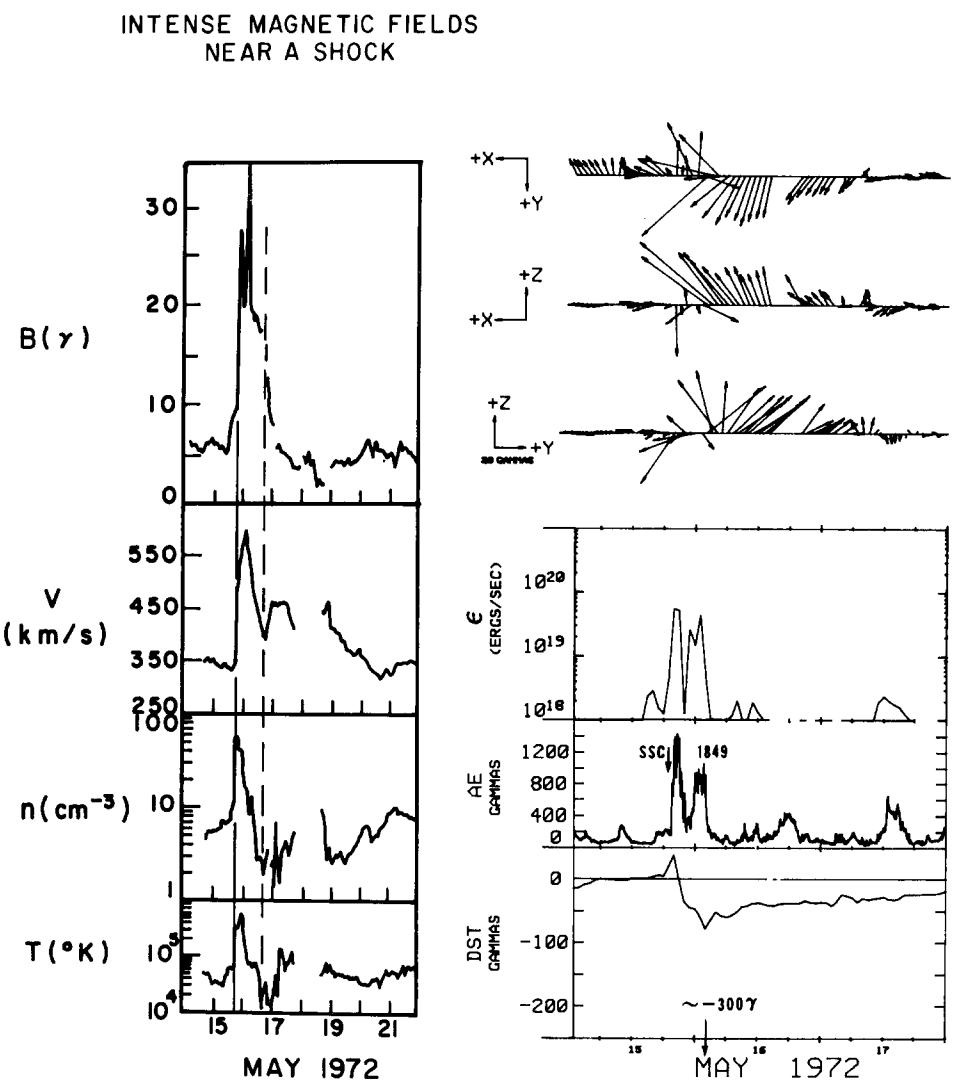

Fig. 36. Same as Figure 35, for the May 15–17, 1972 storm.

Y–Z planes, ε and the AE and Dst indices are shown. In the first case, a large B value and θ caused a major geomagnetic storm. On the other hand, in the second case, the shock produced only a mini-storm. The reason for the failure to develop an intense storm was a small value of θ, namely the northward pointing vector. If the vector of the same magnitude was pointing southward, this storm could have developed into a major storm of $|Dst| \sim 300\gamma$.

Figure 37 shows a large value of B in the vicinity of the interface (Burlaga and King, 1979). Actually, this interface passage can be identified as the passage of the solar current disk, as we examined in Section 6. In the past, various interplanetary discontinuities (such as shock waves and interfaces) were mostly discussed in their

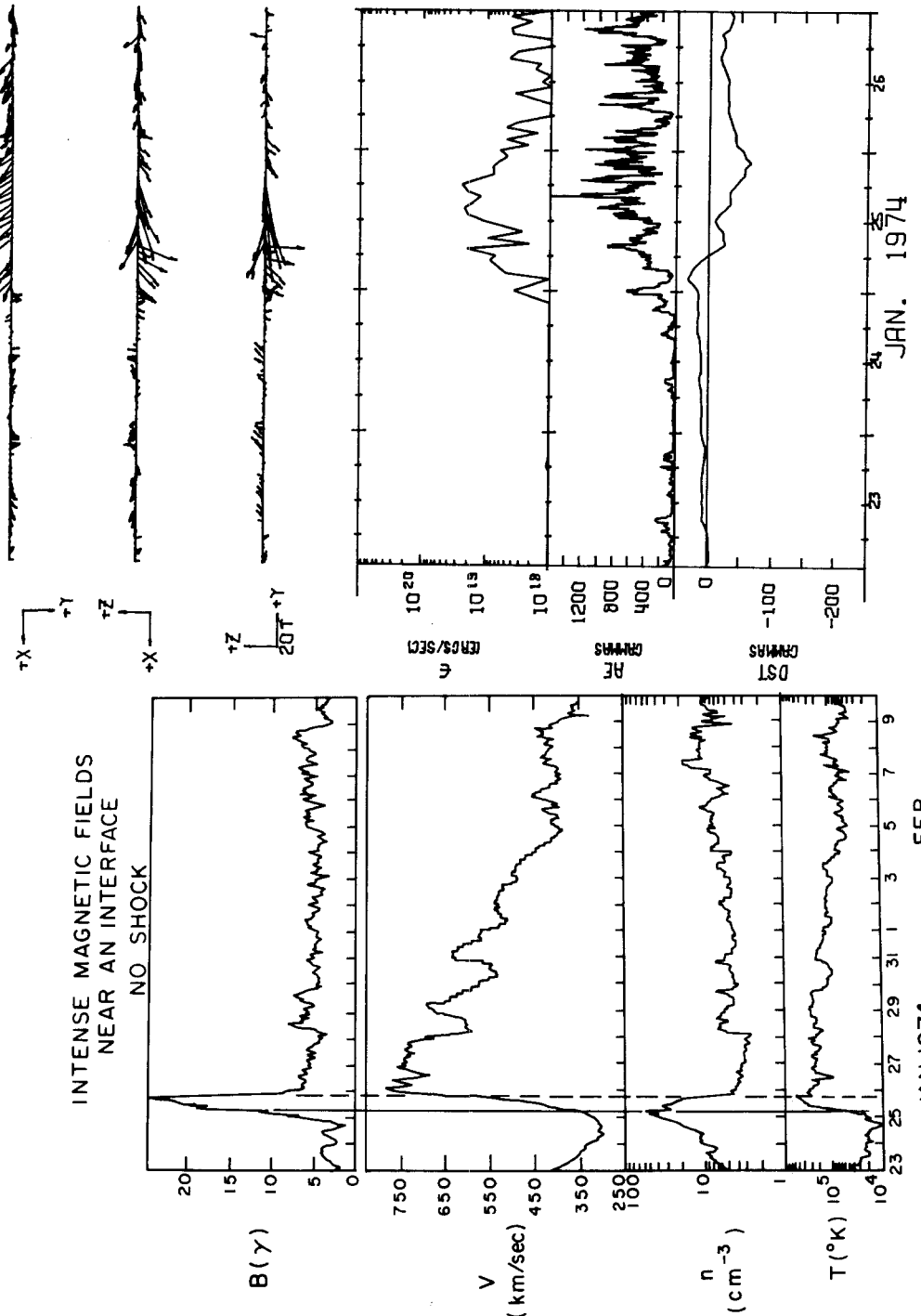

Fig. 37. Same as Figure 35, for the February 23–16, 1974 storm.

equatorial plane projection. However, for a full understanding of such discontinuities, particularly in relation to ε and magnetospheric disturbances, it is essential to understand their structures in the meridian plane. This was the reason why the interface was discussed in terms of the solar current disk in Section 6. When an interface is associated with a sharp change of the IMF ϕ angle from 135° to 335° or from 335° to 135°, it may be identified as the solar current disk. In this example, B was very large at the time of the passage, but the vector was more or less parallel to the solar-magnetospheric equatorial plane. As a result, ε did not exceed $3\times$ $\times 10^{19}$ erg s^{-1}. Figure 38 shows details of the distribution of various solar wind quantities, including ε, during the passage of the interface (and also the solar current disk in this case) observed on February 28–29, 1968. In this particular case, the highest value of ε was concentrated near the interface. However, this is not always the case, as we examined in Section 6. Such a study of ε in the solar wind has just begun.

Since a large value of the IMF magnitude B is often associated with either a shock wave caused by a solar flare or the high speed stream interface which can often be identified as the solar current disk, the passage of a region of a large value of B is more or less predictable with some accuracy by observing solar flares or examining the 27-day recurrence tendency of a high speed stream. On the other hand, it is not understood why the angle θ varies, particularly during the passage of such a large B value region. Therefore, it is essential to find causes of changes of the angle θ in understanding solar activity-terrestrial relationships. Indeed, this problem is, at present, an important missing link between solar disturbances and magnetospheric disturbances. Unfortunately, only a few solar and interplanetary physicists are interested in causes of changes of the angle θ at the present time. Most magnetospheric physicists take it for granted that the angle θ varies at the front of the magnetosphere, and they concentrate only on consequences and effects of the changes in the magnetosphere.

Burlaga and Klein (1980) suggested that a large value of the angle θ during the January 13–14, 1967 storm (Figure 35) was caused by the passage of a magnetic cloud in which the field had a cylindrical geometry; see Figure 39. Such an idea was originally suggested by Gold (1962). Smith (1979) and Akasofu (1979b) suggested that the solar current disk develops, at times, a large-scale radial deformation with a very steep gradient. Figure 40 shows schematically the solar current disk which has developed a wavy structure; the insert shows its meridian cross-section through the Earth. The associated magnetic field lines (namely, the IMF field lines) are expected to have also a large scale gradient in the vicinity of the current disk. Figure 41 shows the suggested changes of the wavy structures at several epochs during an intense storm of July 3–7, 1974 by showing the meridian cross-section of the solar current sheet through the Earth (Akasofu, 1979b). It shows schematically how a large value of θ or Ⓗ can be generated by the wavy structure. Note that this storm was examined in Section 6.

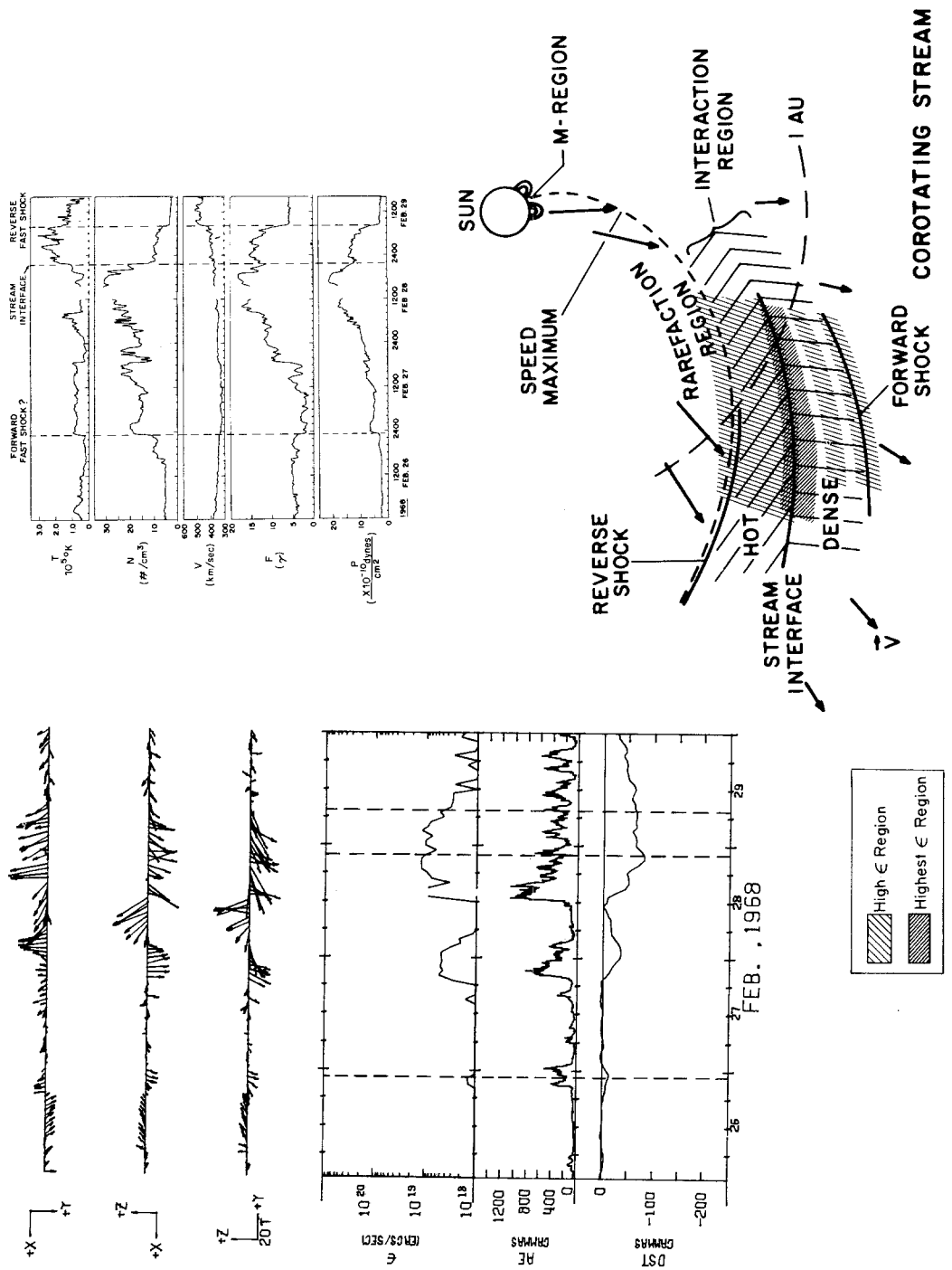

Fig. 38. Same as Figure 35, for the February 26–29, 1968 storm. The insert, taken from Burlaga (1975), illustrates schematically the passage of the interface (the solar current disk in this case) and the distribution of the solar wind-magnetosphere energy coupling function ε.

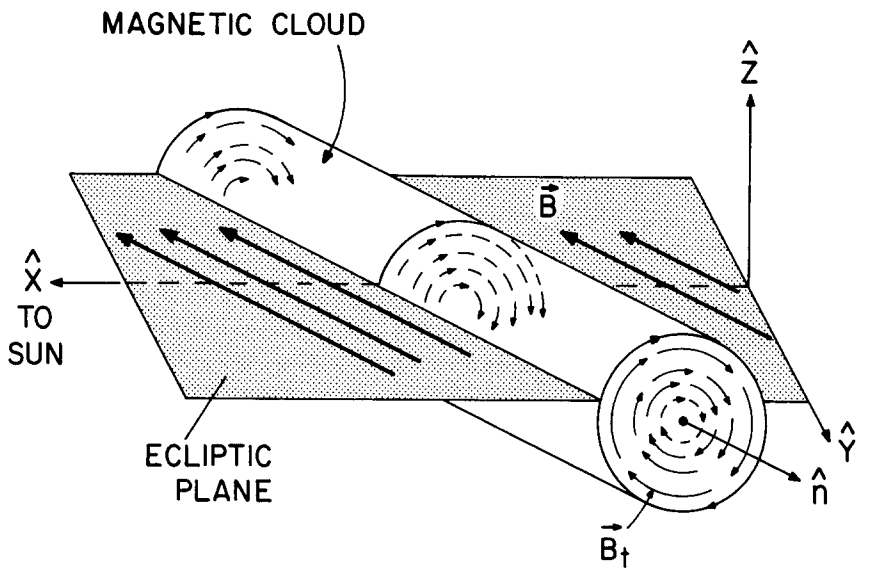

Fig. 39. Schematic illustration of the magnetic cloud and the field distribution in it for the January 12–15, 1967 storm (Burlaga and Klein, 1980).

It is interesting to note that the occurrence of major geomagnetic storms is often associated with the passage of the solar current disk, as we learned in Section 6. This implies that an intense shock wave generated by a solar flare causes a large-scale radial deformation of the solar current disk. As a result, the current disk shifts temporarily upward or downward with respect to the pre-flare location and passes the location of the Earth during its movement. If the radial deformation of the current disk occurs at such times, large changes of the IMF angle θ are also expected. It will become possible in the near future to examine quantitatively such possibilities and others by simulating plausible interplanetary conditions by using a large computer. There is no doubt that a quantitative understanding of this problem is an important future problem to both solar physicists and magnetospheric physicists.

9.2. Transmission of the Dynamo Power $P\,(=\varepsilon)$ to the Inner Magnetosphere and the Ionosphere

It is hoped that the finding of ε alone may serve to eliminate a number of possible mechanisms of the transmission of the power. In the past, it was widely believed that reconnection processes convert stored magnetic energy into substorm energy, so that much theoretical effort has been concentrated on a study of possible conversion mechanisms. The finding of ϵ indicates that the transmission of the generated power to the inner magnetosphere and the ionosphere is a direct process, since $U_T(t)$ correlates well with $\varepsilon\,(t)$. A recent study by Akasofu *et al.* (1981) shows that the power generated by the solar wind-magnetosphere is directly transmitted to the convective motion of magnetospheric plasma and that this convective motion

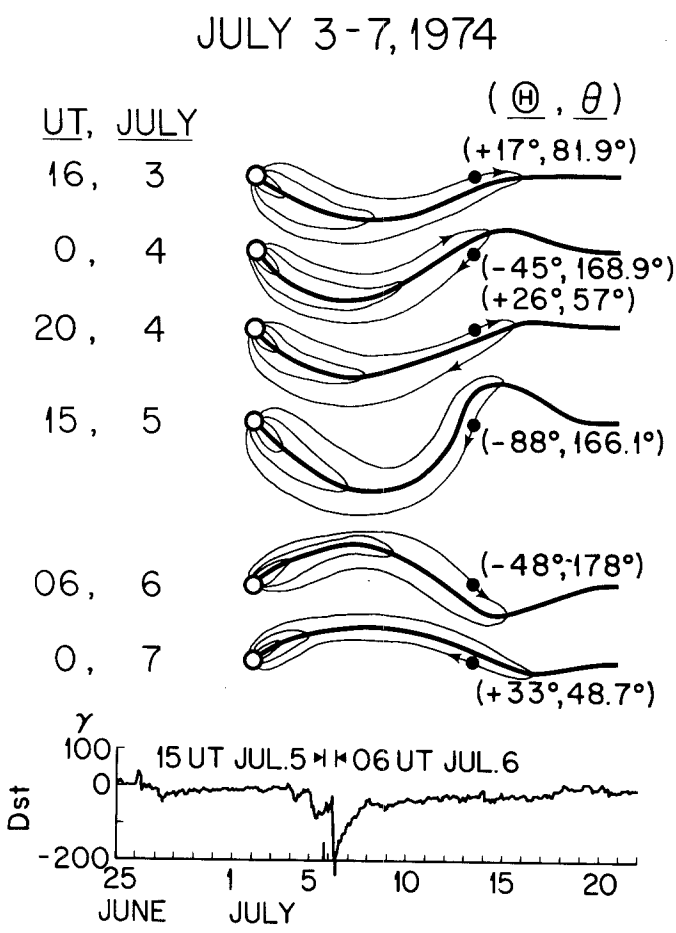

Fig. 40. Schematic illustration of the solar current disk which has developed a wavy structure. The insert shows its meridian cross-section through the Earth.

generates field-aligned currents. This subject is, however, beyond the scope of this paper.

9.3. Improvement of the Expression for the Energy Coupling Function

One of the basic assumptions involved in determining the total energy consumption rate U_T by using the *Dst* and *AE* indices is that a large part of the energy consumed by the magnetosphere is deposited in the inner magnetosphere and the ionosphere. This is a plausible assumption, since the convective motion of magnetospheric plasma is directed toward the Earth. The similarity of time variations of $\varepsilon(t)$ and $U_T(t)$ suggests also that if a significant part of $\varepsilon(t)$ escapes from the magnetosphere without being detected by ground observations (the *Dst* and *AE* indices), such a part is nearly proportional to $U_T(t)$. Otherwise, it is difficult to expect the similarity of $\varepsilon(t)$ and $U_T(t)$. However, it is important to examine further this problem.

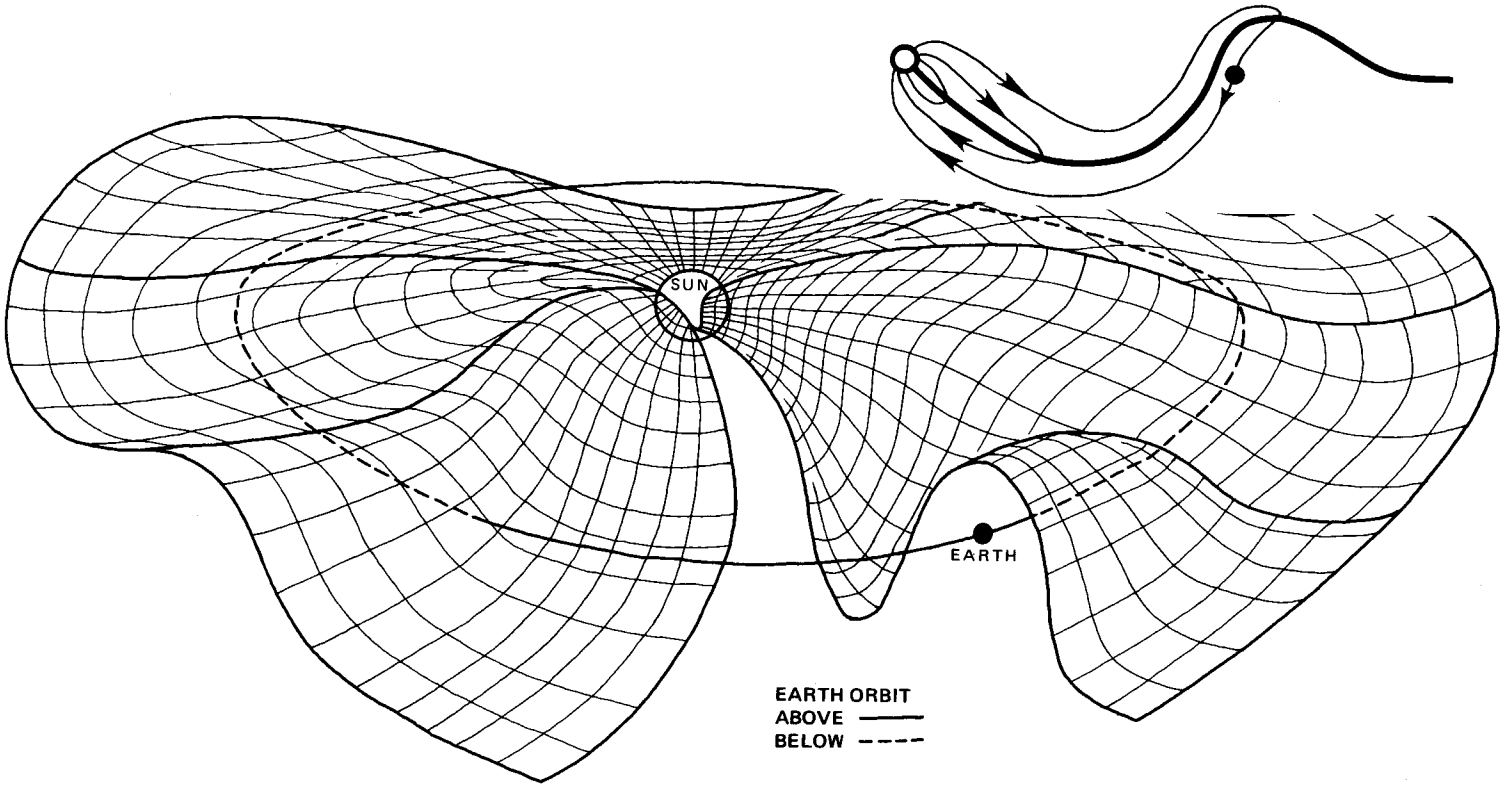

Fig. 41. Schematic illustration of the wavy solar current disk (the meridian cross-section through the Earth) during the July 3–7, 1974 storm.

One of the first tasks in improving the expression for the energy coupling is to improve the estimate of the total energy consumption rate U_T which is given as the sum of U_R, U_J, and U_A. At this stage, it is perhaps of little use to attempt to improve the expression for the energy coupling without improving U_T. For an accurate determination of these quantities, the following steps are needed:

(a) *Accurate determination of the ring current field and its relation to the total energy of the ring current.*

For this purpose, we must recognize at least the following problems.

(i) The ring current is greatly asymmetric during the period when it is rapidly developing. At present, there is no expression to relate the asymmetric ring current field to the total energy of the ring current.

(ii) Effects of the solar wind pressure should be accurately calibrated and be removed from the *Dst* index.

(iii) A part of the magnetic field of the substorm current system (such as the field of ionospheric currents and field-aligned currents) should be removed from the *Dst* index. Altogether, (i), (ii), and (iii) require an advance in understanding of the geomagnetic storm fields.

(iv) The lifetime of the ring current particles should be determined accurately as a function of storm time. Knowing now that the function H in (25) is smaller than unity, the lifetime τ_R of the ring current particles is now the most uncertain parameter and significantly affects our estimate of U_T. Let us assume that τ_R varies smoothly with ε (rather than to assume that $\tau_R = 20$ hr for $\varepsilon < 5 \times 10^{18}$ erg s^{-1} and $\tau_R = 1$ hr for $\varepsilon > 5 \times 10^{18}$ erg s^{-1}) and estimate U_T and compare it with the old U_T. The following values of τ_R are used for this new estimate: $\tau_R = 20$ hr for $\varepsilon < 10^{18}$ erg s^{-1}, $\tau_R = 6$ hr for 10^{18} erg/s$^{-1} < \varepsilon < 5 \times 10^{18}$ erg s^{-1}, $\tau_R = 3$ hr for 5×10^{18} erg s$^{-1} < \varepsilon <$ $< 10^{19}$ erg s^{-1}, $\tau_R = 1.0$ hr for 10^{19} erg s$^{-1} < \varepsilon < 5 \times 1^{19}$ erg s^{-1}, $\tau_R = 0.3$ hr for $5 \times$ $\times 19^{19} < \varepsilon < 10^{20}$ erg s^{-1} and $\tau_R = 0.2$ hr for $\varepsilon > 10^{20}$ erg s^{-1}. The results are shown in Figure 32. Comparing it with Figure 4a, one can see clearly a considerable improvement of the correlation between ε and U_T. This is true for all the storms examined so far. In fact, the estimate of ε can indeed be more certain than that of U_T, and one could perhaps estimate τ_R from ε and U_T (after improving $\partial Dst/\partial t$ by using a finer time resolution data than hourly rates).

(b) *Accurate determination of the production rate of Joule heat U_J and the auroral particle injection rate U_A.*

First of all, it is important to improve the AE index as the *quantitative* index of magnetospheric substorms. Since it is obtained by using the upper limit of positive changes (the AU index) and the lower limit of negative changes (the AL index), it tends to exaggerate effects of locally concentrated currents. For example, a westward traveling surge is often associated with a large concentration of the auroral electrojet in a localized region. Such a current often produces large negative bays which often contribute to the AE index as a large impulsive change. Such a change hardly represents changes of the total current of the auroral electrojet. Since the AE index

is the only index available in estimating the Joule heat production rate on a continuous basis, it is important to relate the Joule heat production rate U_J, estimated by whatever means available, to the AE index. Incoherent scatter radar and satellite probes can be used in this calibration, as suggested in Section 3.

(c) *Accurate determination of the cross-sectional area* l_0^2.

In the empirical analysis described in the above, it was assumed that the cross-sectional area l_0^2 in the energy coupling function ε is constant. The good correlation between U_T and ε suggests that such an assumption is a reasonable first approximation. However, it is quite likely that l_0^2 is only a weak function of ρ, V, B, θ, etc.; otherwise, we would not be able to obtain any correlation between ε and U_T. The distance l_0 may be proportional to the Chapman–Ferraro distance (namely, the distance between the dayside magnetopause and the Earth) or the distance to the neutral point from the Earth by assuming Dungey's model. This analysis may be carried out theoretically on the basis of assumed models, as we attempted in Section 7.2. However, it is difficult to verify such a theoretical analysis until the total energy consumption rate U_T is determined accurately.

10. Summary

The finding of the energy coupling function ε, though it is a first approximation expression, is an important new step in understanding the energy coupling process between the solar wind and the magnetosphere. The finding has now verified that the solar wind and the magnetosphere constitute a dynamo and that the magnetosphere is closer to a driven system than to an unloading system. The finding has also raised the possibility of an accurate forecasting of magnetospheric substorms and storms.

The finding has led us to several new directions along which we should pursue in understanding relationships between solar activity and magnetospheric disturbances. The most important missing link between solar activity and magnetospheric disturbances is the causes of the distortion of the solar current disk, which results in large changes of the IMF angle θ.

An improved understanding of the energy coupling process requires, first of all, an accurate determination of the total energy consumption rate U_T, which requires in turn a better understanding of the geomagnetic disturbance fields and their relations to the dissipated energies.

Acknowledgements

The author would like to thank a number of colleagues who collaborated in the study of the energy coupling function, including J. Chao, J. Kan, L. Lee, and P. Perreault. The work reported in this paper was supported in part by a grant from the National

Science Foundation, Atmospheric Sciences Section ATM77-26522, in part by a grant from the National Aeronautics and Space Administration, NSG-7447, and in part by a contract with the U.S.A.F., F19628-79-C-0067.

References

Akasofu, S.-I.: 1964, *Planet. Space Sci.* **12**, 801.
Akasofu, S.-I.: 1968, *Polar and Magnetospheric Substorms*, D. Reidel Publ. Co., Dordrecht, Holland.
Akasofu, S.-I.: 1974, *Space Sci. Rev.* **16**, 617.
Akasofu, S.-I.: 1977, *Physics of Magnetospheric Substorms*, D. Reidel Publ. Co., Dordrecht, Holland.
Akasofu, S.-I.: 1979a, *Planet Space Sci.* **27**, 425.
Akasofu, S.-I.: 1979b, *Planet. Space Sci.* **27**, 1055.
Akasofu, S.-I.: 1981, *J. Geophys. Res.* (submitted).
Akasofu, S.-I. and Chao, J. K.: 1979, *Geophys. Res. Letters* **6**, 897.
Akasofu, S.-I. and Chao, J. K.: 1980, *Planet Space Sci.* **28**, 381.
Akasofu, S.-I. and Chapman, S.: 1963, *J. Geophys. Res.* **68**, 125.
Akasofu, S.-I. and Chapman, S.: 1972, *Solar-Terrestrial Physics*, Oxford Univ. Press, Oxford.
Akasofu, S.-I., Chapman, S., and Meng, C.-I.: 1968, *J. Atmos. Terr. Phys.* **30**, 227.
Akasofu, S.-I., Perreault, P. D., Yasuhara, F., and Meng, C.-I.: 1973, *J. Geophys. Res.* **78**, 7490.
Akasofu, S.-I., Kamide, Y., Kan, J. R., Lee, L. C., and Ahn, B.-H.: 1981, *Planet. Space Sci.* (submitted).
Alfvén, H.: 1939, *I. Kung, sv. Vet.-Akademiens Handl.* (3) **18**, No. 3.
Alfvén, H.: 1950, *Cosmical Electrodynamics*, Oxford Univ. Press.
Arnoldy, R. L.: 1971, *J. Geophys. Res.*, **76**, 5189.
Axford, W. I.: 1964, *Planet. Space Sci.* **12**, 45.
Axford, W. I.: 1967, *Space Sci. Rev.* **7**, 149.
Axford, W. I.: 1969, *Rev. Geophys.* **1**, 421.
Ballif, J. R., Jones, D. E., and Coleman, Jr., P. J.: 1969, *J. Geophys. Res.*, **74**, 2289.
Bobrov, M. S.: 1973, *Planet. Space Sci.* **21**, 2139.
Brandt, J. C. and Hunten, D. M.: 1966, *Planet. Space Sci.* **14**, 95.
Brekke, A. and Rino, C. L.: 1978, *J. Geophys. Res.* **83**, 2517.
Burch, J. L.: 1972, *J. Geophys. Res.* **77**, 5629.
Burlaga, L. F.: 1975, *Space Sci. Rev.* **17**, 327.
Burlaga, L. F. and King, J. H.: 1979, *J. Geophys. Res.* **84**, 6633.
Burlaga, L. F. and Klein, L.: 1980, 'Magnetic Clouds in the Solar Wind', NASA Tech. Mem., 80668, GSFC, NASA.
Burton, R. K., McPherron, R. L., and Russell, C. T.: 1975, *J. Geophys. Res.* **80**, 4204.
Chapman, S. and Ferraro, V. C. A.: 1931, *Terr. Mag. Atmosph. Elect.* **36**, 77.
Cole, K. D.: 1962, *Australian J. Phys.* **15**, 223.
Cole, K. D.: 1971, *Planet. Space Sci.* **19**, 59.
Crooker, N. U., Feynman, J., and Gosling, J. T.: 1977, *J. Geophys. Res.* **82**, 1933.
Davis, T. N. and Parthasarathy, R.: 1967, *J. Geophys. Res.* **72**, 5825.
Dessler, A. J. and Parker, E. N.: 1959, *J. Geophys. Res.* **64**, 2239.
Dessler, A. J., Hanson, W. B., and Parker E. N.: *J. Geophys. Res.* **66**, 3631.
Dryer, M.: 1975, *Space Sci. Rev.* **17**, 277.
Dryer, M. and Steinolfson, R. S.: 1976, *J. Geophys. Res.* **81**, 5413.
Dryer, M., Smith, Z. K., Smith, E. J., Mihalov, J. D., Wolfe, J. H., Steinolfson, R. S., and Wu, S. T.: 1978, *J. Geophys. Res.* **83**, 4347.
Dungey, J. W.: 1961, *Phys. Rev. Letters* **6**, 47.
Fairfield, D. H. and Cahill, Jr., L. J.: 1966, *J. Geophys. Res.* **71**, 155.
Frank, L. A.: 1971, *J. Geophys. Res.* **76**, 2265.
Garrett, H. B., Hassler, A. J., and Hill, T. W.: 1974, *J. Geophys. Res.* **79**, 4603.
Gold, T.: 1962, *Space Sci. Rev.* **1**, 100.
Gonzalez, W. D. and Mozer, F. S.: 1974, *J. Geophys. Res.* **79**, 4186.

Gosling, J. T., Asbridge, J. R., Bame, S. J., Feldman, W. C., and Zwickl, R. D.: 1980, *J. Geophys. Res.* **85**, 3431.
Hays, P. B., Jones, R. A., and Rees, M. H.: 1973, *Planet. Space Sci.* **21**, 559.
Hoyle, F.: 1949, *Some Recent Researches in Solar Physics*, Chapter 6, Cambridge Univ. Press.
Holzer, R. E. and Slavin, J. A.: 1978, *J. Geophys. Res.* **83**, 3831.
Iijima, T.: 1973, *Rep. Ionosph. Space Re., Japan* **27**, 205.
Kan, J. R. and Akasofu, S.-I.: 1974, *J. Geophys. Res.* **79**, 1379.
Kan, J. R. and Lee, L. C.: 1979, *Geophys. Res. Letters* **6**, 577.
Kan, J. R., Lee, L. C., and Akasofu, S.-I.: 1980, *Planet. Space Sci.* **28**, 823.
Kawasaki, K., Akasofu, S.-I., Yasuhara, F., and Meng, C.-I.: 1971, *J. Geophys. Res.* **76**, 6781.
King, J. H.: 1977, *Interplanetary Medium Data Book*, NSSDC, Goddard Space Flight Center, NASA, September 1977.
Maezawa, K.: 1979, in W. P. Olson (ed.), *Quantitative Modeling of Magnetospheric Processes*, American Geophysical Union, Washington, D.C., p. 436.
Meng, C.-I., Tsurutani, B., Kawasaki, K., and Akasofu, S.-I.: 1973, *J. Geophys. Res.* **78**, 617.
Murayama, T.: 1979, in T. Obayashi (ed.), *Magnetospheric Study 1979*, Japanese IMS Committee, Tokyo, p. 296.
Murayama, T. and Hakamada, K.; 1975, *Planet. Space Sci.* **23**, 75.
Olbert, S.: 1960, in R. L. Carovillano, J. F. McClay, and H. R. Radoski (eds.), *Physics of the Magnetosphere*, D. Reidel Publ. Co., Dordrecht, Holland, p. 641.
Perreault, P.: 1974, 'On the Relationship between Interplanetary Magnetic Fields and Magnetospheric Storms and Substorms', Ph.D. thesis, University of Alaska, August.
Perreault, P. and Akasofu, S.-I.: 1978, *Geophys. J. Roy. Astron. Soc.* **54**, 547.
Rees, M. H.: 1975, *Planet. Space Sci.* **23**, 1589.
Rino, C. L., Wickwar, V. B., Banks, P. M., Akasofu, S.-I., and Rieger, E.: 1974, *J. Geophys. Res.* **79**, 4669.
Rostoker, G. and Fälthammar, C.-G.: 1967, *J. Geophys. Res.* **72**, 5853.
Saito, T.: 1975, *Sci. Rep. Tohoku Univ., Ser. 5* **23**, 37.
Schieldge, J. P. and Siscoe, G. I.: 1970, *J. Atmosph. Terr. Phys.* **32**, 1819.
Schulz, M.: 1973, *Astrophys. Space Sci.* **24**, 371.
Sckopke, N.: 1966, *J. Geophys. Res.* **71**, 3125.
Siscoe, G. L. and Cummings, W. D.: 1969, *Planet. Space Sci.* **17**, 1795.
Siscoe, G. L., Formisano, V. and Lazarus, A. J.: 1968, *J. Geophys. Res.* **73**, 4869.
Smith, D. J., Tsurutani, B. T., and Rosenberg, R. L.: 1978, *J. Geophys. Res.* **83**, 717.
Smith, E. J.: 1979, in H. R. Rosenbauer (ed.), *Solar Wind IV.*
Smith, E. J. and Wolfe, J. H.: 1979, *Space Sci. Rev.* **23**, 217.
Snyder, C. W., Neugebauer, M., and Rao, U. R.: 1963, *J. Geophys. Res.* **68**, 6361.
Sonnerup, B. U. Ö.: 1974, *J. Geophys. Res.* **79**, 1546.
Svalgaard, L.: 1977, in *Coronal Holes and High Speed Wind Streams*, Colorado Associated University Press, Boulder, p. 371.
Svalgaard, L. and Wilcox, J. M.: 1976, *Nature* **262**, 766.
Tinsley, B. A.: 1976, *J. Geophys. Res.* **81**, 6193.
Wilcox, J. M. and Ness, N. F.: 1965, *J. Geophys. Res.* **70**, 5793.
Yeh, T., Kan, J. R. and Akasofu, S.-I.: 1981, *Planet. Space Sci.* (in press).